

NEOTECTONICS AND SEISMICITY OF
EASTERN SİMAV GRABEN, KÜTAHYA – TURKEY

A THESIS SUBMITTED TO
THE GRADUATE SCHOOL OF NATURAL AND APPLIED SCIENCES
OF
MIDDLE EAST TECHNICAL UNIVERSITY

BY

MUSTAFA KAPLAN

IN PARTIAL FULFILLMENT OF THE REQUIREMENTS
FOR
THE DEGREE OF MASTER OF SCIENCE
IN
GEOLOGICAL ENGINEERING

SEPTEMBER 2014

Approval of the thesis:

**NEOTECTONICS AND SEISMICITY OF
EASTERN SİMAV GRABEN, KÜTAHYA – TURKEY**

submitted by **MUSTAFA KAPLAN** in partial fulfillment of the requirements for the degree of **Master of Science in Geological Engineering Department, Middle East Technical University** by,

Prof. Dr. Canan Özgen
Dean, Graduate School of **Natural and Applied Sciences**

Prof. Dr. Erdin Bozkurt
Head of Department, **Geological Engineering**

Prof. Dr. Ali Koçyiğit
Supervisor, **Geological Engineering Dept., METU**

Examining Committee Members:

Prof. Dr. Erdin Bozkurt
Geological Engineering Dept., METU

Prof. Dr. Ali Koçyiğit
Geological Engineering Dept., METU

Prof. Dr. F. Bora Rojay
Geological Engineering Dept., METU

Prof. Dr. Reşat Ulusay
Geological Engineering Dept., HÜ

Assist. Prof. Dr. A. Arda Özacar
Geological Engineering Dept., METU

Date: 03.09.2014

I hereby declare that all information in this document has been obtained and presented in accordance with academic rules and ethical conduct. I also declare that, as required by these rules and conduct, I have fully cited and referenced all material and results that are not original to this work.

Name, Last Name: Mustafa Kaplan

Signature:

ABSTRACT

NEOTECTONICS AND SEISMICITY OF EASTERN SİMAV GRABEN, KÜTAHYA – TURKEY

Kaplan, Mustafa

M.S., Department of Geological Engineering

Supervisor: Prof. Dr. Ali Koçyiğit

September 2014, 121 pages

The Simav graben is an about 1-9 km wide, 50 km long and approximately WNW-trending active depression. It is located along the western section of a seismogenic belt with a depth of 10-15 km. It is the 10-30 km wide and approximately 500 km long active fault system, namely the Akşehir-Simav fault system. The Simav graben was developed on the northern Menderes Massif under the control of active faults comprising the Simav section of the Akşehir-Simav fault system.

The Simav and Akdere grabens include two different fills separated by an intervening angular unconformity: (a) Early Miocene-Middle Miocene deformed graben fill, and (b) Quaternary modern and undeformed graben fill. Geological structures and stratigraphic relationships reveal that there are four tectonic periods differentiated in the study area: (a) N-S extension along the Simav detachment fault, (b) E-W extension and formation of Demirci, Akdere and Selendi grabens, (c) NW-SE compression period characterized by strike-slip faulting, deformation of older graben fills, separation and displacement of the Akdere and Demirci grabens and

“non-deposition” in the region, (d) NNE-SSW extension controlled neotectonic period that is characterized by normal faulting and development of both the modern Simav and Akdere grabens.

The Simav County and a number of settlements in the size of town and villages are located on and very close to the graben margin-bounding normal faults. Most of them are active and have a capacity of creating destructive earthquakes. This was proved once more by the occurrence of two recent earthquakes. These are the 17 February 2009 Naşa (Simav) ($M_w = 5.3$) and the 19 May 2011 Söğüt (Simav) ($M_w = 5.9$) earthquakes. The source of the Söğüt earthquake is the Nadarçanı or Seyirkaya fault comprising the Simav fault zone. These faults are normal faults dipping towards NNE. NNE extension and normal faulting mechanism is consistent with the focal mechanism solutions, epicenter location and focus depth and GPS velocity analysis. Simav and a number of settlements located around the active faults are under the threat of earthquake hazard. For this reason, deterministic seismic hazard maps of the study area were prepared to define the earthquake hazard in the Simav region by using the available geological and seismological data as well as a reasonable attenuation relationship for the region. PGA value for Simav city center soil site condition is 0.398 g.

Keywords: neotectonic, seismicity, seismic hazard, Simav graben, Simav fault zone, GPS, PGA, DSHA

ÖZ

SİMAV GRABENİ DOĞU KESİMİNİN NEOTEKTONİĞİ VE DEPREMSELLİĞİ

KAPLAN, Mustafa

Yüksek Lisans, Jeoloji Mühendisliği Bölümü

Tez Yöneticisi: Prof. Dr. Ali KOÇYİĞİT

Eylül 2014, 121 sayfa

Simav grabeni yaklaşık 1-9 km genişlikte, 50 km uzunlukta BKB uzanımlı aktif bir çöküntü alanıdır. Simav grabeni 10-15 km derinlikteki bir sismik kuşağın batı kesiminde yer alır. Bu sismik kuşak 10-30 km genişlikte ve 500 km uzunlukta olan Akşehir-Simav fay sistemidir. Simav grabeni, Akşehir-Simav fay sisteminin Simav kısmını oluşturan aktif fayların kontrolünde kuzey Menderes Masifinde gelişmiştir.

Simav ve Akdere grabenleri aradaki açılma uyumsuzlukla birbirinden ayrılan iki farklı dolgu içerir. (a) Erken Miyosen-Orta Miyosen deforme olmuş dolgu, ve (b) deforme olmamış Kuvaterner dolgu. Jeolojik yapılar ve stratigrafik ilişkiler bölgede ayırılabilen 4 farklı tektonik dönem olduğunu göstermiştir. (a) Simav sıyrılma fayı üzerinde K-G genişleme, (b) D-B genişleme ve Demirci, Akdere ve Selendi grabenlerinin oluşması, (c) Doğrultu atımlı faylanma, eski graben dolgusunun deforme olması, Akdere ve Demirci grabenlerinin ayrılması ve ötelenmesi, ve bölgede çökelimin duraksamasıyla temsil edilen KB-GD sıkışma dönemi, ve (d)

normal faylanma ve güncel Akdere ve Simav grabenlerin oluşumu ile karakterize edilen, KKD-GGB genişleme kontrolündeki neotektonik dönem.

Simav ilçesi ve köy-kasaba büyüklüğündeki birçok yerleşim birimi Simav grabenini sınırlayan normal fayların üzerinde ya da çok yakınında bulunmaktadır. Bu fayların çoğu aktiftir ve yıkıcı deprem üretme potansiyeline sahiptir. Bu durum yakın zamanda meydana gelen iki depremle birkez daha kanıtlanmıştır. Bu depremler 17 Şubat 2009 Naşa (Simav) ($M_w=5.3$) ve 19 Mayıs 2011 Söğüt (Simav) ($M_w=5.9$) depremleridir. Söğüt depreminin kaynağı Simav fay kuşağını oluşturan Nadarçamı ya da Seyirkaya faylarıdır. Bu faylar KKD eğimli normal faylardır. KKD genişleme ve normal faylanma mekanizması, odak mekanizması çözümleri, episantır konumu, odak derinliği ve GPS hızları analiziyle uyumludur. Aktif fayların çevresinde bulunan Simav ve birçok yerleşke deprem tehlikesi tehdidi altındadır. Bu nedenle, Simav bölgesindeki deprem tehlikesini ortaya koymak için, mevcut jeolojik ve sismolojik verilerle birlikte bölge için uygun azalım ilişkileri kullanılarak deterministik ve olasılıksal deprem tehlike haritaları hazırlanmıştır. Simav şehir merkezi toprak zemin sınıfı için PGA değeri 0.398 g olarak bulunmuştur.

Anahtar kelimeler: neotektonik, depremsellik, deprem tehlikesi, Simav grabeni, Simav fay zonu, GPS

To my family,

ACKNOWLEDGEMENTS

First of all, I would like to thank my supervisor Prof. Dr. Ali Koçyiğit for his clear guidance, endless support, encouragement, sharing his knowledge and critically editing of the manuscript. Studying under his supervision was a priceless experience for me to learn about structural geology and tectonics. He is more than a supervisor for me and words will never be enough to express my sincere gratefulness to him.

I am grateful to Prof. Dr. Erdin Bozkurt for fruitful discussions about the thesis and giving valuable insight into the discussions on the views about extension in the region. His attitude always inspired and encouraged me during the writing of this thesis. I want to express my gratitude to Prof. Dr. Reşat Ulusay for the time he spent reading the thesis without missing any typing mistake and inconsistency. I am thankful to Prof. Dr. F. Bora Rojay who critically reviewed the thesis and shared his knowledge about not only for the geology of the region but also for the geology of Turkey. I would also thank to Assist. Prof. A. Arda Özacar for critically reviewing the thesis and providing smart solutions whenever I was in despair.

I would like to M. Abdullah Kelam, Haydar Merdin, İlkay Mudun, Aydın Çiçek, Hakan Tanyaş and Erhan Gülyüz for their valuable helps during different stages of this work. Your helps and efforts made great effect on this study.

I also want to thank to my friends at the department, Okay Çimen, Mustafa Y. Kaya, Yavuz Kaya, Felat Dursun, Faruk Berber, Arzu Arslan, Özge Ünlüce, Bülent Tokay as well as other friends and staff for their friendship and support.

I am so glad I have my friends out of the department Erçin Savur, Niyazi Gürsoy, Bahtiyar Yılmaz, Ebru Topsakal, Can Barış Agbay and others who always gave support without questioning.

At last but not the least, I want to thank to my family for patience and encouragement before and during my studies. Especially, I am grateful to my beloved, Hülya, for her continuous support, love and confidence to me.

TABLE OF CONTENTS

ABSTRACT	v
ÖZ	vii
ACKNOWLEDGEMENTS	x
TABLE OF CONTENTS	xi
LIST OF TABLES	xv
LIST OF FIGURES	xvi
CHAPTERS	
1. INTRODUCTION	1
1.1 Purposes and Scope.....	1
1.2 Method of Study	2
1.3 Location	3
1.4 Previous Works.....	3
1.5 Regional Tectonic Setting.....	9
2. STRATIGRAPHY	15
2.1 Pre-Miocene Rocks.....	15
2.1.1 Menderes Crystalline Rocks	15
2.1.2 Simav Metamorphics	17
2.1.3 Budağan Limestone.....	19
2.1.4 Dağardı Mélange.....	19
2.2 Miocene Units.....	20
2.2.1 Eğrigöz – Koyunoba Plutons	21

2.2.2	Taşbaşı Formation	21
2.2.3	Kızılbük Formation	23
2.2.4	Civanadağı Tuffs	25
2.2.5	Naşa Basalt	28
2.3	Neotectonic Units	29
2.3.1	Toklargözü Formation	29
2.3.2	Alluvial Deposits	30
3.	STRUCTURAL GEOLOGY	31
3.1	Beds	31
3.2	Unconformities	32
3.3	Folds	33
3.4	Faults	35
3.4.1	Simav Fault Zone	35
3.4.1.1	Öreylar fault	36
3.4.1.2	Beyce fault	37
3.4.1.3	Simav fault	37
3.4.1.4	Hisarardı fault	38
3.4.1.5	Mamak fault	38
3.4.1.6	Nadarçanı fault	38
3.4.1.7	Küçüktaştepe fault	41
3.4.1.8	Seyirkaya fault	42
3.4.1.9	Kocakırtepe fault	45
3.4.2	Naşa Fault Zone	45
3.4.2.1	Güneyköy fault	46
3.4.2.2	Balıklar fault	46

3.4.2.3	Karaçayırbaşı fault	48
3.4.2.4	Naşa fault	48
3.4.2.5	Bayram fault.....	48
3.4.2.6	Hüsüm fault.....	49
3.4.2.7	Eynal fault	50
3.4.2.8	Muradınlar fault	51
3.4.3	Akdere Fault Zone.....	51
3.4.3.1	Akdere fault	51
3.4.3.2	Hamzabey fault	52
3.4.4	Other faults.....	52
3.4.4.1	Kibletaştepe fault	52
3.4.4.2	Secondary normal fault	54
3.4.4.3	Faults with two overprinted sets of slickenlines	55
3.4.4.4	Buried faults.....	58
4.	SEISMICITY AND GPS ANALYSIS	59
4.1	Historical Seismicity	59
4.2	Recent Seismicity.....	60
4.3	Focal Mechanism Solutions.....	62
4.4	GPS Analysis of the region.....	67
4.4.1	Theoretical Background of GPS	68
4.4.2	Usage of GPS in Active Tectonics.....	69
4.4.3	GPS Analysis in Western Anatolia and Simav Graben	70
5.	DISCUSSION ON EVOLUTIONARY HISTORY OF THE SIMAV AND AKDERE GRABENS.....	75
6.	SEISMIC HAZARD ASSESSMENT OF SIMAV REGION.....	81

6.1	Theoretical Background	81
6.2	Deterministic Seismic Hazard Assessment of Simav Region.....	83
6.2.1	Source Characterization	83
6.2.2	Selecting Reasonable Attenuation Relationship	83
6.2.3	Calculating Ground Motion	87
7.	CONCLUSIONS.....	91
	REFERENCES.....	93
	APPENDICES	
A.	TABLES AND PLATES.....	105

LIST OF TABLES

TABLES

Table 4-1: Seismic parameters of the focal mechanism solutions of earthquakes occurred in study area	65
Table 6-1: Earthquake and ground motion parameters of 24.05.2014 Gökçeada earthquake and properties of accelerometer installed in Simav County (ERD, 2014a)	84
Table 6-2: Accelerometer readings that are selected for attenuation relationship	86
Table 6.3: Recorded PGA values and calculated PGA values from attenuation relationships	87
Table A-1: Seismic parameters of the earthquakes with magnitudes larger than 3.5 occurred in the period of 1944-2014. Epicenter distribution of the Simav graben between 38.5-39.5N 28.5-29.5E coordinates. Data source: Earthquake Research Institute (ERD, 2014b)	105

LIST OF FIGURES

FIGURES

- Figure 1-1: **a.** Simplified tectonic of Turkey and adjacent areas showing major structural elements and plate boundaries. CAFS. Central Anatolian Fault System, DSFS. Dead Sea Fault System, EAFS. East Anatolian Fault System, NAFS. North Anatolian Fault System. **b.** Simplified neotectonic map showing the study area and its regional geological setting (Courtesy of Prof. Dr. Ali Koçyiğit). 4
- Figure 1-2: Simplified map showing the location of the study area, major tectonic structures and neotectonic domains in Turkey and surrounding areas (Different colors represent different neotectonic domains that are numbered and explained on the figure) (DFZ: Doğanbey Fault Zone; BFZ: Başkale Fault Zone; YFZ: Yüksekova Fault Zone) (courtesy of Prof. Dr. Ali Koçyiğit). 10
- Figure 2-1: Generalized tectono-stratigraphic column of the study area. E-K Gr. Eğrigöz and Koyunoba granites 16
- Figure 2-2: Close-up view of migmatite (near 1km south of Akdağ town)..... 17
- Figure 2-3: Close-up view of schist-marble alternation (near Rahimler village) 18
- Figure 2-4: Close-up view of serpentinitized rocks included in the Dağardı mélangé (along Samat-Hıdırdıvanı road) 20
- Figure 2-5: Close-up view of reddish polygenetic boulder-block conglomerates of Taşbaşı formation (near east of Kabaşlar Village)..... 22
- Figure 2-6: General view of the unconformity between Budağan Limestone (JKb) and Taşbaşı Formation (Tt) (near Sivrikır Hill between Koyunoba and Kabaşlar villages, view to north)..... 23
- Figure 2-7: Close-up view of sandstone-siltstone-mudstone alternation of Kızılbük Formation (near south of Yeşilköy town) 24

Figure 2-8: Close-up view of internal structure of highly jointed rhyolitic dome in Kızılbük Formation (quarry, along Simav-Karamanca road, 3km SW of Kalkan Village).....	25
Figure 2-9: Geological map showing units exposed in the Akdere graben and line of measured section.	26
Figure 2-10: General view of Civanadağı Tuffs (Büyükgüney Hill, 2 km north of Naşa, view to NW).....	26
Figure 2-11: Measured section of Civanadağı tuffs along the line on Figure 2.9.....	27
Figure 2-12: Close-up view of the vesicular Naşa Basalt (north of Eynal thermal facility).....	28
Figure 2-13: General view of a fault terrace included in Toklargölü Formation which unconformably overlies Naşa Basalt (1 km NW of Eynal thermal facility, view to NE).....	30
Figure 3-1: Contour diagram of poles to bedding planes collected in Kızılbük Formation on equal angle lower hemisphere stereonet.....	34
Figure 3-2: Contour diagram of poles to bedding planes collected in Civanadağı tuffs on equal angle lower hemisphere stereonet.	34
Figure 3-3: Step like morphology resulted from the basinward dipping parallel faults comprising the Simav Fault Zone. F1.Seyirkaya fault, F2. Küçüktaştepe fault, F3. Nadarçanı fault (view to SW).	36
Figure 3-4: Close-up view of the slickenside developed on the Hisarardı fault (S-4 in Figure A-1 in Appendix, 670238E-4328471N).	39
Figure 3-5: Slip plane data taken from Hisarardı fault (S-4 in Figure A-1 in Appendix) and kinematic solution using Angelier's direct inversion method on Schmidt's lower hemisphere. (black arrows show local extension direction).....	39
Figure 3-6: General view of the Nadarçanı fault scarp, trace (F-F) and the sudden break in the slope amount along the Nadarçanı fault (near Nadarçanı Recreation Area, view to East).....	40

Figure 3-7: A sketch block diagram illustrating a relay ramp resulted from the transfer of movement along two overstepping normal fault segments dipping in the same direction. (Ferrill & Morris, 2001).....	41
Figure 3-8: General view of steeply sloping fault scarp of the Küçüktaştepe fault (near north of Küçüktaştepe Hill, view to southwest).....	42
Figure 3-9: General view of the step-like morphology, the back-tilting and the total throw amount of 250 m formed along the Seyirkaya fault (view to east).....	43
Figure 3-10: Close-up view of the Seyirkaya fault slickenside (S-6 in Figure A-1 in Appendix).....	44
Figure 3-11 Slip plane data taken from Seyirkaya fault (S-6 in Figure A-1 in Appendix) and kinematic solution using Angelier's direct inversion method on Schmidt's lower hemisphere. (black arrows show local extension direction)	44
Figure 3-12: General view of the Güneyköy fault scarp and trace (F-F) (view to north).	46
Figure 3-13: Close up view of the mesoscopic synthetic fault of the Güneyköy fault (S-1 in Figure A-1 in Appendix)	47
Figure 3-14 General view of the Balıklar fault scarp and trace (F-F) (view to north)	47
Figure 3-15: General view of Naşa fault scarp (F-F) (view from 1.5 km northwest of Hüsüm District, view to northeast)	49
Figure 3-16: General view of the suspended fault terrace along the Hüsüm fault (view to north).....	50
Figure 3-17: Close-up view of a synthetic mesoscopic fault running parallel to the Akdere fault (along the Eğirler road).	52
Figure 3-18: Slip plane data taken from fault plane (S-2 in Figure A-1 in Appendix) and kinematic solution using Angelier's direct inversion method on Schmidt's lower hemisphere. (black arrows show local extension direction)	53

Figure 3-19: Close-up view of a mesoscopic fault and its well-developed slickenlines observed along Simav-Samat road (S-3 in Figure A-1 in Appendix).....	54
Figure 3-20: Slip plane data taken from fault plane (S-3 in Figure A-1 in Appendix) and kinematic solution using Angelier’s direct inversion method on Schmidt’s lower hemisphere. (black arrows show local extension direction)	55
Figure 3-21: a. Close-up view of the set of slickenlines depicting dextral faulting (SL1), b. Close-up view of the set of slickenlines depicting normal faulting, c. General view of the slip plane with two overprinted sets of slickenlines (SL1, SL2) (See figure 3.24 for location).	56
Figure 3-22: Kinematic analysis of the slip plane data by using the Angelier’s direct inversion method on Schmidt’s lower hemisphere net; 1 st phase of deformation obtained from the overprinted older slickenlines (SL1 in Figure 3.22). (black arrows show local extension and compression directions)	56
Figure 3-23: Kinematic analysis of the slip plane data by using the Angelier’s direct inversion method on Schmidt’s lower hemisphere net; 2 nd phase of deformation obtained from the overprinted older slickenlines (SL2 in Figure 3.21). (black arrows show local extension and compression directions)	57
Figure 3-24: Location map showing the site of overprinted slickenline measurement (Courtesy of Prof. Dr. Ali Koçyiğit)	57
Figure 4-1: Cumulative number of earthquakes with magnitude $M \geq 3.5$ recorded in and near environ of the Simav graben (ERD,2014b).....	61
Figure 4-2: Seismotectonic map of the study area (Data is from ERD,2014b).	63
Figure 4-3: Focal mechanism solutions and their distribution in the study area. Seismic parameters are given in Table 4.1.....	64
Figure 4-4: Schmidt lower hemisphere plot of Win Tensor rotational optimization solution of available focal mechanisms (Delvaux et al., 2003) (Red arrows indicate local extension direction of earthquake area).....	66
Figure 4-5: Stress field orientation derived from focal mechanisms (Görgün, 2014).....	67

Figure 4-6: GPS velocity field of Western Anatolia which is relative to Eurasia fixed reference frame. Error ellipses are at 95% confidence interval. Simav graben is shown as black box inserted in the figure.....	71
Figure 4-7: Maximum and minimum horizontal strain axes (black arrows), Minimum horizontal stress (extension) direction taken from World Stress Map project (red arrows) Heidbach et al., 2008	72
Figure 4-8: Rigid body rotations in the study area according to GPS velocities.	73
Figure 5-1: Sketch map view, cross-sections and major events depicting proposed evolutionary history of Simav and Akdere grabens	78
Figure 6-1: Correlations between earthquake magnitude values for Turkish earthquake catalogue (r: correlation coefficient; S.D.: standard deviation) (Ulusay et al., 2004).....	85
Figure 6-2: Deterministic seismic hazard map of Simav region prepared by using Ulusay et al. (2004) attenuation relationship formula and $M_w = 6.73$ scenario earthquake sourced from Simav fault zone.	88
Figure 6-3: Deterministic seismic hazard map of Simav region prepared by using Ulusay et al. (2004) attenuation relationship formula and $M_w = 5.34$ scenario earthquake sourced from Naşa fault zone.	89
Figure A-1: Geological map of the study area.....	117
Figure A-2: Geological cross sections along A-B and C-D lines (position of the lines are shown in figure A-1). For details of the well logs readers are referred to see (Güven et al., 1985)	119
Figure A-3: Geological cross sections along A-B and C-D lines (sites of the lines are shown in figure A-1). For details of the well logs readers are referred to see (Erkan et al.,1977; Erkan, 1978; Erişen et al.,1985; Erişen et al.,1986; Erişen et al.,1989)	121

CHAPTER 1

INTRODUCTION

1.1 Purposes and Scope

Western Anatolia is one of the most well-known regions under the effect of tensional tectonics. This region is characterized by graben-horst systems and their nearly E-W trending margin-boundary faults. One of the well-developed members of the graben-horst system is the Simav graben. It is the study area located in the western part of the 10-30 km wide and 500 km long Akşehir-Simav fault system, which comprises the northern part of the western Anatolia extensional tectonic province. Both the neotectonics and active tectonics of the grabens are still under debate due to composite tectonic history. There are two main points that are still being discussed in the region: commencement age and the cause of the extension. This discussion also raised a disagreement about the onset of neotectonic regime. Neotectonic term is used for tectonic periods that started anytime in the geologic past but not finished, i.e. corresponding tectonic regime is still present. There are numerous studies in the region in this scope proposing different views which will be introduced in detail in the regional tectonic setting section; however, most of the time there is not enough evidence given by one author to refute other views. Different authors interpret similar geological data as evidences of different evolutionary models. Moreover proposed driving mechanisms of the tectonic movements may have been operating synchronously, therefore the resulting geological data of different mechanisms could be formed at the same time in different places. Simav graben is a key location to observe the field-based records of the tectonic periods. Part of the Akdere and Selendi grabens with older and deformed units are included in the study area as well

as younger Simav modern graben. Therefore, the main aim is to test the coherence of the views on the neotectonic regime in the Simav graben. Moreover, there is no a common agreement about the source of the 19 May 2011 Söğüt earthquake, which led to heavy damage in Simav County and its near environ. There are different views about the geometry and the nature of the source fault, which will be determined by detailed geological mapping. The nature of the active faults will also be key evidences that will be used to understand the nature of neotectonic regime. Moreover, the main shock and its aftershocks presented valuable seismological data to analyze its source in terms of active tectonics. Consequently, in order to contribute to the neotectonic characteristics and evolutionary history of the Simav graben, a detailed geological map was prepared. Additionally, active fault parameters collected from the field were evaluated together with the available seismological data. Finally, deterministic seismic hazard map of the region was prepared as a guide for quantitative assessment of the earthquake hazard for inhabiting and construction processes.

1.2 Method of Study

The study has been carried out in three main stages which are preliminary works, field studies and office works.

During the preliminary works, available literature was reviewed. The area was analyzed using satellite images in order to plan the fieldwork.

Second stage of field work is mainly composed of geological mapping of the study area at 1/25000 scale. During geological mapping, stratigraphic, igneous and tectonic contacts were mapped and documented by taking photographs. Geological structures such as folds and faults were mapped and documented in terms of their geometrical properties. Also field observations performed by previous researchers were verified and updated if new field data is available. Faults were identified by using the slip plane data, geological offsets and geomorphological indicators. Sketch cross-sections were drawn to show the important features, relationships of the rock units and the structure of the Simav graben.

The last stage of the study is office work where preliminary work and fieldwork results were evaluated. Office work includes kinematic analysis of the faults by using slip-plane data. Kinematic analysis was performed to find out the paleostress orientations by using “Tector” software developed by Angelier (1989). This method is based on correct measurement and interpretation of slickensides of faults. The method assumes the slip lines on the fault plane represent the plane having maximum resolved shear stress. Resolved stress tensor of best fitting fault plane and relative magnitudes of principal stresses are calculated. This program assumes pure shear and homogenous deformation. The misfit of each slip vector with the reduced tensors is calculated and some of the measurements are omitted by hand. Therefore, orientations of local principal stress axes are found using fault plane slip data. Seismological data, such as earthquake catalogue and available focal mechanism solutions, were also collected to discuss the seismicity originated from the mapped faults in the study area. Available GPS velocities were processed on the Velocity Interpolation to Strain Rates v2.0 (VISR2) software (Shen et al., 1996) to present the active deformation in the study area. The detail of this procedure will be explained in relevant chapter. Lastly, deterministic seismic hazard map was prepared for the study area by using geological and seismological data as well as a reasonable attenuation relationship.

1.3 Location

Study area is located between 39.00 N - 39.25 N latitudes and 28.875 E – 29.125 E longitudes in the eastern part of the Simav graben (Figure 1.1). It lies within J21c2,c3 and J22d1,d4 1/25000 topographical maps and covers an area around 200km². The whole area can be accessed in all seasons except for the mountainous parts with dirt roads (Figure 1.1)

1.4 Previous Works

It is necessary to categorize previous studies carried out in and around the Simav graben into two groups. The first group is about the general geology of the region as well as paleotectonic and neotectonic evolution of the Simav graben. The studies,

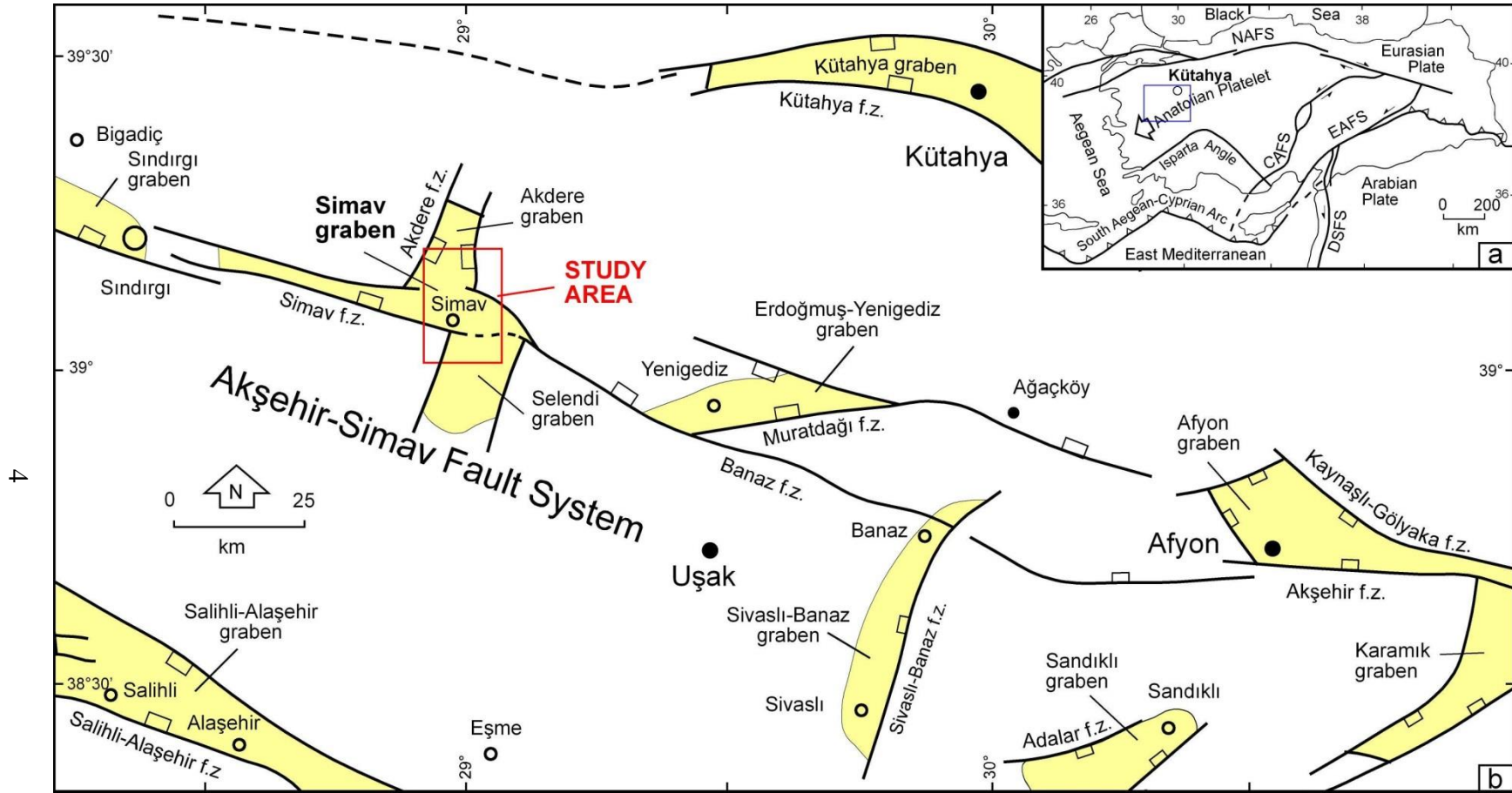


Figure 1-1: **a.** Simplified tectonic of Turkey and adjacent areas showing major structural elements and plate boundaries. CAFS. Central Anatolian Fault System, DSFS. Dead Sea Fault System, EAFS. East Anatolian Fault System, NAFS. North Anatolian Fault System. **b.** Simplified neotectonic map showing the study area and its regional geological setting (Courtesy of Prof. Dr. Ali Koçyiğit).

which are included in the first group and are relevant to the neotectonic evolution of the region and the study area, will be discussed in the Regional Tectonic Setting part of this chapter. Second group is about the active tectonics of the Simav graben and particularly the source mechanism of recent earthquakes such as the 19 May 2011 Söğüt earthquake. The studies belonging to the both groups will be summarized respectively in a chronological order.

Simav graben is first named as a 100 km long depression by Zeschke (1954).

The rock units exposed in the southern margin of the Simav graben were firstly studied in detail on a scale of 1/25000 by Akdeniz and Konak (1979), who worked in the region covering Simav, Emet, Tavşanlı, Dursunbey and Demirci towns. They proposed that basement rocks in the region are the Simav metamorphics and Menderes Massif core rocks composed mostly of granitic gneiss-migmatites. They are overlain with an angular unconformity (nonconformity) by the Sarıcasu Formation and the low grade metamorphic cover rocks of the Menderes Massif. The Jurassic-Cretaceous Budağan Limestone overlies unconformably older units. The Upper Cretaceous Dağardı mélangé has a tectonic contact with older units. The Eğrigöz granite intruded into older units during Paleocene. Lower Miocene Taşbaşı Formation, which is mainly composed of metamorphic rock fragments, unconformably overlies the Eğrigöz granite and older units. The Kızılbük Formation is overlain by Civandağı Tuffs and Akdağ Volcanics. Toklargölü Formation is cut by “Quaternary” Naşa Basalt. Konak (1982) proposed that the Dağardı mélangé was thrust towards south onto the Simav metamorphics in Late Cretaceous. He also reported that there is a 5.5–6 km right lateral offset between the same metamorphic rocks exposed on both the southern and northern margins of the Simav graben.

Öztunalı (1973) studied the Eğrigöz granite and reported that the Eğrigöz granite has formed by the anatexis during the early Alpine phase. He also reported that the granite has a calc-alkaline character and an age of 167 ± 17 Ma and 217 ± 33 Ma based on the methods of Rb/Sr and K/Ar respectively.

Ercan et al. (1984) reported that the origin of volcanic activity, which first started in Middle-Late Miocene in and around the Simav graben, is the anatexis of continental

lithosphere and emplacement of calc-alkaline Eđrigöz and Koyunoba plutons. This first strong volcanism also produced pyroclastic flows of the Akdađ Volcanics made up of thick tuff deposition, agglomerates and lava flows distributed over a large region. The second volcanic activity took place in Middle-Late Pliocene. It was the Payamtepe Volcanics resulted from an alkaline basaltic volcanism. They also stated that the last volcanic activity occurred in Quaternary, and it resulted in thick and dark colored basaltic flows of the Nařa Basalts. However, later on, the age of the Nařa Basalts were determined as 15.2 ± 0.2 Ma and 15.8 ± 0.3 Ma (Middle Miocene) based on K/Ar method by Ercan et al. (1996).

Oygür and Erler (2000) studied vein-type Pb-Zn-Cu mineralizations and proposed that these mineralizations occurred along a fracture zone running parallel to the WNW-trending “dextral Simav Fault Zone”. He also stated that the neotectonic regime was changed from compressional to tensional character during early Pliocene, and then the Simav fault started to behave like a normal fault as a natural response to the N-S extension, i.e., the Simav Fault Zone is an originally compressional (strike-slip) paleotectonic structure reactivated to be an extensional feature during the tensional neotectonic period.

Iřık et al. (2003) proposed that the extension in western Anatolia started at the beginning of Tertiary. It produced south-dipping Büyükmenderes, north-dipping Alařehir and the north-dipping Simav detachment faults. They also stated that this resulted in formation and then exhumation of syn-tectonic granodioritic intrusions such as the Eđrigöz and Koyunoba plutons. This process also resulted in ductile deformation in the deeper part of crust, while it changes to a brittle deformation at the top, at or near the ground surface. The Simav detachment fault separates high-grade metamorphics and syn-tectonic granodiorites in the footwall block from the low-grade metamorphics and unmetamorphosed rock units at the top. They also reported that the Simav detachment fault had been inactive 15 Ma before present and then cut across and offset in vertical direction by the younger margin-boundary faults of the Selendi and Demirci grabens. However, the Alařehir detachment fault is still active. These observations reveal that the Simav detachment fault is older than the

Alaşehir detachment fault. The intrusion of the Eğrigöz granodioritic pluton was dated as 20-24 Ma based on the K/Ar in biotite (Bingöl et al., 1982), 20.19 ± 0.28 Ma based on $^{40}\text{Ar}/^{39}\text{Ar}$ in biotite (Tekeli et al., 2001) and 20 Ma based on U/Pb zircon methods (Reischmann et al., 1991).

Akay (2009) studied a series of Oligo-Miocene granitic plutons such as the Ezine, Evciler, Eybek, Kozak, Alaçam, Koyunoba, Eğrigöz and the Baklan plutons exposed on the northern margin of the Menderes Massif, and then reported some similarities among them based on the internal structures, emplacement mechanisms and petrological characteristics. Akay (2009) argued that all these plutons show calc-alkaline I-type and post-collisional characteristics. He also concluded that the Eğrigöz and Koyunoba granites are shallow-seated and collisional in origin.

Hasözbeek et al. (2010a; 2010b) carried out geochemical analysis and radiogenic age determination on the Koyunoba and Eğrigöz granites and found out that they were contaminated by Menderes Massif's rocks by using U-Pb intercept ages. They also concluded that emplacement of these granitic bodies are not related to a low-angle detachment fault.

Bozkurt et al. (2011) sampled low-grade mylonites (foliated cataclasites) from the exposed Simav detachment Fault Zone and obtained ages of 30 Ma for Rb-Sr on muscovite, 17-13 Ma for brown biotite and 12-10 Ma for green biotite. They also reported that ca. 46 Ma muscovite age obtained from the metamorphic rocks is also the age of the regional main Menderes Massif metamorphism. They argued that these ages probably correspond to the followings: (a) the extensional exhumation started 30 Ma ago, (b) a period of tectonic quiescence occurred between 18-12 Ma ago, (c) reactivations of Simav detachment fault occurred between 12 Ma ago and 8 Ma ago respectively. Lastly they concluded that these ages point out that the activity on the Simav detachment fault is episodic not continuous.

The following studies also made some valuable contributions to the neotectonic evolution of the Simav graben in respect of geometry and kinematics of faults in the study area.

Koçyiğit (1984) mapped and named the Akşehir-Simav fault system (ASFS) at a regional scale for the first time and reported that the ASFS is one of the most seismically active zones characterized by the WNW-ESE-trending oblique-slip normal faults. He focused on neotectonic evolution of the region and proposed an initiation age (Late Miocene-Early Pliocene) for the neotectonic regime in this region.

Eyidoğan and Jackson (1985) reported that the Simav graben is bounded by normal faults. Their idea is based on the northward sloping of the graben floor and position of streams on the northern side of the graben. However, Westaway (1990) argued that Miocene sediments are dipping towards south, and therefore, the major fault is on the southern side.

Seyitoğlu (1997) suggested that the Simav graben cuts NE-SW-trending Selendi, Demirci and Akdere basins and is Plio(?)–Quaternary in age. He also reported that the Simav fault has a listric geometry, and the 25 March 1969 Demirci earthquake of $M_s = 6.5$ was originated from it.

There are a number of GPS studies carried out on the crustal deformation (Kahle et al., 1998; McClusky et al., 2000; Reilinger et al., 2006). Based on both the regional elastic and block-like behavior models, they proposed a current extension of NNE-SSW direction in the Simav region.

Koçyiğit and Deveci (2005) studied the Akşehir-Simav fault system in detail. They proposed that this fault system, located between Karaman in the SE and Sındırgı in the NW, is an approximately 500 km long, 10–30 km wide zone of active deformation characterized by normal faulting governed by a tensional neotectonic regime. They also pointed out that there is a long-term seismic gap (Çobanlar-Çukurören seismic gap) in the area between Çobanlar (Afyon) and Çukurköy (Kütahya) settlements included in the ASFS.

Doğan and Emre (2006) used both the geomorphological features and the geological offsets, proposed that the Simav fault is a segment of the Sındırgı-Sincanlı Fault Zone, which they regard as a transition zone between Aegean graben system and the North Anatolian Fault System. However, they did not prove whether the geological

offsets occurred in paleotectonic or neotectonic periods, and did not do a kinematic analysis based on slip-plane data measured from the faults comprising the Simav Fault Zone.

Yolsal-Çevikbilen et al. (2013) analyzed teleseismic long period 28 P and 3 SH waveforms and concluded that the source of the 19 May 2011 Söğüt earthquake is a normal fault with a minor amount of strike-slip component. They also concluded that the probable source fault, along which a vertical displacements of 50-190 cm occurred during the main shock, strikes 287° , dips at 58°N and has a rake of 86°E .

1.5 Regional Tectonic Setting

Turkey is located in the Alpine-Himalayan belt near the junction of Eurasian, African and Arabian plates (Bozkurt and Mittwede, 2001). The relative motion and interaction between these plates resulted in complex deformation patterns and high seismic activity in different tectonic domains. African plate is subducting beneath the Anatolian Platelet in north direction while the Arabian plate is colliding to Eurasia at a rate faster than that of the African plate in eastern Anatolia. Resulting major structures are the dextral North Anatolian Fault System (NAFS), the sinistral East Anatolian Fault System (EAFS), the sinistral Dead Sea Fault System (DSFS) and the South Aegean-Cyprus Subduction zone or Arc (SACA) (Figure 1.2).

Using the Eurasia fixed Global Positioning System (GPS) velocities, movement rate of the Arabian plate is 8 mm/yr towards north near South Aegean-Cyprus Arc while southwestward movement of western Anatolia is 35 mm/yr at the same place (McClusky et al., 2000). This is resulted from retreating of trench due to roll-back geometry of slab (Le Pichon and Angelier, 1979; Royden, 1993). Also the northward movement rate of the Arabian plate with respect to Eurasia is 15 mm/yr (Kahle et al., 1998). Differential velocities between African and Arabian plates make the nature of the Dead Sea Fault System left lateral. In the same way, the collision of Arabia with

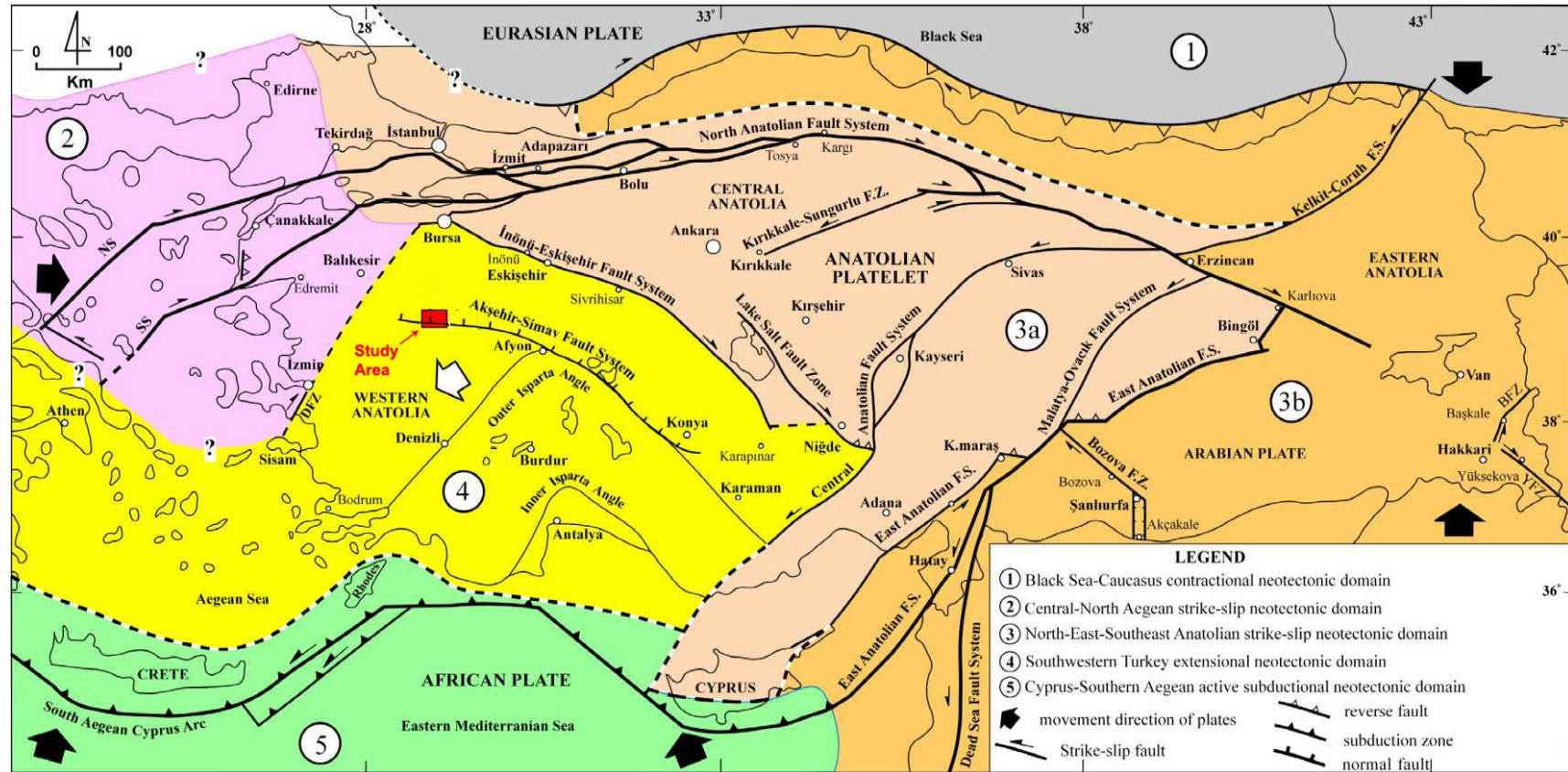


Figure 1-2: Simplified map showing the location of the study area, major tectonic structures and neotectonic domains in Turkey and surrounding areas (Different colors represent different neotectonic domains that are numbered and explained on the figure) (DFZ: Doğanbey Fault Zone; BFZ: Başkale Fault Zone; YFZ: Yüksekova Fault Zone) (courtesy of Prof. Dr. Ali Koçyiğit).

Eurasia makes the Anatolian platelet to escape from the collision zone towards west at a rate of 20 mm/yr along both the dextral North Anatolian and the sinistral East Anatolian fault systems (Şengör, 1979; Oral et al., 1992; Reilinger et al., 1997; McClusky et al., 2000).

Based on the nature of governing tectonic regimes, Turkey and its near environ can be divided into five neotectonic domains and related neotectonic regimes, that operate side by side. These domains are the Black Sea-Caucasus contractional neotectonic domain, Central-North Aegean strike-slip neotectonic domain, North-East-Southeast Anatolian strike-slip neotectonic domain, Southwestern Turkey extensional neotectonic domain and the Cyprus-South Aegean active subductional neotectonic domain. The study area is located in the southwestern Turkey extensional neotectonic domain (Figure 1.2). This neotectonic domain is mainly characterized by the N-S extension and E-W trending graben-horst systems bounded by active normal faults.

The cause and onset age of the neotectonic extension in western Anatolia has long been subject of a debate. There are four different ideas: (a) Tectonic escape model resulted from the westward extrusion of Anatolian plate due to Arabia-Eurasia collision (Şengör et al., 1985; Dewey and Şengör, 1979; Şengör, 1987), (b) Back-arc spreading model caused by southwestward migration of trench due to the slab roll-back (McKenzie, 1978; Meulenkamp et al., 1988, Le Pichon and Angelier, 1979), (c) Orogenic collapse model which refers to spreading of overthickened crust (Seyitoğlu and Scott, 1991, 1992) and (d) Episodic two stage graben model which is the combination of both the orogenic collapse and tectonic escape model (Koçyiğit et al., 1999; Koçyiğit et al., 2000; Bozkurt, 2002; Koçyiğit and Özacar, 2003; Koçyiğit, 2005; Bozkurt and Sözbilir, 2004; Bozkurt and Rojay, 2005)

Tectonic escape model is based on the squeezing and westward extrusion of the wedge-shaped Anatolian platelet. This wedge-shape brings accommodation space in further west, where effect of contractional neotectonic regime is relatively diminished. It has been suggested that the Tectonic escape of Anatolian platelet commenced in Tortonian due to the Arabia-Eurasia collision took place in Langhian-

Serravalian (Dewey and Şengör, 1979; Şengör et al., 1985). Seyitoğlu et al. (1996) argues that this model cannot be the triggering mechanism of N-S extension of western Anatolia, because the age of the rocks (ca. 20 Ma) which formed under the control of the extensional tectonics, predates the Eurasia-Arabia collision. Later on Koçyiğit et al. (1999) suggested that the North Anatolian and East Anatolian intracontinental transform fault systems were formed in Early Quaternary and then the escape of Anatolian platelet started.

Back-arc spreading model suggests that the cause of the southward migration of the south Aegean Cyprus arc is the retreating of northward subducting slab and resulting extension in western Anatolia. However, the age of subduction is being proposed differently as 13 Ma (Le Pichon and Angelier, 1979), 5 Ma (McKenzie, 1988) and at least 26 Ma (Meulenkamp et al., 1988).

Orogenic collapse model proposes that the cause of the spreading and thinning of overthickened crust is the collision and tectonic uplift (Dewey, 1988). After the removal of lateral forces, which buildups vertical stress and results in topographic high, the isostatic and gravity forces took place and spread the overthickened crust as a rebound. The closure of İzmir-Ankara-Erzincan ocean took place in latest Paleocene to early Miocene. Immediately after the cessation of collision, the orogenic collapse took place (Seyitoğlu and Scott, 1991, 1992). Şengör et al., (1985) suggested that the crust in western Turkey was thickened up to 50-55 km. This model is supported by extensive calc-alkaline magmatism sourced from the anatexis of continental lithosphere and emplacement of granitic melt (Seyitoğlu and Scott, 1991; Bozkurt and Park, 1994).

Fourth and more recent model was proposed by Koçyiğit et al. (1999). It is the episodic two stage extension for the evolution of the west Anatolian graben-horst systems. Based on this model, the evolution of the graben and horsts in southwestern Anatolia is episodic, i.e., they evolved at two tensional periods interrupted by an intervening short-term compressive episode. This model suggests that the early-middle Miocene extension is the result of orogenic collapse occurred along the İzmir-Ankara-Erzincan suture zone. It was interrupted by a short term contraction

presumably resulted from a change in the kinematics of Eurasian and Arabian plates. The second phase of N-S extension resulted from the westward escape of Anatolian plate as a natural response to the seafloor spreading of Red sea (Hempton, 1987). Koçyiğit et al. (1999) reported that Early middle Miocene sedimentary rock assemblage deposited in supradetachment basins and /or grabens intercalated with calc-alkaline volcanics are intensely folded and is overlain with an angular unconformity by the non-deformed (nearly flat-lying) early Quaternary sediments. This angular unconformity between two graben fills is the most diagnostic stratigraphic evidence for the episodic two stage extension model for the evolutionary history of graben-horst systems in southwestern Turkey. This model is also supported by the Early Quaternary age of both the NAFS and EAFS.

CHAPTER 2

STRATIGRAPHY

The rock units exposed in the Simav region were first named and mapped by Akdeniz and Konak (1979). These are, from oldest to youngest, the Menderes crystalline rocks (Kalkan Formation), the Simav metamorphics, the Budağan Limestone, the Dağardı Mélange, the Eğrigöz and Koyunoba granites, the Taşbaşı Formation, the Kızılbük Formation, the Civanadağı tuffs, the Naşa basalt, the Toklargölü Formation and Quaternary alluvium (Figure 2.1, Figure A-1 in Appendix).

The main concern of this study is the neotectonic evolution of the Simav graben and related fills. Hence, based on the graben fills and the tectonic regime, under which they were deposited, the units can be divided into three categories: (a) Pre-Miocene Rocks (basement rock units formed in previous paleotectonic periods), (b) Early Miocene-Middle Miocene units (latest paleotectonic units), and (c) Neotectonic units. These three categories of rock units are described briefly below.

2.1 Pre-Miocene Rocks

2.1.1 Menderes Crystalline Rocks

Menderes Crystalline Rocks are known as the lowermost basements units exposed in a wide region around the Simav graben and its surroundings. It is a lithodemic rock unit, therefore, it must be named as a lithodeme. The Menderes Crystalline Rocks were first named by Akdeniz and Konak (1979) as the “Kalkan Formation”. It exposes in a wide region including southern, northwestern and eastern margins of the Simav graben (Figure A-1 in Appendix). The bottom of the Kalkan Formation is not

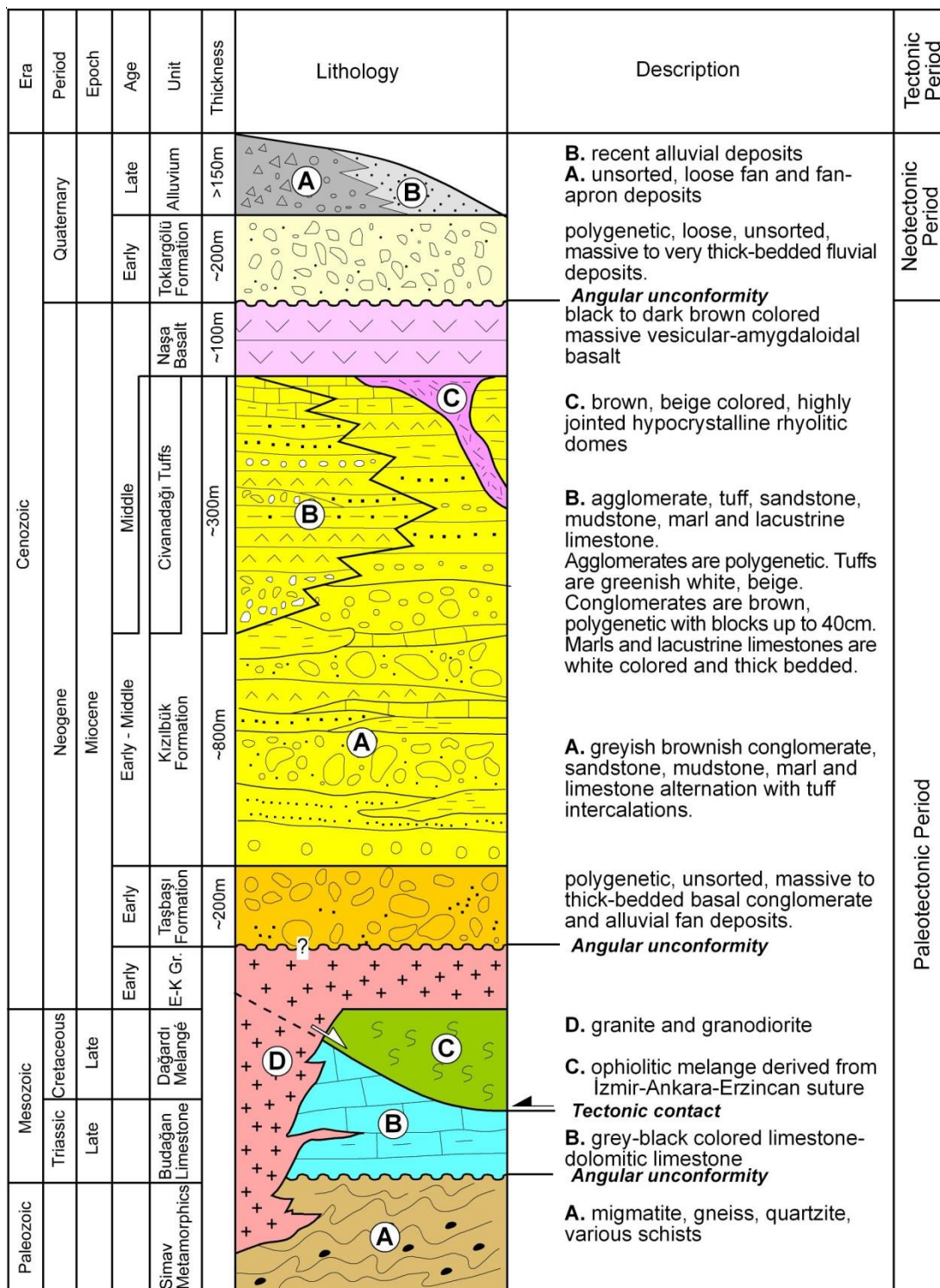


Figure 2-1: Generalized tectono-stratigraphic column of the study area. E-K Gr. Eğrigöz and Koyunoba granites

observed in the study area. It is overlain tectonically by the Simav Metamorphics. There is a cataclastic zone between these units (Konak, 1982). The Kalkan Formation is composed mainly of dark cream, brown, reddish colored and high-grade metamorphic rocks of migmatite, gneiss, banded-gneiss, migmatitic gneiss, biotite gneiss, aplite-pegmatoid veins, amphibolites and marble bands to lenses. Migmatites and gneisses are roughly foliated, folded and banded (Figure 2.2).



Figure 2-2: Close-up view of migmatite (near 1km south of Akdağ town)

They experienced intense partial melting, therefore protolith cannot be determined. Main mineral composition is quartz, orthoclase, plagioclase, biotite, sillimanite and rarely garnet. Gneisses are augen-gneisses and banded gneisses. They are jointed indicating deformation in cataclastic zone. Schists are also highly crushed and deformed in cataclastic zone, for this reason their primary textures are not observed. Marbles are 1-25 m thick, laminated to banded in structure.

2.1.2 Simav Metamorphics

This unit was first named by Akdeniz and Konak (1979). They divided the Simav Metamorphics into three sub-units, such as the Simav Metamorphics, the Sarıcasu

Formation and the Arikaya Formation. Differentiation of these units is not in the scope of this study. Hence they altogether will be referred as the Simav Metamorphics. They are exposed near south of Simav town, in the area between Koyunoba and Kabaşlar villages, along the Simav-Samat road, near Taşlık Village and especially around the Koyunuba and Eğrigöz plutons (Figure A-1 in Appendix). The Simav metamorphics have been metamorphosed in greenschist facies from the rocks of different facies along an active continental margin (Konak, 1982). The Simav Metamorphics are commonly referred as the “Menderes Massif cover rocks” in the literature. It overlies tectonically the Menderes Crystalline Rocks while is overlain with a nonconformity by the Upper Triassic- Jurassic Budağan lacustrine limestone.

The Simav Metamorphics are composed of muscovite-albite-quartz-chlorite schists, amphibolites, quartzite, calc-schist, bands and lenses of marble alternation with metabasic-ultrabasic tectonic slices at the lower and middle parts. Towards the top, the unit passes into recrystallized limestone-marble only (Figure 2.3).



Figure 2-3: Close-up view of schist-marble alternation (near Rahimler village)

Schists change in thickness from several centimeters to several meters. They are highly jointed-brecciated and folded. The unit passes into white-gray, medium to thick-bedded, folded, highly jointed and recrystallized limestone- marble-dolomite alternation.

2.1.3 Budağan Limestone

The unit was first named by Kaya (1972) as the Budağandağ Limestone in the Tavşanlı (Kütahya) area. The Budağan Limestone exposes along the Samat-Hıdırdıvanı road and in the west of Akdere graben (Figure A-1 in Appendix). The unit overlies unconformably the Simav Metamorphics while it has a tectonic contact with the overlying Dağardı Mélange.

The Budağan Limestone is characterized by the discontinuous and lense-shaped siltstone-shale-limestone alternation at the bottom while it is composed of dolomitic limestone to limestone towards the top of formation. It was deposited in shallow-marine environment. Clastic levels are composed of quartz-rich and recrystallized sandy limestone. Dolomitic limestones are light grey, grey, dark grey, and white colored, partially recrystallized, massive and highly-jointed crossed frequently by the calcite veins. Limestones are light grey, dark grey, white, beige colored, thick bedded and folded. Dolomitized parts include thin chert bands. Based on the fossil assemblage of *Involunita* sp., *Trcholina* sp. and *Triasina* sp., the age of the Budağan Limestone is late Triassic and possibly Norian-Rhaetian (Konak, 1982). Total thickness of the unit changes between 150-600m in the region.

2.1.4 Dağardı Mélange

Dağardı Mélange was first named by Akdeniz and Konak (1979). It exposes between Samat and Hıdırdıvanı villages in the study area (Figure A-1 in Appendix). The Dağardı Mélange overlies tectonically the Budağan Limestone while it is overlain with an angular unconformity by Miocene sedimentary units (older graben fill).

Dağardı Mélange is composed of intensely sheared and altered (silicified, carbonitized) chaotic mixture of listvenite, serpentinite, peridotite, diabase, gabbro, radiolarite, pelagic limestone, massif lacustrine limestone, quartzite and schist blocks

set in an ophiolitic material-rich scaly matrix. Spaces between blocks are filled with highly deformed sandstone, shale, and mudstone. Block sizes vary from several meters to mappable dimensions (Figure 2.4). Observable thickness of the Dağardı Mélange is about 200 m in the study area Akdeniz and Konak (1979).



Figure 2-4: Close-up view of serpentinitized rocks included in the Dağardı mélange (along Samat-Hıdırdivanı road)

Akdeniz (1980) reported that the Dağardı Mélange is overlain with an angular unconformity by the Eocene basal conglomerates near Başlamış village in the southwest of study area. Radiolarite-bearing red limestones of the Dağardı Mélange taken from east of Şaphane Mountain consists of *Globotruncana* sp. *Praeglobotruncana* sp. *Rotalipora apenninica*. Based on this fossil assemblage, formation age of the Dağardı Mélange should be late Cretaceous.

2.2 Miocene Units

Miocene units in the study area are the Eğrigöz and Koyunoba granites, the Taşbaşı Formation, the Kızılbük Formation, the Civanadağı Tuffs and the Naşa Basalt (Figure A-1 in Appendix). Except for the intrusions, rest of units is the older graben fill exposed along the margins of both the N-S-trending Akdere and the E-W-trending Simav grabens.

2.2.1 Eđrigöz – Koyunoba Plutons

Eđrigöz granite exposes between Kalkan and Söđüt villages to the NE of the study area, and covers an area of around 500 km². The Koyunoba granite exposes around Koyunoba village along the western margin of the Akdere graben, and covers an area of around 100-150 km². Stratigraphic position and mineralogical composition of both granites are similar, therefore they will be described together. The Eđrigöz and Koyunoba plutons have intrusive contact with the Menderes Crystalline Rocks and the Simav Metamorphics in the study area while they are overlain unconformably by the Middle Miocene volcanic and sedimentary rocks.

Both intrusions are composed of granodiorite, monzonite, granite, monzodiorite and diorite (Işık et al., 2004). Their texture is holocrystalline and mineral sizes are generally similar in each sample. Mineralogical composition is quartz, feldspar, biotite, rarely muscovite and hornblende. Aplites are generally intruded into the granite bodies in the form of dykes.

HasözbeK (2010a) reported that the Eđrigöz and Koyunoba granites are Early Miocene in age, I-type in origin and calc-alkaline in chemical composition. Their source magma has been contaminated by the Menderes Massif rocks during its upwelling processes. Their emplacement and cooling ages are 22-19 Ma and 18.77 ± 0.19 Ma respectively based on the Rb/Sr biotite closure temperature. Also, U-Th-Pb SIMS zircon dating of the Eđrigöz and Koyunoba syn-extensional granites gives 21 ± 0.2 to 20.7 ± 0.6 Ma (Ring and Collins, 2005)

2.2.2 Taşbaşı Formation

This unit was first named by Akdeniz and Konak (1979) in the Simav region. Its type locality is the Taşbaşı Village in the Demirci graben. The Taşbaşı Formation is the oldest graben fill deposited in the NNE-trending Selendi, Demirci and Akdere grabens during their early evolutionary stage (Figures A-1, A-2 in Appendix). Southern half of the Akdere graben is included in the study area while the rest two grabens are outside of it.

The Taşbaşı Formation is characterized by the reddish-brownish-colored, loosely packaged, weakly cemented and polygenetic boulder block conglomerates deposited into alluvial fans by the high energy fluvial systems (Figure 2.5).



Figure 2-5: Close-up view of reddish polygenetic boulder-block conglomerates of Taşbaşı formation (near east of Kabaşlar Village)

Bedding planes are generally unclear and it is very thick-bedded to massive. The source of the pebbles are generally augen-gneiss, schist, quartz, calc-schist, radiolarite, marble, recrystallized limestone, dolomite, serpentinite, peridotite and andesite derived from older rock units except for the Koyunoba and Eğrigöz plutons. Relative abundance of fragments depends on the proximity to source rock to the site of deposition. Fragments are generally sub-angular to angular especially in the lower parts and the unit. Overall, the unit is generally matrix-supported and unsorted. Grain size is changing from millimeters to several meters (up to 5 m in diameter), which gradually decreases towards the top of the formation. The Taşbaşı Formation is exposed well between Kabaşlar and Güneyköy villages in the study area, where it overlies with an angular unconformity all of the Pre-Miocene units (Figure 2.6).

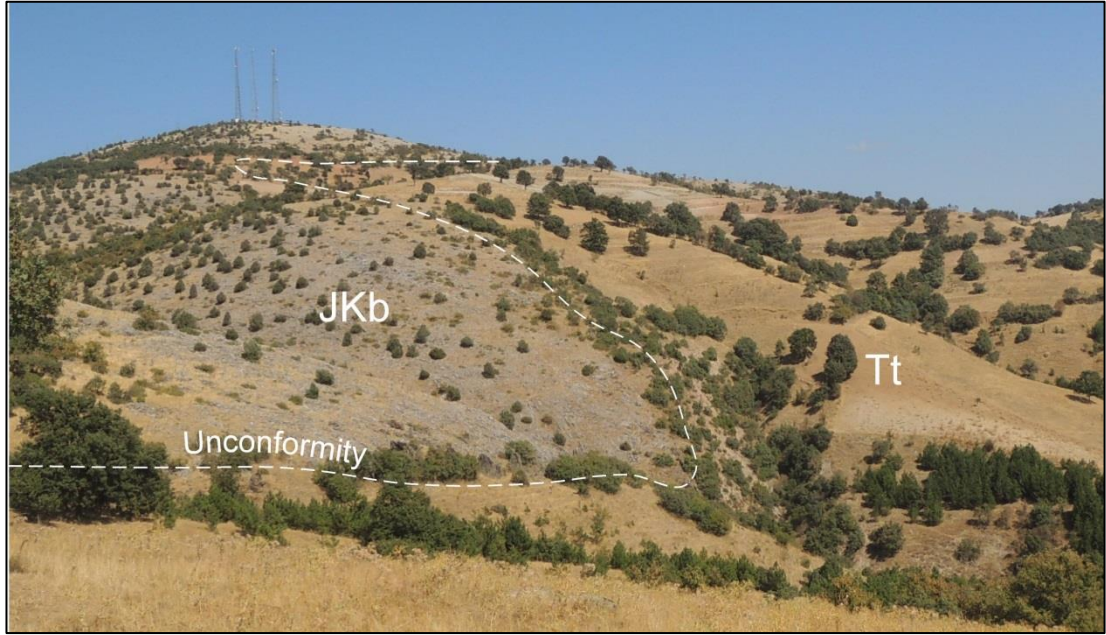


Figure 2-6: General view of the unconformity between Budağan Limestone (JKb) and Taşbaşı Formation (Tt) (near Sivrikır Hill between Koyunoba and Kabaşlar villages, view to north)

The Taşbaşı Formation shows lateral and vertical gradations with the Kızılbük Formation of Middle-Late Miocene age (Akdeniz and Konak, 1979). The total thickness of the Taşbaşı Formation in the study area is around 200 m. Based on the lithofacies and stratigraphical position, the Taşbaşı Formation can be correlated with the Kurtköyü Formation exposed in the Selendi graben (Ercan et al., 1978).

2.2.3 Kızılbük Formation

This unit was first named by Akdeniz and Konak (1979). It is composed of pale yellowish, brownish sandstone, mudstone, marl and clayey limestone alternation with tuff intercalations (Figure 2.7).

The Kızılbük formation is exposed in the northern tip of the Selendi graben in the study area (Figures A-1, A-3 in Appendix). Sandstones are brown, pale yellow, grey colored, thin bedded to thick-bedded, well sorted and graded. Sandstone grains are subrounded in shape, and include quartz, feldspar and mica minerals. It is calcite cemented and well-lithified. In addition, coal- and organic material- rich layers of



Figure 2-7: Close-up view of sandstone-siltstone-mudstone alternation of Kızılbük Formation (near south of Yeşilköy town)

several meters in thickness are also seen as intercalations in this formation near Karamanca in the eastern part of the study area. Marls are light green, light yellow, pale yellow and thick-bedded. Clayey limestones are grey, beige, greenish in color, and show alternation with marls. Tuff levels are lense-shaped, massive to thick-bedded and rhyolitic to dacitic in composition. The topmost part of the Kızılbük Formation consists of thick-bedded lacustrine limestone and shale alternation. Based on both the lithofacies and syn-sedimentary features, the Kızılbük Formation might have been deposited in a fluvio-lacustrine depositional setting. Sedimentary structures observed in the Kızılbük Formation are graded bedding, cross-trough bedding, lamination, ripple mark, flute mark, mudcracks, abandoned channels, growth faults and bioturbation. The Kızılbük Formation has both the lateral and vertical gradations with the the overlying Civanadağı Tuffs while it is cut across by the rhyolitic dykes and domes (Figure 2.8). The rhyolitic domes are observed in the northern side of Selendi graben (Figure A-1 in Appendix). The unit is light brown colored and has aphanitic texture. It is highly jointed and displays blocky texture. It cuts and deforms the surrounding rocks as anticlines and then overlies them as lava flows. Stratigraphic position and the composition of rhyolitic domes and tuffs are similar, therefore that are thought to have similar ages (Figure 2.1).



Figure 2-8: Close-up view of internal structure of highly jointed rhyolitic dome in Kızılbük Formation (quarry, along Simav-Karamanca road, 3km SW of Kalkan Village)

2.2.4 Civanadağı Tuffs

Civanadağı Tuffs were first named by Akdeniz and Konak (1979). They are exposed well along the Hamzaköy-Kabaşlar road and to the north-northwest of Efir village in the Akdere graben (Figure 2.9).

The Civanadağı Tuffs overly unconformably the Taşbaşı Formation at the bottom and has a lateral and vertical gradations with the Kızılbük Formation at the top. It is overlain conformly by the Middle Miocene Naşa basalts. The Civanadağı Tuffs are composed of agglomerate, tuff, tuffite, sandstone, siltstone, mudstone, marl and limestone alternation. Agglomerates are medium bedded to thick-bedded, deposited by lahar flows and pyroclastic basal flows. They pinch out into tuff layers towards east which implies to that its source is in western side. Pebbles in the agglomerate are angular to sub-angular rhyolite, rhyodacite, dacite, andesite, schist, gneiss, marble and ophiolitic fragments of all sizes up to 40 cm in diameters. Tuffs are white, beige, light grey, greenish grey colored, medium bedded to very thick-bedded and rhyolitic, dacitic to rhyodacitic in composition. Plagioclase, biotite, quartz, hornblende and other volcanic fragments are observed in the matrix. The Civanadağı tuffs grade into brown to yellow colored fluvio-lacustrine sequence towards the top of the unit. The Koyunoba granite has been exposed just before the deposition of the fluvial section

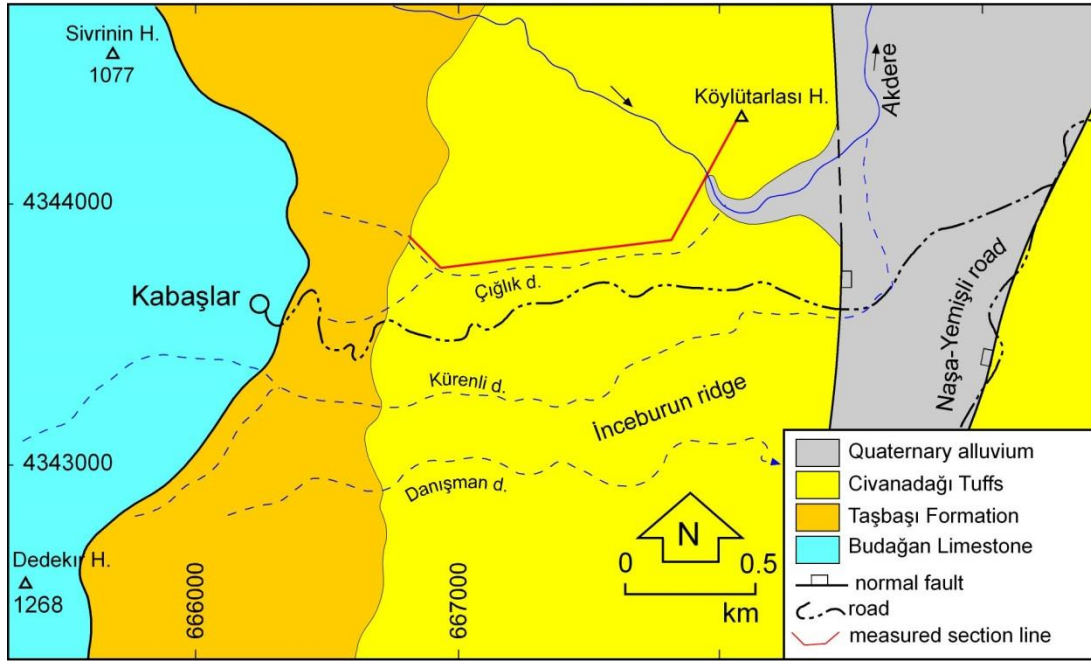


Figure 2-9: Geological map showing units exposed in the Akdere graben and line of measured section.

of the Civandağı Tuffs. Conglomerates and sandstones are light brown to light grey colored, medium to thick-bedded, polygenetic, graded and well sorted. Mudstones are light brown colored, thick-bedded to massive. The unit passes into marl and limestone at the topmost part of the unit in the upper parts (Figures 2.10, 2.11).



Figure 2-10: General view of Civandağı Tuffs (Büyüküney Hill, 2 km north of Naşa, view to NW)

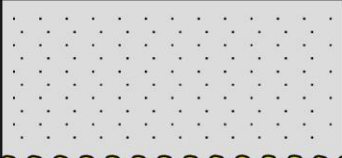

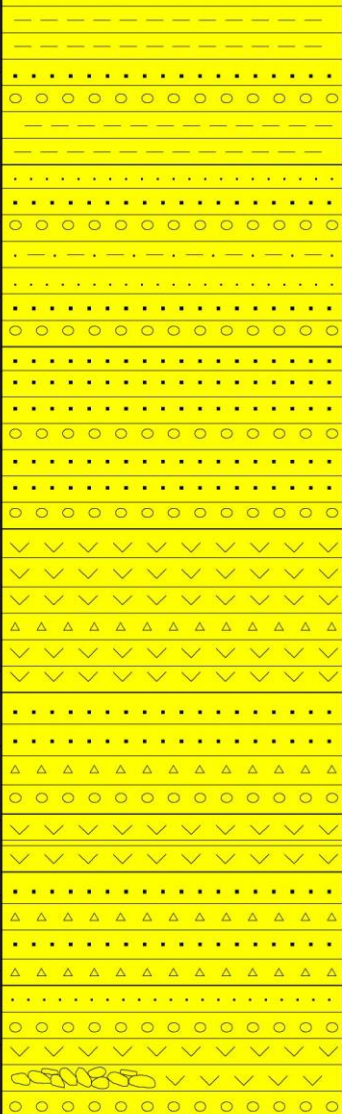
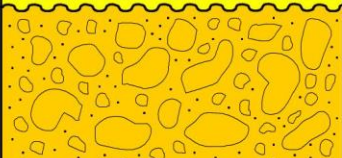
Age	Unit	Total Thickness	Thickness	Lithology	Description
Quaternary	Alluvium				recent sediments deposited along river valleys
Middle Miocene	Civanadağı Tufts	>152m	150		disconformity
			100		light brown thick bedded mudstone alternation with thin bedded polygenetic conglomerate and sandstone. conglomerates include angular tuff fragments and rounded granite fragments fluvial conglomerate, sandstone, siltstone alternation composed of angular volcanic fragments, semirounded metamorphic and granitic fragments, granite pebble is observed in the section for the first time alternation of polygenetic coarse sandstone and conglomerate. conglomerate is composed of large angular metamorphic blocks up to 10 cm in a white volcanic rich matrix. coarse sandstones include mostly angular fragments of volcanic rocks white to brownish white tuff with grains up to 2 cm alternating with volcanic breccia alternating with angular metamorphic blocks alternation of polygenetic light grey colored thin bedded conglomerate, lahar flow including angular fragments of metamorphic rocks up to 40 cm and well sorted coarse sandstone well lithified tuff composed of angular volcanic fragments in a white matrix alternating with thin silica layers alternation of polygenetic light gray to greenish gray coarse sandstone with angular fragments and volcanic breccia composed of volcanic fragments and angular metamorphic rock fragments polygenetic conglomerate, massive tuff, sandstone, agglomerate (lahar?) alternation. fining upward, well-lithified, grain supported. grain size is up to 40cm
Early Miocene	Taşbaşı Formation	~200m			angular unconformity reddish-brownish colored, loosely packed and weakly cemented massive boulder block conglomerates which are transported by high energy fluvial systems into alluvial fans

Figure 2-11: Measured section of Civanadağı tufts along the line on Figure 2.9

The Civanadağı Tuffs overly with an angular unconformity the Lower Miocene Taşbaşı Formation, while they are overlain conformably by the Middle Miocene Naşa Basalt (Ercan et al., 1996). Based on these contact relationships, the Civanadağı Tuffs must be Middle Miocene in age.

2.2.5 Naşa Basalt

Naşa basalt was first named by Akdeniz and Konak (1979). It exposes between Naşa, Karacaören and Eğirler villages along the northern margin of the Akdere graben. The Naşa Basalt overlies conformably the Civanadağı Tuffs while it displays a free erosional top surface.

Appearance of the Naşa Basalt is black-dark brown, porphyritic and vesicular in texture. Vesicles are sometimes filled with calcite. It is alkaline basalt with olivine and plagioclase phenocrysts (Figure 2.12). The total thickness of the Naşa Basalt is around 100 m and decreases towards the Simav graben based on the data obtained from the Eynal thermal facility well logs (Figure A-3 in Appendix).



Figure 2-12: Close-up view of the vesicular Naşa Basalt (north of Eynal thermal facility)

Akdeniz and Konak (1979) first reported that the Naşa Basalt has same age with Kula Basalt (1.1 Ma, Borsy et al., 1972) according to its stratigraphic position, and then they assigned a Quaternary age for the Naşa Basalt. However later on, Ercan et al. (1996) pointed out that the age of the Naşa Basalt is 15.2 Ma and 15.8 ± 0.3 Ma (Middle Miocene) based on the K/Ar radiometric dating of samples taken from it.

2.3 Neotectonic Units

2.3.1 Toklargölü Formation

This unit was first named by Akdeniz and Konak (1979). It is the modern graben fill deposited by the fluvial system under the control of the current tensional tectonic regime (neotectonic regime). The Quaternary Toklargölü Formation overlies with an angular unconformity whole of the Pre-Miocene rocks. The Toklargölü Formation exposes as the fault terraces along the margins (Figure 2.13), while it is buried beneath the recent alluvial sediments in the depocenters of both the Simav and Akdere grabens. Terrace deposits occur particularly on both sides of the Mustafa Kemalpaşa Çay, which drains the Akdere graben in N-S direction. Both the eastern and the western fault-bounded margins of the modern Akdere graben and the north to northeastern margin of the Simav graben are indicated by a series of uplifted (up to 30 m), dissected, discontinuous and fault-suspended fault terrace conglomerates (Figure 2. 13). They are the stratigraphically lowermost facies of the modern graben fill. Terrace conglomerates are composed of conglomerates and sandstone alternation with red to brown mudstone intercalations. Conglomerates are unsorted, polygenetic, weakly lithified to loose in nature. They consist of well-rounded augen gneiss, quartzite, quartz, various schists, marble, various ophiolitic rocks, granite, andesite, basalt, marl and lacustrine limestone clasts set in a sandy matrix. The Toklargölü Formation ranges between a few meters to 30 m in the field but it is observed up to 200 m in thickness on a geothermal well (Erişen et al., 1989). Age of the unit is Early Quaternary since it contains Late Pliocene limestone pebbles (Akdeniz and Konak, 1979).



Figure 2-13: General view of a fault terrace included in Toklargölü Formation which unconformably overlies Naşa Basalt (1 km NW of Eynal thermal facility, view to NE)

2.3.2 Alluvial Deposits

These are the coarse-grained marginal and the finer-grained depocentral facies of Late Quaternary age. Marginal deposits are represented by both the fan and fan-apron facies surrounding fault-bounded margins of both the Akdere and Simav modern grabens. In general, fan deposits occur at the mouths of transverse drainage system flowing from the peaks of the fault bounded-graben margins into the grabens. However, the fan-apron deposits form a blanket surrounding the graben margins. They are produced by the coalescence of both the talus cones to slope scree deposits with the alluvial fans deposits. Both the fan and fan-apron deposits are composed of unconsolidated, unsorted to polygenetic boulder to blocks up to 1-2 m in diameters. They have been transported and deposited into fans. Both the fan and fan-apron deposits grade into finer grained depocentral deposits made up of red-brown mudstone deposited in flood plain and the organic material-rich silt, clay and mud alternation accumulated in swamp and stream beds. They range from tens of meters up to 150 m in total thickness based on the data obtained from exploration wells (Erişen et al., 1989).

CHAPTER 3

STRUCTURAL GEOLOGY

This chapter deals with the description and tectonic meaning of the geological structures such as beds, unconformities, folds and faults observed in the study area and their kinematic analysis. According to tectonic periods during which these structures formed, they can be classified into two categories: (a) Paleotectonic structures, and (b) Neotectonic structures.

Since the aim of this study is to contribute to the neotectonic evolution of the Simav graben, and there are some ideas arguing that the neotectonic regime started during Miocene, the units deposited during Miocene and later will be analyzed. The data to be analyzed were obtained in terms of the field geological mapping at 1/25000 scale in the study area. Dip and strike measurements of beds were analyzed on stereonet to describe the geometrical characteristic of folds. Slip plane data including dip, strike, rake and sense of motion were analyzed by using a computer software programme entitled “Tector” and its sub-programs “Tensor”, “Diagra” and “Mesure” (Angelier, 1989).

3.1 Beds

Based on both the tectonic regime and the deformation pattern, the units deposited in study area can be divided into two groups: (a) Akdere and Selendi paleotectonic graben fill and (b) Neotectonic Simav graben fill. The paleotectonic graben fill is deformed (steeply-tilted to folded), while the neotectonic graben fill is nearly flat-lying (undeformed). The Akdere and Selendi graben infill are composed of Lower Miocene Taşbaşı Formation, Lower-Middle Miocene Kızılbük Formation and

Middle Miocene Civanadağı Tuffs. Taşbaşı Formation is characterized by loosely packaged, weakly cemented and polygenetic boulder block conglomerates deposited in alluvial fans by the high-energy fluvial systems. It is exposed well on the western side of the Akdere graben. The bedding planes cannot be observed in the Taşbaşı Formation.

The Kızılbük Formation is characterized by sandstone, mudstone, marl and clayey limestone alternation with tuff intercalations. It is observed in the north of Selendi graben. Thicknesses of the beds vary from centimeter to meters. It is intensely folded unit. The predominant dip amount is about 30° for the Kızılbük Formation.

The Civanadağı Tuffs are characterized by volcano-sedimentary sequence of agglomerate, tuff and sandstone passing into the fluvio-lacustrine sequence of conglomerate, sandstone, marl and limestone alternation. It is observed well in the Akdere graben. Its bed thickness changes between centimeters to several meters. The unit has been deformed into a series of anticlines and synclines with the axes running parallel to the general trend of the graben margins. Beds dip up to 38° while their predominant dip amount is about 20°.

3.2 Unconformities

Based on both the age and the type of the rock units below and above the erosional surface, the unconformities observed in the study area can be classified into three categories. These are, from oldest to youngest, the nonconformity, an angular unconformity-nonconformity and the angular unconformity. The nonconformity, which is the oldest erosional surface in the study area, is observed between the underlying pre-Lower Miocene units (Simav Metamorphics, Budağan Limestone, Dağardı Mélange) and the overlying Lower Miocene Taşbaşı and the Lower-Middle Miocene Kızılbük Formations (Figure A-1 in Appendix, Figure 2.6, A-B and E-F geological cross-sections in Figures A-2, A-3 in Appendix respectively). This is the oldest erosional gap in the study area. The second erosional gap is in the type of partly nonconformity and partly angular unconformity. It is observed among the bottom of Middle Miocene Civanadağı Tuffs, the Naşa Basalt, older basement rocks

and the Early Miocene Taşbaşı Formation. Earlier two rock units overly with an angular unconformity both the Early Miocene Taşbaşı Formation and the Pre-Miocene basement rocks such as the Simav Metamorphics (Figure A-1 in Appendix and geological cross-sections A-B- and G-H in Figures A-2, A-3 in Appendix respectively). The third and youngest erosional gap observed in the study area lies between the bottom of the Quaternary neotectonic fill (Toklargölü Formation and alluvial sediments) and the underlying Pre-Quaternary rock units such as the metamorphic rocks and the non-metamorphic but highly deformed (folded) Miocene units (Taşbaşı and Kızılbük Formations, the Civanadağı Tuffs and the Naşa Basalt) (Figure 13, Figure A-1 in Appendix and the G-H geological cross-section in Figure A-3 in Appendix).

3.3 Folds

In general, folds are observed in the Early-Middle Miocene rocks, especially Kızılbük Formation in north of Selendi graben (Figure A-1 in Appendix). Drainage pattern is parallel to dendritic in style and is dominantly oriented in N-S direction. Therefore dip and strike measurements are collected along N-S traces along valleys where outcrops are observed well. Along these valleys, there are numerous parallel and sub-parallel folds which generally trend in WNW-ESE direction (Figure A-1 in Appendix) and plunge towards WNW. Folds are asymmetric and moderately to steeply plunging in type (Figure A-1 in Appendix, Figure 3.1). Dip and strike measurements are plotted on a stereonet to illustrate general trend and geometry of folds in the Kızılbük Formation (Figure 3.1). Although the folds are relatively small and have high frequency, their mean orientation shows a general trend of N79°W/88°NE axial plane and 27°/282°N fold axis. Mean fold envelope is open and symmetric. Dip amounts vary between 10° and 55° in the Kızılbük Formation. Folds observed in Akdere graben trends in N-S direction. Unlike the folds in Selendi graben, Folds in Akdere graben are gentle. Mean orientation of the hinge plane is N02°W/85NE and fold axis is 02°/357°N. They are parallel to the graben margins so that they are considered to be formed under the control of the margins (Figure 3.2). Although the ages of the folded units

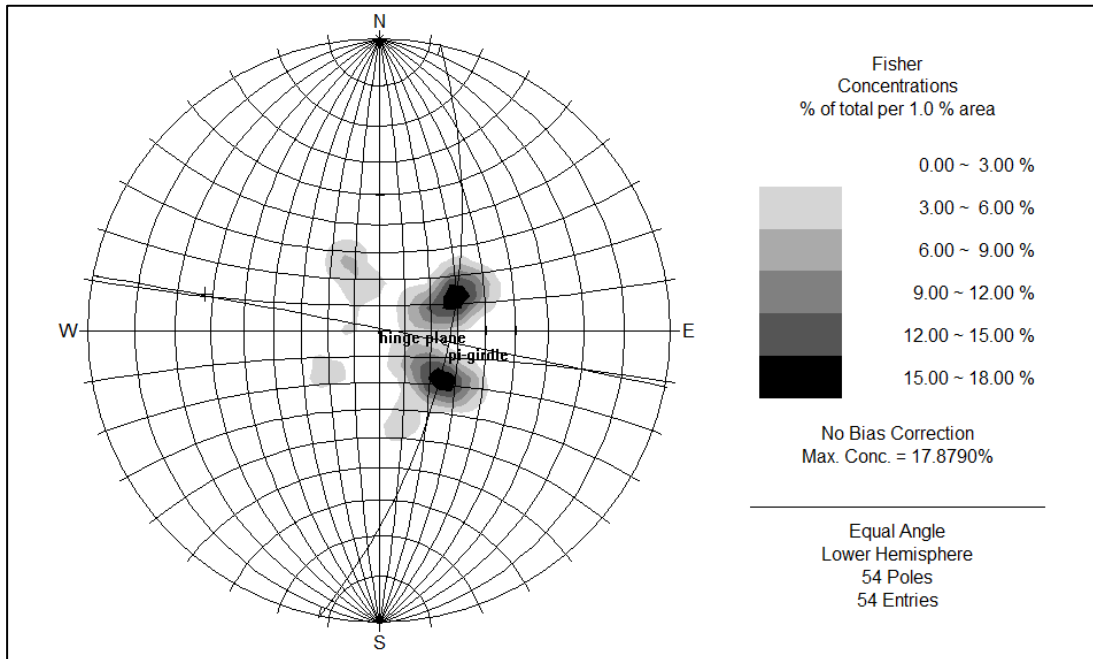


Figure 3-1: Contour diagram of poles to bedding planes collected in Kızılbük Formation on equal angle lower hemisphere stereonet.

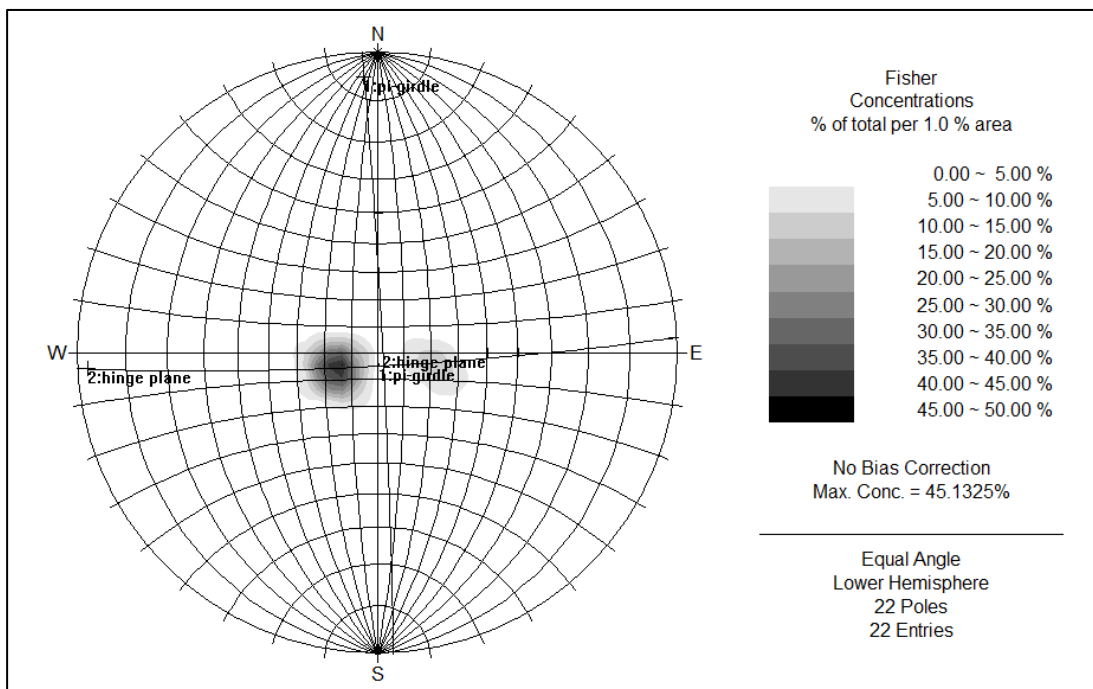


Figure 3-2: Contour diagram of poles to bedding planes collected in Civanadağı tuffs on equal angle lower hemisphere stereonet.

are similar, fold orientations are different, this could be resulted from either different age of folding or different folding mechanism for folds observed Akdere and Selendi grabens. However modern (neotectonic) graben fill is not deformed. This shows that only the Early-Middle Miocene units were deformed into a series of anticlines and synclines before the deposition of the modern graben infill.

3.4 Faults

3.4.1 Simav Fault Zone

Simav Fault Zone is an about 5 km wide, 80 km long WNW-ESE trending active zone of deformation which determines and controls southern margin of the modern Simav graben. It is located between Sındırgı Town in the northwest and Banaz Town in the southeast (Figure 1.1). Most of the Simav Fault Zone is outside the study area. It comprises a series of closely spaced, parallel to sub-parallel high-angle normal faults with minor amount of strike slip components. Lengths of the fault segments vary from 2 km to 10 km (Figure A-1 in Appendix). These fault segments cut, displace and juxtapose various rocks of dissimilar age and type such as the Paleozoic Simav Metamorphics, the Middle Miocene Kızılbük Formation with the Quaternary neotectonic fill. Minimum total vertical offset of the faults included in the Simav graben are approximately 800m (Figure A-2 in Appendix). Fault segments mapped in the study area dip towards the depocenter of the Simav graben and display step-like morphology (Figure 3.3; Figures A-1, A-2, A-3 in Appendix).

The most common morphotectonic to fault plane-related criteria observed and used for the recognition of faults are the steeply sloping fault scarps, sudden break in the slope amount, step-like morphology, linear alignment of hot and cold water springs, deeply incised valleys, hanging valleys, deflected and offset streams, uplifted and suspended terrace conglomerates, triangular facets, degraded alluvial fans, tectonic juxtaposition of modern graben fill with different older rock units, extensional veins, crushed to sheared strips of rocks and the slickensides. Faults comprising the Simav Fault Zone are, from west to east, the Öreyler, Beyce, Simav, Mamak, Nadarçamı,

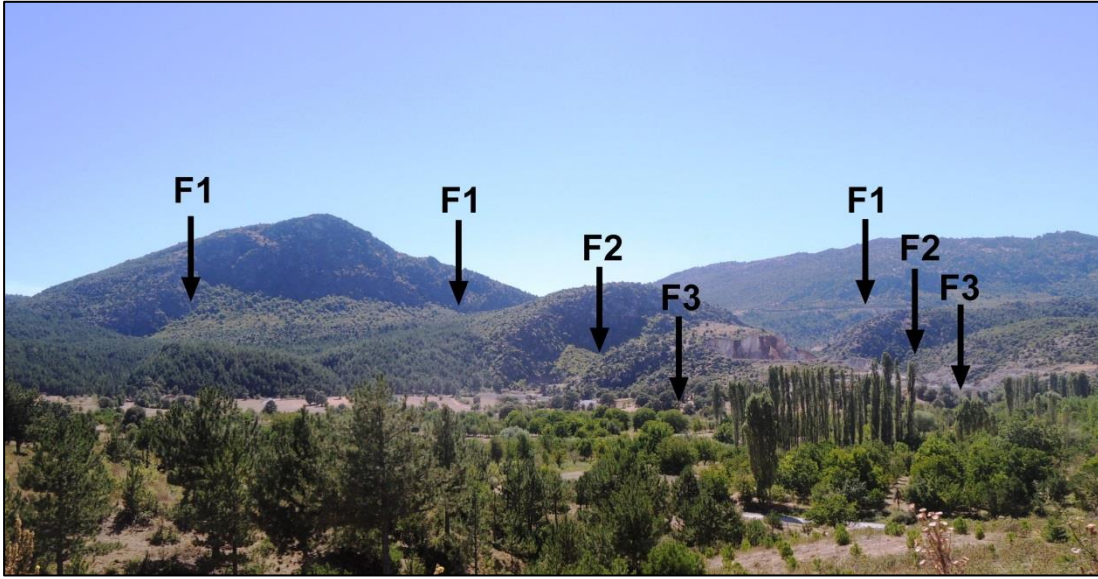


Figure 3-3: Step like morphology resulted from the basinward dipping parallel faults comprising the Simav Fault Zone. F1.Seyirkaya fault, F2. Küçüktaştepe fault, F3. Nadarçami fault (view to SW).

Küçüktaştepe, Seyirkaya and the Kocakırtepe faults These faults are described separately in more detail below.

3.4.1.1 Öreyler fault

It is a 6 km long and nearly WNW-ESE trending normal fault which dips around 60°-65° N-NE. It starts from near southwest of Öreyler Town which is outside of the study area and continues eastwards up to the near southeast of Demirci Town (Figure A-1 in Appendix). The Öreyler fault cuts and displaces in vertical direction the Pre-Miocene basement rocks and the overlying pre-modern (neotectonic) graben fill. It juxtaposes the modern graben fill with the Pre-Miocene basement rocks. Sudden break in the slope, deeply incised valleys, deflected streams, almost perfectly linear alignment of numerous water springs are common morphotectonic criteria observed along the Öreyler fault. Öreyler fault also controls deposition of the Late Quaternary alluvial fans composed of all-sized fragments derived from the basement rocks. However, a slickenside couldn't be observed along the Öreyler fault. A geological cross-section passing through the Öreyler fault is drawn by using geological observations and geothermal well data (Figure A-1 in Appendix). If the elevation of

the Simav Metamorphics in the graben and the margin are used as piercing points, total vertical offset along the Öreyler fault and possible undifferentiated synthetic faults are about 700 m (C-D geological cross-section in Figure A-2 in Appendix).

3.4.1.2 Beyce fault

It is a 2 km long, approximately WNW-ESE trending and northerly steeply dipping normal fault. It starts from south of the Pazar district of the Demirci Town and continues up to the Hürriyet district of Beyce village (Figure A-1 in Appendix). It forms the tectonic contact between recent alluvial fans and the Pre-Miocene basement rocks such as the Simav Metamorphics. Sudden break in the steep slope of the basement rocks, incised to hanging valleys and the disappearance of intermittent streams are diagnostic morphotectonic features used to recognize the Beyce fault.

3.4.1.3 Simav fault

It is a 7 km long, nearly WNW-ESE trending and steeply north-dipping normal fault. The Simav fault starts from south of Beyce village, runs through Simav County and then ends in Kartal Hill located in the eastern of Simav Town (Figure A-1 in Appendix). The Simav fault cuts and displaces the Simav Metamorphics and tectonically juxtaposes them with the modern graben fill. Sudden break in the slope amount, development of alluvial fan system, highly deformed and crushed to sheared rocks are the morphotectonic indicators of the Simav fault. The source of the 17 February 2009 earthquake occurred in the Simav region (See Figure 4.3, Table 4.1 in Chapter IV) is attributed to the faults bounding the northern margin of the Simav graben. Whereas, the epicenter location, earthquake focal mechanism solution and the site focus depth strongly reveal that the Simav fault is the most reasonable candidate for the source of this earthquake. In addition, the epicenter of the mainshock falls in a somewhere further north of the northern margin of the Simav graben. If the northern margin-boundary faults were the sources, the epicenter site would be in the south side of the faults, whereas the northern margin-boundary faults dip southward. On the other hand, the Simav fault fits well with both the site of epicenter and the depth of focus of the 17 February 2009 Simav earthquake.

Consequently, the Simav fault is the source of the 17 February 2009 earthquake and is active as indicated by both the seismological and field data.

3.4.1.4 Hisarardı fault

It is an approximately 2.5 km long, north-easterly steeply dipping normal fault with small amount of strike slip component. The Hisarardı fault starts from Karşiyaka district in the southeast of Simav County, and then continues up to the near south-southwest of Simav County along the southern margin of the Simav graben, lastly joins with the Simav master fault near south of the Çavdır district (Figure A-1 in Appendix). Hisarardı fault cuts and displaces the Pre-Miocene rocks in vertical direction and forms the tectonic contact between the Quaternary modern graben fill and the Simav Metamorphics. Sudden break in the slope amount, steep fault scarp and crushed-sheared strips of rocks are common morphotectonic criteria observed along this fault. Hisarardı fault also displays well-developed and preserved slickenside (Figure 3.4).

Slip plane data analysis of the Hisarardı fault slickenside data by using the Angelier's direct inversion method (Angelier, 1994) indicates the NNE-SSW extension and normal faulting in the Simav region (Figure 3.5). Also relative magnitudes of σ_1 and σ_3 are higher than σ_2 which reveals that this fault is being governed by the combination of both the gravitational force and the regional tensional force.

3.4.1.5 Mamak fault

It is a 3 km long, WNW-ESE trending and northerly dipping normal fault. It cuts and displaces the Middle Miocene Kızılbük Formation and the basement rocks, and tectonically juxtaposes them with to each other (Figure A-1 in Appendix).

3.4.1.6 Nadarçanı fault

It is an 8 km long, WNW-ESE trending normal fault dipping towards north-northeast. The Nadarçanı fault starts from 1 km west of the Nadarçanı recreation area and continues up to the Gelincikkayası Hill (Figure A-1 in Appendix). The



Figure 3-4: Close-up view of the slickenside developed on the Hisarardı fault (S-4 in Figure A-1 in Appendix, 670238E-4328471N).

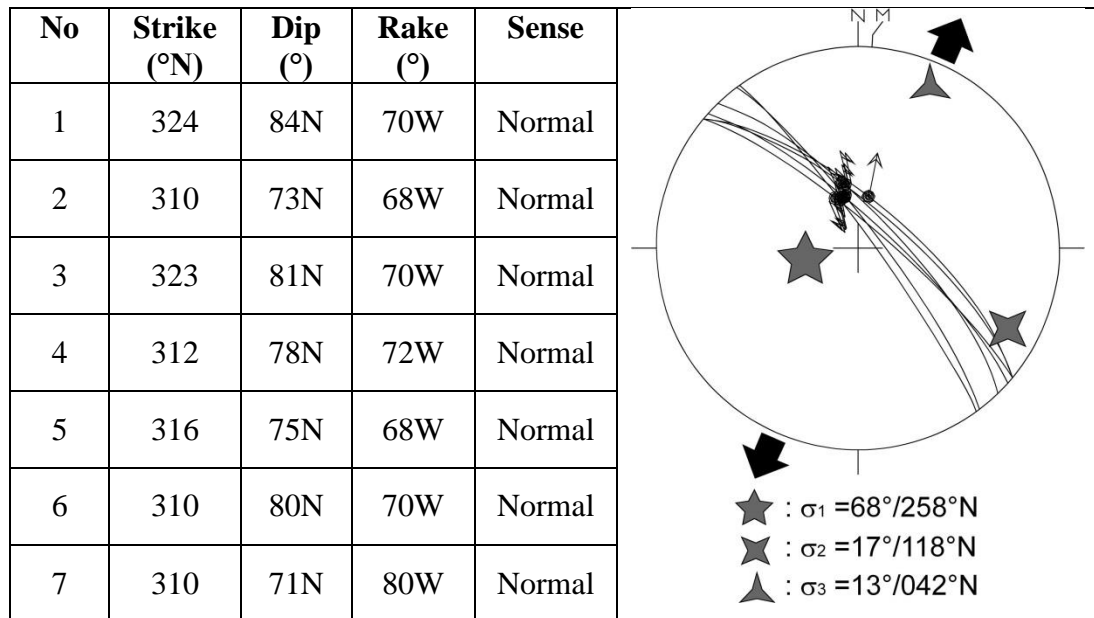


Figure 3-5: Slip plane data taken from Hisarardı fault (S-4 in Figure A-1 in Appendix) and kinematic solution using Angelier's direct inversion method on Schmidt's lower hemisphere. (black arrows show local extension direction)

Nadarçamı fault cuts and displaces in vertical direction the Simav Metamorphics. Sudden break in the slope amount, steeply sloping fault scarp to triangular facets are diagnostic morphotectonic indications of the Nadarçamı fault (Figure 3.6).



Figure 3-6: General view of the Nadarçamı fault scarp, trace (F-F) and the sudden break in the slope amount along the Nadarçamı fault (near Nadarçamı Recreation Area, view to East)

In the western section, steep scarp disappears and the fault becomes morphologically invisible. However, in the eastern part of the Nadarçamı fault both the displacement along the fault and its morphotectonic reflection increase and fault becomes quite clear, i.e., a relay ramp geometry forms between the Hisarardı and Nadarçamı faults. In general, relay ramps occur between two parallel faults which dip in the same direction and resulted from the transfer of displacement between synthetic faults (Morley et al., 1990). It is illustrated in Figure 3.7.

Relay ramps occur when two synthetic normal faults are overstepped. During progressive deformation along the faults, a relay ramp starts to form. In the same way the transfer faults form along the upper and lower ramps to accommodate the deformation in the relay ramp. The dips of the faults control the type of deformation along the relay ramp. If the faults are steeply dipping, transfer faults are normal, if

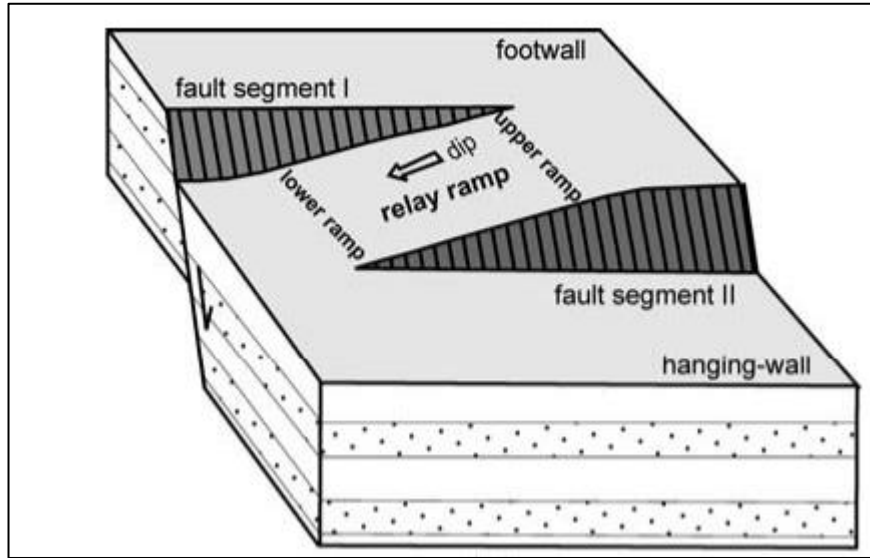


Figure 3-7: A sketch block diagram illustrating a relay ramp resulted from the transfer of movement along two overstepping normal fault segments dipping in the same direction. (Ferrill & Morris, 2001).

the dips of the faults are gentle, strike slip component of transfer faults increases. In the case of steeply dipping Nadarçamı and Hisarardı faults, transfer fault should be normal. However, transfer fault is not observed in the region (Figure A-1 in Appendix).

3.4.1.7 Küçüktaştepe fault

It is a 3 km long normal fault which dips steeply towards north. This fault is exposed well around Küçüktaştepe Hill located 3 km south of Yeşilköy. This fault cuts and displaces vertically both the Kızılbük Formation and older units, and tectonically juxtaposes the Simav Metamorphics with the Quaternary alluvial sediments. The vertical offset (throw amount) along the Küçüktaştepe fault is about 150 m based on the faulted bottom contacts of the Kızılbük Formation on both blocks of the Küçüktaştepe fault (C-D geological cross-section in Figure A-1 in Appendix). Sudden break in the steep slope amount of the fault scarp is a diagnostic morphotectonic reflection for the Küçüktaştepe fault (Figures 3.3 and 3.8).



Figure 3-8: General view of steeply sloping fault scarp of the Küçüktaštepe fault (near north of Küçüktaštepe Hill, view to southwest)

3.4.1.8 *Seyirkaya fault*

It is an 8 km long normal fault. It trends in WNW direction and dips at 70°-75° towards north-northeast. The Seyirkaya fault starts from Çapkın Hill in the northwest, runs towards southeast along Seyirkayası Hill and then ends in the area 1 km east of Kibletas Hill (Figure A-1 in Appendix). The Seyirkaya fault is the southernmost fault included in the step-like morphology shaping the southern margin of the Simav graben (Figure 3.3). This fault cuts and displaces in vertical direction the Simav Metamorphics, the Budağan Limestone, the Kızılbük Formation and tectonically juxtaposes them with to each other. The deflected drainage pattern, steeply sloping fault scarp, deeply incised valleys, waterfalls, extensional veins and backtilting of rock units are common morphotectonic criteria observed and used to recognize the Seyirkaya fault. The total throw amount accumulated on the Seyirkaya

fault is about 250 m (Figure 3.9) based on the comparison of the bottom contacts of the Kızılbük Formation on both blocks of the fault (E-F geological cross-section in Figure A-3 in Appendix).

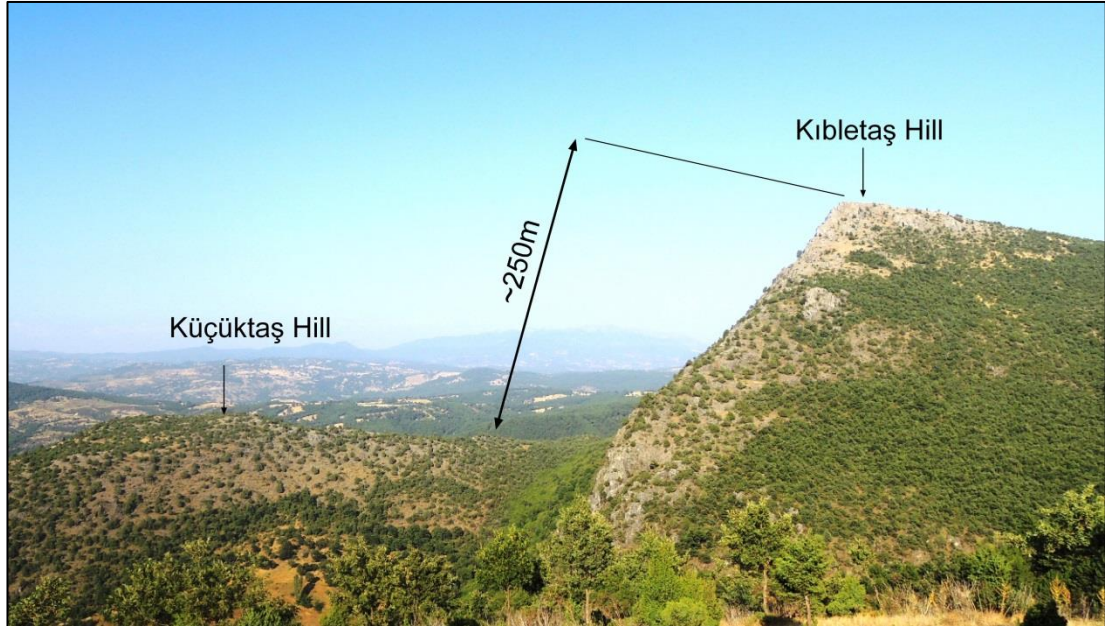


Figure 3-9: General view of the step-like morphology, the back-tilting and the total throw amount of 250 m formed along the Seyirkaya fault (view to east)

Seyirkaya fault also displays well-developed and preserved slickenlines (Figure 3.10). The stereographic plots of slip-plane data on the Schmidt's lower hemisphere net indicate that the Seyirkaya fault is an oblique-slip normal fault with minor amount of dextral strike-slip component (Figure 3.11).

The slip-plane data analysis also reveals that relative magnitudes of the σ_1 is higher than σ_2 and σ_3 which indicate that this fault is being governed mainly by the gravitational force. The epicenter of the 19 May 2011 Simav earthquake of $M_w = 5.7$ is located near Söğüt settlement. The seismic data recorded by several stations indicate that the source of this earthquake is a normal fault, focus depth is 24.4 km and its epicenter is located in a somewhere further north of the northern margin of the Simav graben (Figure 4.3, Table 4.1 in Chapter IV). According to catalogue data,

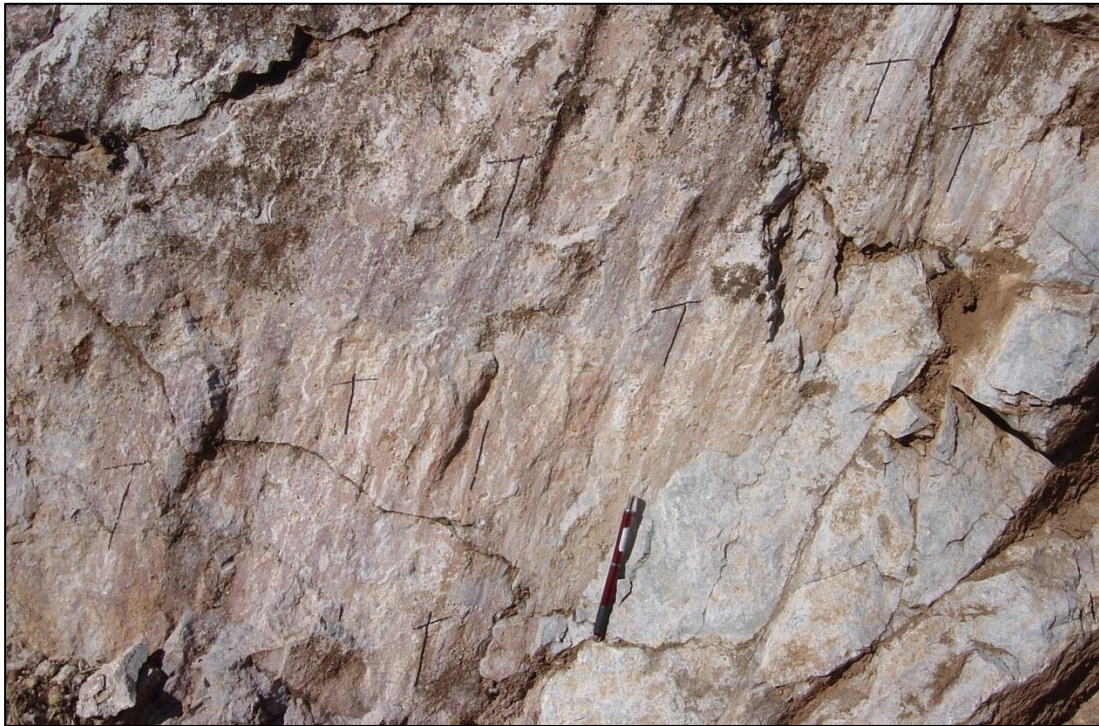


Figure 3-10: Close-up view of the Seyirkaya fault slickenside (S-6 in Figure A-1 in Appendix).

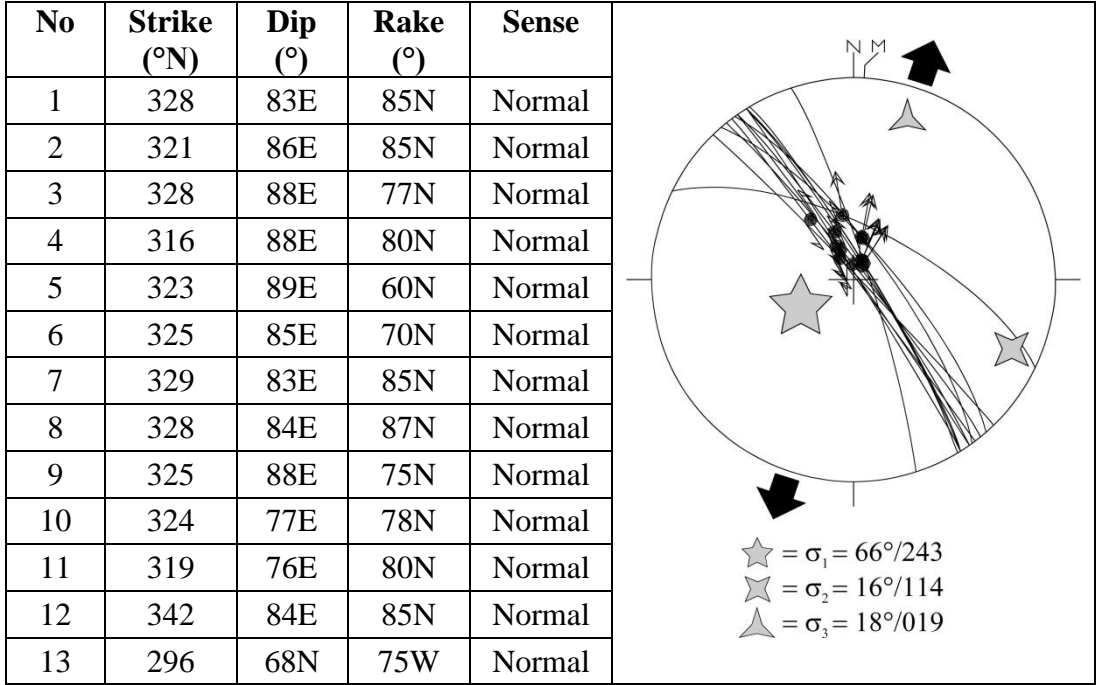


Figure 3-11 Slip plane data taken from Seyirkaya fault (S-6 in Figure A-1 in Appendix) and kinematic solution using Angelier's direct inversion method on Schmidt's lower hemisphere. (black arrows show local extension direction)

one of both the Seyirkaya and the Nadarçanı faults is the most reasonable candidate for the source of the 19 May 2011 Simav earthquake. Therefore those faults are active based on both the seismic and field data. Focal mechanism solution data of this earthquake also reveal a normal fault dipping at 40° at the focus of 24.4 km depth. In contrast, dip amount of the fault measured at the surface is about 70° - 75° degrees. These values indicate that the source fault of the 19 May 2011 Simav earthquake is listric in geometry. This is also supported by the back-tilting of blocks along the source fault (Figure 3.9).

3.4.1.9 Kocakırtepe fault

It is a 4.5 km long and WNW-trending normal fault dipping towards southwest. It starts from 1 km north of Yeşilköy settlement, runs for about 4.5 km distance and then disappears near Gözet Hill (Figure A-1 in Appendix). The Kocakırtepe fault cuts and displaces in vertical direction both the Miocene Kızılbük Formation and older rock units and then tectonically juxtaposes them. Fault-parallel alignment of springs and drainage system, back-tilting of the Selendi graben fill and the highly deformed, crushed to sheared rock units are the common morphotectonic criteria observed and used for the recognition of the Kocakırtepe fault. Slip plane data couldn't be obtained from the Kocakırtepe fault.

3.4.2 Naşa Fault Zone

The Naşa Fault Zone is an approximately 1 km wide 15 km long , in general NNW-trending zone of deformation characterized by normal faulting. The Naşa Fault Zone determines and controls both the north and northeast margin of the Simav graben (Figure A-1 in Appendix). It consists of a series of closely-spaced fault segments of dissimilar trends and length. Some of the segments are different in orientation, however they are included in Naşa fault zone. Lengths of the fault segments vary from 2 to 7 km. These fault segments are, from north-northwest to south-southeast, the Güneyköy, Balıklar, Karaçayırbaşı, Bayram, Naşa, Hüsüm, Eynal, Muradınlar, and Kalkan faults respectively. They cut and displace different rock units and tectonically juxtapose them with the modern graben fill.

3.4.2.1 Güneyköy fault

It is a 7 km long, WNW-trending and southwesterly dipping normal fault. It starts from Örenli Town in the northwest and continues towards southeast up to the Naşa fault and then terminates. It determines and controls the northern margin of the Simav graben. Older basement rocks such as the Simav Metamorphics, the N-S-trending Akdere graben and its older graben fills (the Taşbaşı Formation, the Civanadağı Tuffs) are cut, displaced in vertical direction and then tectonically juxtaposed with the Quaternary modern graben fill by the Güneyköy fault (Figure A-1 in Appendix). Sudden break in the slope and deeply incised narrow valleys are observed along the Güneyköy fault as morphotectonic criteria (Figure 3.12).



Figure 3-12: General view of the Güneyköy fault scarp and trace (F-F) (view to north).

Slickenside couldn't be observed along the Güneyköy fault. However a well-developed outcrop-scaled synthetic normal fault and its brecciated surface with the attitude of N28°W/60°SW (Figure 3.13) reveal that the nature of the Güneyköy fault is also normal.

3.4.2.2 Balıklar fault

It is an 1.5 km long and WNW-trending normal fault dipping towards north. It starts from 1 km northwest of Güneyköy Village and continues eastwards up to Balıklar Hill. The Balıklar fault is also a synthetic structure to the Güneyköy fault. It cuts and displaces in vertical direction both the Akdere graben and its paleotectonic fill,



Figure 3-13: Close up view of the mesoscopic synthetic fault of the Güneyköy fault (S-1 in Figure A-1 in Appendix)

and juxtaposes tectonically this older fill with the Quaternary modern fill of the Simav graben (Figure A-1 in Appendix). The sudden break in slope amount and alluvial fans accumulated at the foot of basinward-facing steep fault scarp are common morphotectonic criteria observed and used to recognize the Balıklar fault (3.14).



Figure 3-14 General view of the Balıklar fault scarp and trace (F-F) (view to north)

3.4.2.3 *Karaçayırbaşı fault*

It is a 3 km long, NW-trending and southwest dipping normal fault. It starts from Karaçayırbaşı Hill located 1 km southwest of Naşa town and continues towards Northwest until it joins with the margin-boundary faults of the N-S-trending Akdere graben (Figure A-1 in Appendix). The Karaçayırbaşı fault cuts and displaces vertically both the Naşa Basalt and the Civandağı Tuffs exposed along the northeastern margin of the Simav graben. It also juxtaposes tectonically the Lower Quaternary Toklargölü Formation (modern grabenfill) with the Middle Miocene Naşa Basalt and Civandağı Tuffs. Sudden break in the slope amount, crushed and deformed basalts and the deeply incised and suspended narrow valley are common morphotectonic criteria observed along the Karaçayırbaşı fault.

3.4.2.4 *Naşa fault*

It is a 5 km long, NNW-trending and southwesterly dipping normal fault. It starts from the Hüsüm district in the southeast and continues in northwest direction up to 3 km north-northwest of Naşa town and then terminates (Figure A-1 in Appendix). The Naşa fault cuts and displaces vertically the Toklargölü Formation and the Naşa Basalt and tectonically juxtaposes them with the Upper Quaternary Alluvial sediments. Sudden break in the slope amount, a linear trace and crushed rocks and the hot waters coming out of the earth's surface on the hanging block of the Naşa fault are the characteristic morphotectonic criteria observed along the Naşa fault. In addition, based on the field and borehole data, the total throw amount accumulated along the Karaçayırbaşı, Naşa and the buried fault in the Simav graben is about 750 m (C-D geological cross-section in Figure A-2 in Appendix).

3.4.2.5 *Bayram fault*

It is a 2.5 km long and ENE- trending normal fault dipping towards southeast. It starts from Naşa town and continues along a stream valley in ENE direction and then terminates (Figure A-1 in Appendix) The Bayram fault cuts and displaces vertically the Naşa Basalt and the underlying Civandağı tuff.



Figure 3-15: General view of Naşa fault scarp (F-F) (view from 1.5 km northwest of Hüsüm District, view to northeast)

3.4.2.6 *Hüsüm fault*

is a 5 km long, approximately E-W-trending and southerly dipping normal fault. It starts from the Hüsüm district and continues towards east until 1 km south of Kapıkaya Village, where it joins with the Eynal fault (Figure A-1 in Appendix). The Hüsüm fault cuts and displaces vertically the Naşa Basalt, the underlying Simav Metamorphics and the Lower Quaternary Toklargölü Formation and juxtaposes tectonically them with to each other. Suspended fault terraces (Figure 3.16), crushed and sheared rocks and step-like land shape are the common morphotectonic criteria observed and used to recognize the Hüsüm fault.

The throw amount accumulated along the Hüsüm fault is about 50 m based on the comparison of the bottom contacts of the Toklargölü Formation on both blocks of the fault (G-H- geological cross-section in Figure A-3 in Appendix). Vertical



Figure 3-16: General view of the suspended fault terrace along the Hüsüm fault (view to north).

displacement along Hüsüm fault is proven by geothermal wells opened by MTA (Figure A-3 in Appendix).

3.4.2.7 *Eynal fault*

It is a 5 km long, E-W trending and southerly dipping normal fault. It starts from the Hüsüm district and continues eastwards up to 2 km distance to the Kapıkaya Village across the Eynal Thermal facility (Figure A-1 in Appendix). The Eynal fault cuts and displaces vertically the Lower Quaternary Toklargölü Formation and the underlying older rocks and juxtaposes them with the Upper Quaternary alluvial sediments. Sudden break in the slope amount, deeply incised narrow valley with steep slopes, linear and fault-parallel drainage pattern and the occurrence of an artesian geothermal wells are some diagnostic morphotectonic criteria for recognition of the Eynal fault. Based on the field geological and the borehole data, the total throw amount accumulated on the Eynal fault is about 70 m (G-H-geological cross-section in Figure A-3 in Appendix). Both the field and seismic data reveal that the Eynal fault is an active normal fault. This is proved by fault-parallel alignment of some aftershocks occurred after the 19 May 2011 Simav earthquake, during which the Eynal Thermal Hotel was damaged and collapsed.

3.4.2.8 Muradınlar fault

It is a 2.5 km long and NW-trending normal fault dipping towards southwest. It cuts and vertically displaces vertically both the Early Quaternary Toklargölü Formation and the underlying Simav Metamorphics. It also juxtaposes them with the Upper Quaternary alluvial sediments in the Simav graben. The basinward-facing step-like fault scarp, crushed and sheared rocks, suspended fault terrace conglomerates and the triangular facets are most common morphotectonic criteria observed and used to recognize the Muradınlar fault.

3.4.3 Akdere Fault Zone

Indeed the Akdere graben is a superimposed basin dominated by two graben fills such as the pre-Quaternary older fill and the Quaternary modern or neotectonic fill. Older fill is deformed (folded) and separated from the overlying undeformed neotectonic (modern) fill by an angular unconformity. The Akdere fault zone forms the faulted-boundary between the older and uplifted older fill and the nearly flat-lying modern fill exposing intervening narrow and linear depocenter of the graben (Figure A-1 in Appendix). The Akdere fault zone a 2.5 km wide, 30 km long and N-S-trending normal fault zone running along the central section of the N-S-trending Akdere graben. It begins from the 2 km north-northwest of Naşa Town and then continues northwards along both sides of the Akdere Stream, which drains the graben, until the Köleler district in the further north and outside the study area. Only southern 6 km long part of the Akdere fault zone is included in the study area (Figure A-1 in Appendix). The mapped part of the Akdere fault zone consists of two faults. These are the Akdere fault and the Hamzabey fault.

3.4.3.1 Akdere fault

It is a 7 km long, N-S trending and westerly dipping normal fault. It controls eastern margin of the Akdere neotectonic graben. Akdere fault cuts and displaces the Civanadağı Tuffs and tectonically juxtaposes them with the Quaternary alluvial sediments. Sharp fault scarp, crushed and sheared rocks, synthetic mesoscopic faults

(Figure 3.17), sudden break in slope amount and triangular facets are common morphotectonic criteria observed along the Akdere fault.

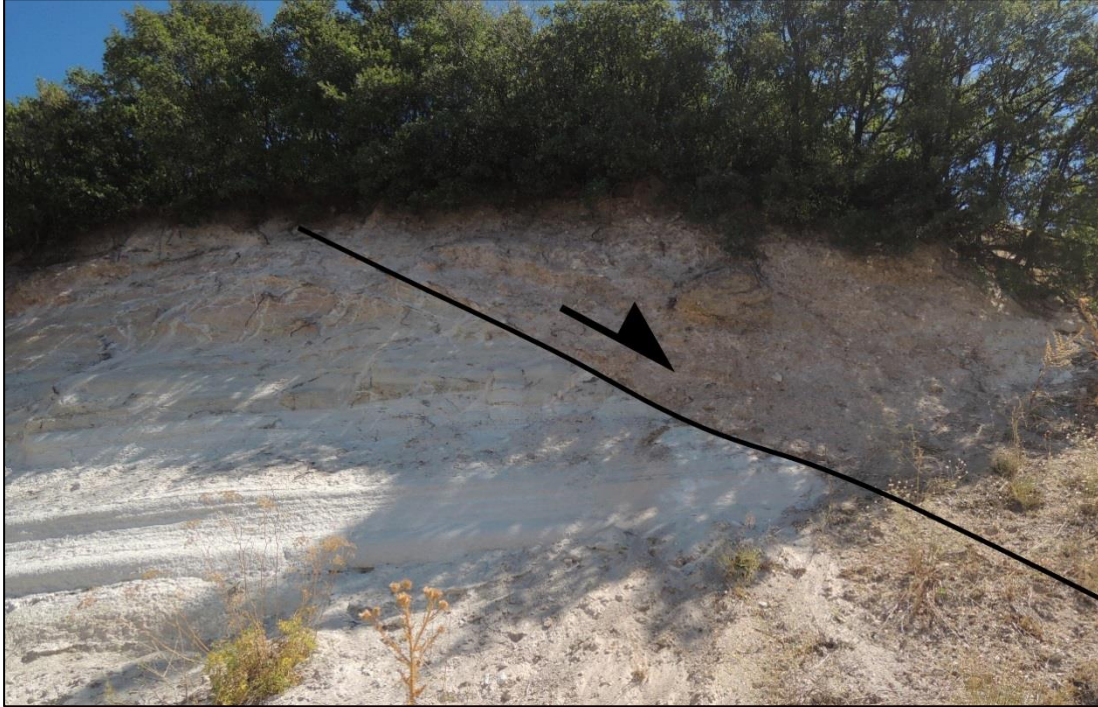


Figure 3-17: Close-up view of a synthetic mesoscopic fault running parallel to the Akdere fault (along the Eğırler road).

3.4.3.2 *Hamzabey fault*

It is a 6 km long, N-S trending and easterly dipping normal fault. The Hamzabey fault cuts and displaces vertically the Middle Miocene Civanadağı tuffs. It juxtaposes tectonically Middle Miocene tuffs with the Quaternary alluvial sediments. The Hamzabey fault starts from 1.5 km northeast of Güneyköy village and then continues up to further north outside the study area. It controls western margin of the modern Akdere graben (Figure A-1 in Appendix).

3.4.4 **Other faults**

3.4.4.1 *Kibletaştepe fault*

Apart from the above-described faults, several outcrop-scaled to mapable faults were also observed in the study area. One of them is exposed well along the Simav-Samat

road cut (S-2 in Figure A-1 in Appendix). It was here termed as the Kibletaştepe fault. It is a NNE-trending and easterly steeply (80°) dipping oblique-slip normal fault, which determines and controls the western margin of the N-S-trending Selendi graben. It cuts and displaces the Simav Metamorphics and tectonically juxtaposes them with the Lower-Middle Miocene Kızılbük Formation. It displays a well-developed and preserved fault slickenside. The stereographic plots of slip-plane data taken from this slip plane on the Schmidt's lower hemisphere net indicate that the Kibletaştepe fault is an oblique-slip normal fault with the local extension in WNW-ESE direction (Figure 3.18).

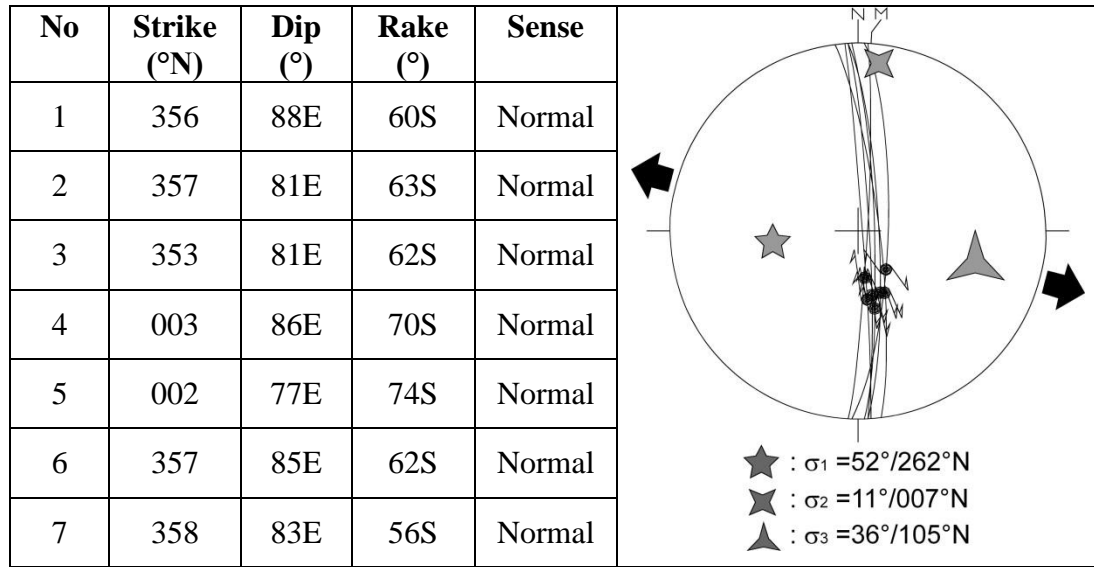


Figure 3-18: Slip plane data taken from fault plane (S-2 in Figure A-1 in Appendix) and kinematic solution using Angelier's direct inversion method on Schmidt's lower hemisphere. (black arrows show local extension direction)

In addition, the relative magnitude of σ_3 is higher than σ_1 and σ_2 which indicates that this fault was governed mainly by the tensional force. Since this fault controls the tectonic contact between the Simavdağı Horst to the west and the Paleotectonic graben infill of the N-S-trending Selendi graben, it should be related to the paleotectonic regime operated during the early evolutionary history of Selendi graben. Consequently there was an approximately E-W trending extension in the Selendi graben during paleotectonic period.

3.4.4.2 Secondary normal fault

A small-scale oblique-slip secondary normal fault was observed in the Simav fault zone along the southern margin of the Simav graben. It cut and deformed the Simav Metamorphics (S-3 in Figure A-1 in Appendix). It displays well-developed and preserved slickenside (Figure 3.19).



Figure 3-19: Close-up view of a mesoscopic fault and its well-developed slickenlines observed along Simav-Samat road (S-3 in Figure A-1 in Appendix)

This fault is an antithetic structure to the Nadarçamı normal fault described in foregoing sentences (Figure 3.6). Stereographic plots of slip-plane data on the Schmidt' lower hemisphere net reveals a NNE-SSW neotectonic extension (Figure 3.20).

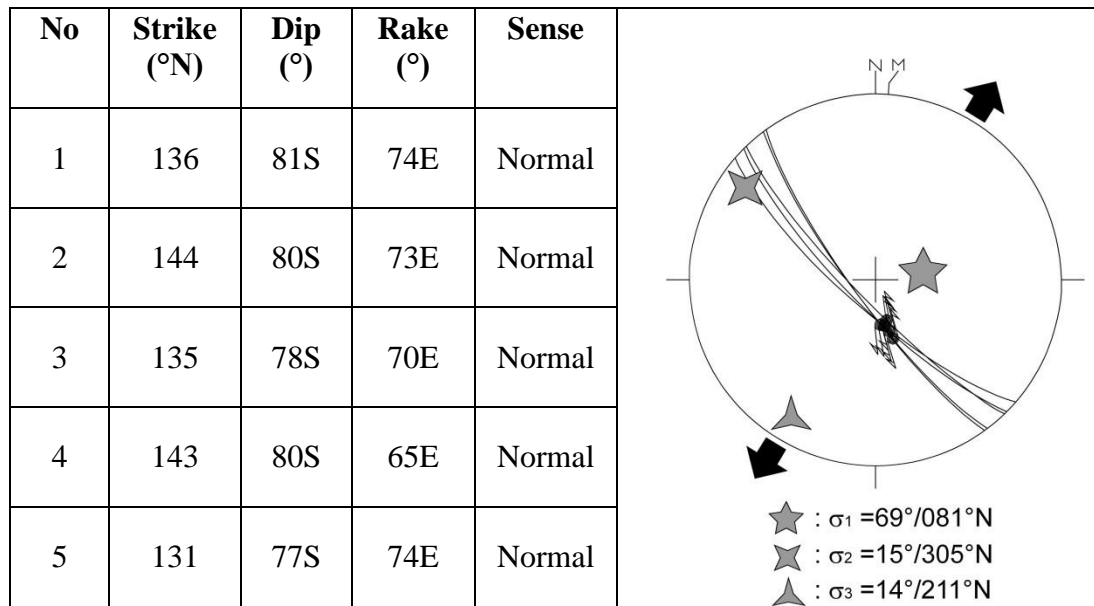


Figure 3-20: Slip plane data taken from fault plane (S-3 in Figure A-1 in Appendix) and kinematic solution using Angelier's direct inversion method on Schmidt's lower hemisphere. (black arrows show local extension direction)

3.4.4.3 Faults with two overprinted sets of slickenlines

A fault slickenside with two overprinted sets of slickenlines was observed along the faulted contact between the Middle Miocene Civanadağı Tuffs and the Simav Metamorphics 5 km west-northwest of Öreyler Town and outside the study area (659008E, 4334127N) (Figure 3.21). Older set of slickenlines, which is crossed by the younger set, is the record of dextral strike-slip faulting operated during the compressive paleotectonic period. However younger set of slickenlines is the record of normal faulting occurred in the Quaternary neotectonic period, i.e., this fault formed originally to be a dextral strike-slip fault during the end of paleotectonic period (possibly Late Pliocene) but later on (in the Quaternary neotectonic period) it reactivated to be a normal fault. In addition, older set of slickenlines also represents the short-term strike-slip faulting phase which interrupted the early evolutionary history of the grabens in the Simav region. The kinematic analysis of slip-plane data measured on this fault slickenside (Figure 3.21) by using the Angelier's direct inversion method (Angelier,1994) reveals a strike slip faulting that was replaced later by the NE-SW extension during post-Miocene period (Figure 3.22 3.23).

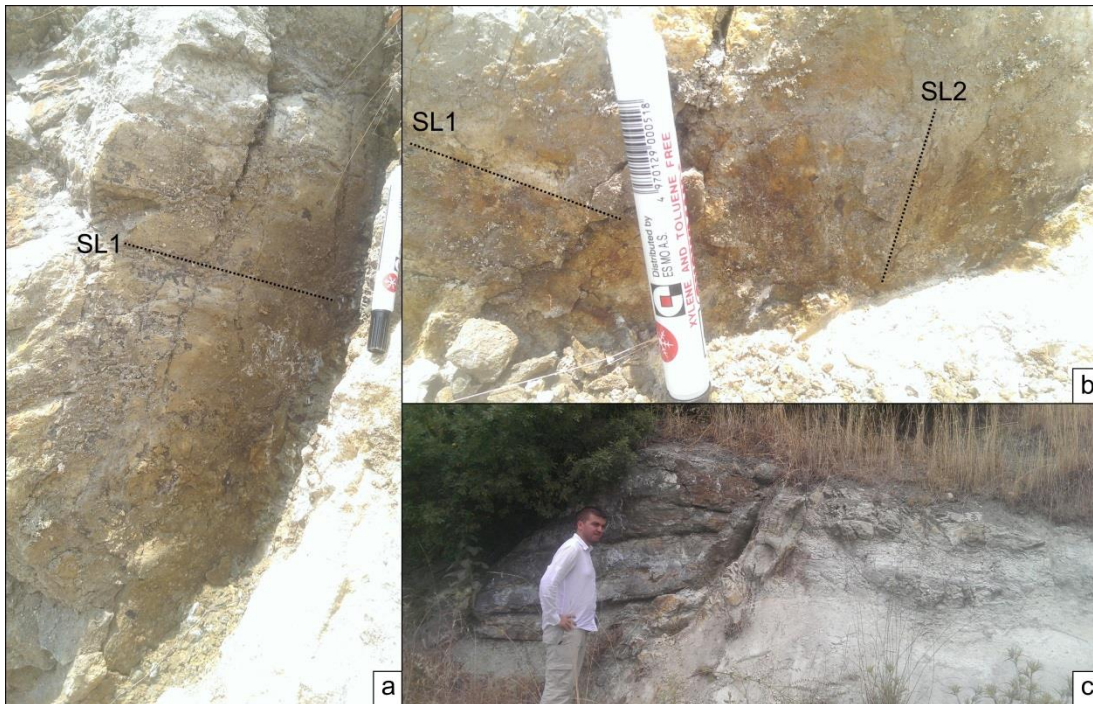


Figure 3-21: a. Close-up view of the set of slickenlines depicting dextral faulting (SL1), b. Close-up view of the set of slickenlines depicting normal faulting, c. General view of the slip plane with two overprinted sets of slickenlines (SL1, SL2) (See figure 3.24 for location).

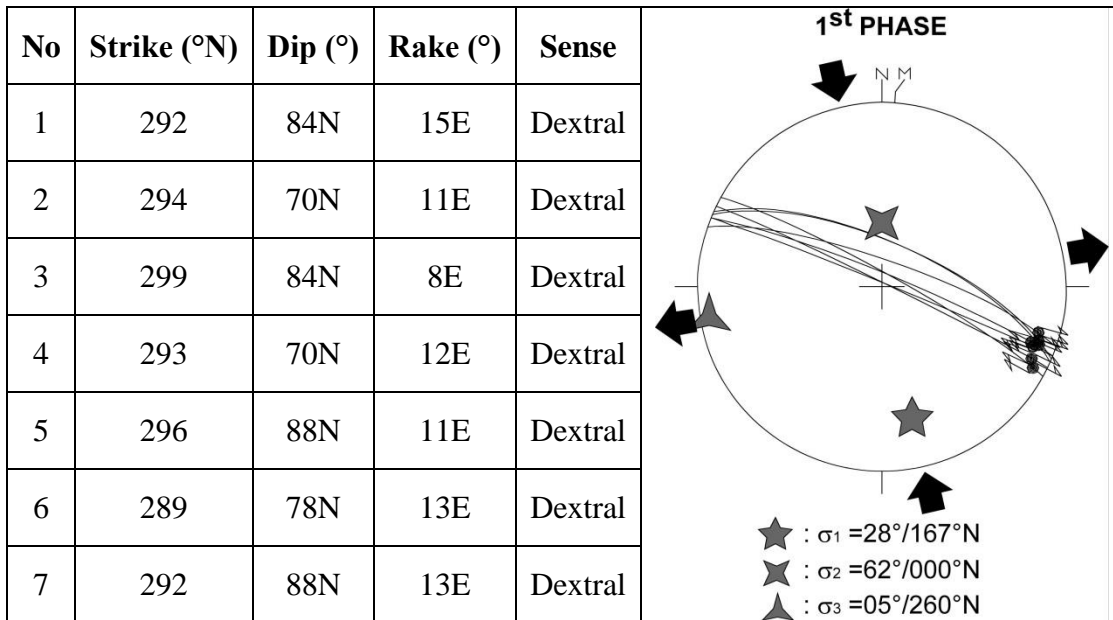


Figure 3-22: Kinematic analysis of the slip plane data by using the Angelier's direct inversion method on Schmidt's lower hemisphere net; 1st phase of deformation obtained from the overprinted older slickenlines (SL1 in Figure 3.22). (black arrows show local extension and compression directions)

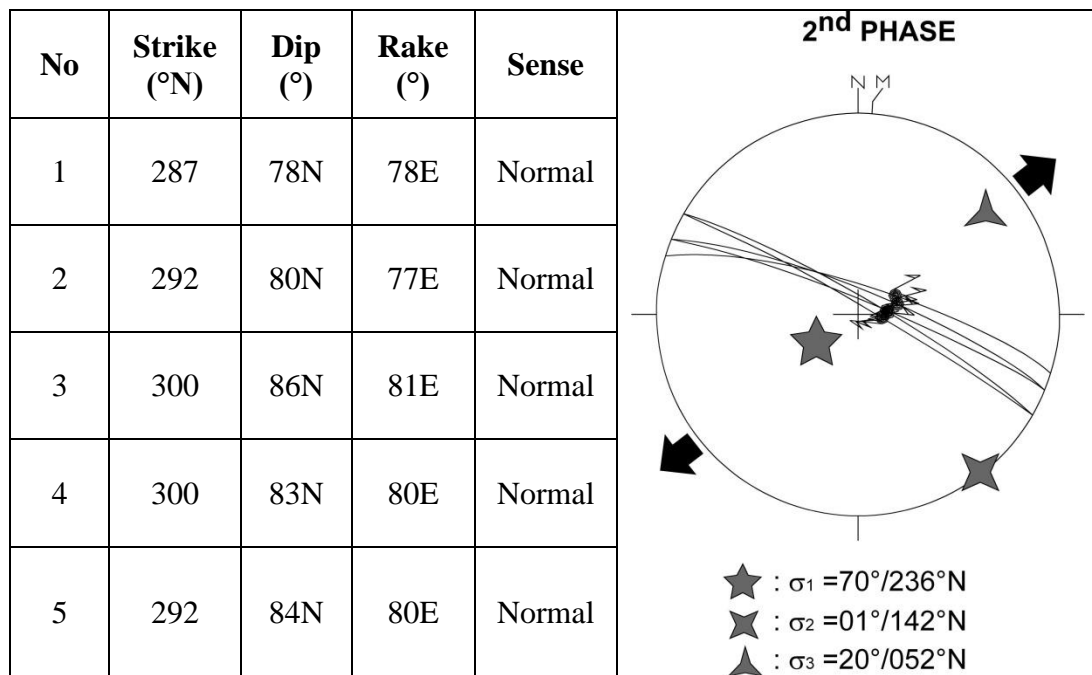


Figure 3-23: Kinematic analysis of the slip plane data by using the Angelier's direct inversion method on Schmidt's lower hemisphere net; 2nd phase of deformation obtained from the overprinted older slickenlines (SL2 in Figure 3.21). (black arrows show local extension and compression directions)

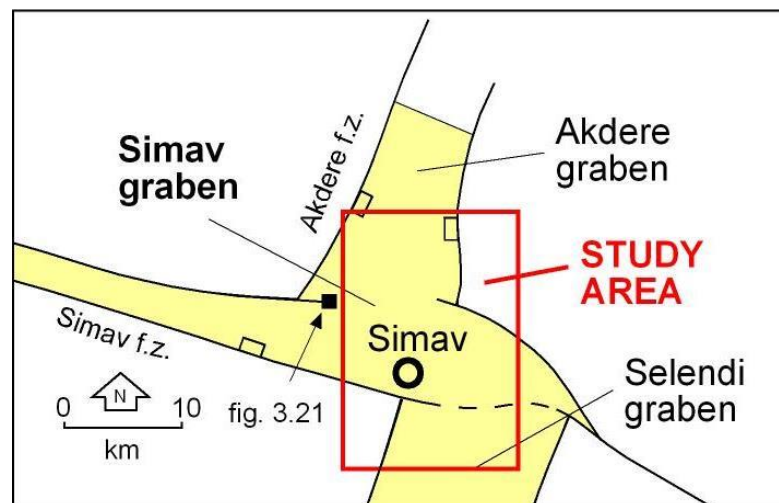


Figure 3-24: Location map showing the site of overprinted slickenline measurement (Courtesy of Prof. Dr. Ali Koçyiğit)

This phase is coeval with the compressive phases observed in the region (Gürboğa et al., 2013). This compressive period may have been related to local block rotations during the west, southwestern escape of the Anatolia platelet or a regional

compressive period that interrupts the regional extension (Koçyiğit et al., 1999; Rojay et al., 2005). Resulting fault mechanism may differ in places where the dominance of synchronously operating different tectonic regimes change. That is, if there is a compression in the east and extension in the west, the interface between these regimes may strike slip regime and complex faulting patterns of same age.

3.4.4.4 Buried faults

As has been described in detail in the aforementioned sentences, the north-northeastern margin of the Simav graben is bounded by a series of active fault segments, which display basinward-facing and steeply sloping fault scarps. A thick fan-apron sedimentary pile have been accumulated along the feet of these active fault scarps owing to the high rate of transportation and sedimentation. For this reason some of the faults are not exposed, but they are located beneath the overlying thick sedimentary pile or modern graben fill. Three buried faults were determined beneath the graben fill in terms of a series of boreholes drilled around Naşa and Eynal thermals along northeastern margin of the Simav graben (Figure A-3 in Appendix). The total throw amount accumulated along these buried faults is about 400 m based on the offset boundaries of the Middle Miocene Civanadağı Tuffs and the Naşa Basalt exposed on both the down-thrown and up-thrown blocks of these buried faults (C-D and G-H-geological cross-sections in Figures A-2, A- 3 in Appendix).

CHAPTER 4

SEISMICITY AND GPS ANALYSIS

Western Anatolia is one of the most seismically active regions in Turkey and the surroundings. Particularly, Simav Fault Zone located in Akşehir Simav Fault System is a major active seismic source displaying frequent earthquake activities in the recent years and arousing the earthquake scientists' interest. This earthquake activity has also been proved by historical period destructive earthquakes (Öcal ,1968; Ergin et.al, 1967; Pınar and Lahn,1952) and the ones in instrumental period recorded by Boğaziçi University Kandilli Observatory and Disaster and Emergency Management Presidency. To understand the long term activity, various characteristics of the seismic sources (faults) in the Simav graben and the tectonic meaning of seismological data will be described and discussed. Also the statistical and descriptive parameters obtained from analysis of seismological data will be used as a major input in the seismic hazard analysis which will be discussed in another chapter.

4.1 Historical Seismicity

There are two well-documented and reported historical earthquake records in and around Simav which occurred in 1875 and 1896. Other earthquakes have insufficient information such as that either their epicenters and/or intensities are not given properly. For example, according to Ambraseys (2009), an earthquake occurred on 16 September 1728, caused heavy damage in Simav, was felt in İzmir but its details are missing. Among the well-documented earthquakes, first one (coordinates 39° N – 29° E) was reported that it occurred in 1875 and has an intensity of VIII (Öcal, 1968). Öcal (1968) also calculated the magnitude of this earthquake as 6.1. The

second earthquake occurred in Emet in 1896 near southeast of Simav County, and it was felt within a circular area with a radius of 200 km. During this earthquake, it was reported that numerous buildings have been damaged, some minarets were collapsed, hot waters came out of the Earth's surface and discharge of some springs were either decreased to dried up or increased (Pinar and Lahn, 1952).

4.2 Recent Seismicity

The 2009 Naşa and the 2011 Söğüt earthquakes occurred in the Simav region are the most recent seismic events that attracted interest of researchers and lead to an increase in the number of seismotectonic studies. Indeed, the earthquake activity and the seismic potential of the region have been proved several times by damaging earthquakes in the last century. These are 1928 ($M_s = 6.1$) Emet, 1944 ($M_s = 6.0$) Şaphane, 1970 ($M_w=7.2$) Gediz, and 1970 ($M_s=5.9$) Çavdarhisar earthquakes (Kalafat et. al., 2011). Particularly the 28 March 1970 Gediz earthquake caused a significant damage and casualties such as 1260 people lost their lives, more than 10000 buildings were damaged and there were around 80000 homeless. Gediz County was relocated to a new place after this earthquake. It was reported that 1086 of the damaged buildings were in villages of Simav County (Erinç et. al, 1970). The 28 March 1970 Gediz earthquake, which was sourced from an active fault segment included in the ASFS, indicated that the damaging potential of the Akşehir-Simav Fault System (ASFS) was quite high.

According to Kandilli Observatory Earthquake Research Institute (KOERI) earthquake catalogues, 468 earthquakes occurred in and near environ of the Simav Graben in the instrumental period covering a time slice between 1900 and 2014 years (Table A-1 in Appendix). 454 of these earthquakes were recorded later than 1968 owing to the earthquake catalog completeness (Figure 4.1). It is clearly seen that there are three jumps in the number of recorded earthquakes (Figure 4.1). First one is in 1968 and due to installation of nearby seismograms that helped recording small-sized earthquakes. Second one is in 1976 which reflects a number of small and moderate-scale earthquake activities in the region. Third and the last one is in 2011

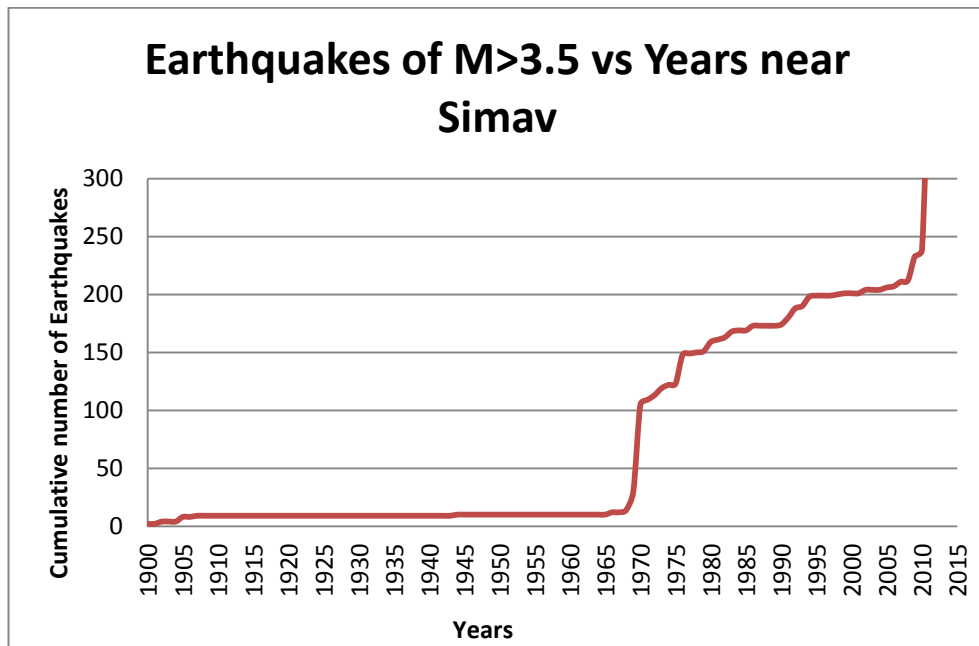


Figure 4-1: Cumulative number of earthquakes with magnitude $M \geq 3.5$ recorded in and near environ of the Simav graben (ERD,2014b)

which is mainly due to aftershocks of the 19 May 2011 Söğüt earthquake. Therefore, the earthquake catalog for this area should be considered as later than 1968.

The information available in earthquake catalogs is mainly origin time, epicenter coordinates, depth and the magnitude. These are key instrumental parameters to calculate earthquake activity. Since epicenter is the vertical projection of focus of an earthquake, depth of the focus of each earthquake should be considered for relating the earthquakes to the dipping faults. Epicenter location is calculated using crustal velocity model and the duration for seismic wave to reach the seismogram. Origin time and the crustal velocity model in a small region is not known precisely, therefore, locating small earthquakes with global or regional models can be misleading in small scales. This is called as the coupled hypocenter-velocity problem (Thurber, 1992). This problem can be overcome to some extent by using more number of seismograms. There are broadband stations in Simav, Tavşanlı and Gediz Counties that help better epicenter distribution resolution. Spatial epicenter distribution of the earthquakes occurred in the study area is available and plotted on a map to illustrate their relationship with the known active faults (Figure 4.2).

Epicenter distributions of large earthquakes are more reliable in terms of both depth and location compared to smaller earthquakes. Epicenter of the 19 May 2011 earthquake is located 1km north of Söğüt village and its focus depth is about 24.4 km. The focal mechanism solution indicates a normal faulting with very small amount of strike-slip component. There are several hypotheses about the type of source fault of this earthquake. These are the strike-slip (Doğan and Emre, 2006), southerly dipping normal fault (Kalafat et al., 2012), and the northerly dipping normal fault (the Simav Fault Zone) in this study. The focal mechanism solutions prepared and published by all available sources show that the source fault should be a nearly ENE-WSW striking normal fault. Hence strike-slip faulting mechanism is not supported by seismological data. Southerly dipping normal fault hypothesis seems to be compatible with the focal mechanism solution. In normal fault systems, earthquakes and aftershocks occur on main fault, antithetic and synthetic faults. All of these faults generate earthquakes with epicenter located in hanging-wall block. Also the depth and epicenter of the 19 May 2011 earthquake mainshock and large aftershocks altogether indicate that southerly dipping normal fault should be at least 20 km north of northern margin of the Simav Graben. However, there is no southerly dipping active normal fault identified in the region which is on the northern side of the earthquake cluster. Therefore, most probable source fault for the 19 May 2011 earthquake should be a northerly dipping normal fault segment included in the Simav Fault Zone, which determines and controls the southern margin of the Simav graben.

4.3 Focal Mechanism Solutions

Focal mechanism solution of an earthquake is a diagram showing the direction of radiating compressional and tensional seismic P-waves around the focus. These directions are determined by using first P-wave arrivals to the seismograms located in different directions. These first P-wave arrivals and their takeoff angles are plotted on a stereogram. Resulting diagram is a beach ball plot with compressional white and tensional black regions. Available focal mechanism solutions of earthquakes are plotted with numbered epicenters on the study area (Figure 4.3).

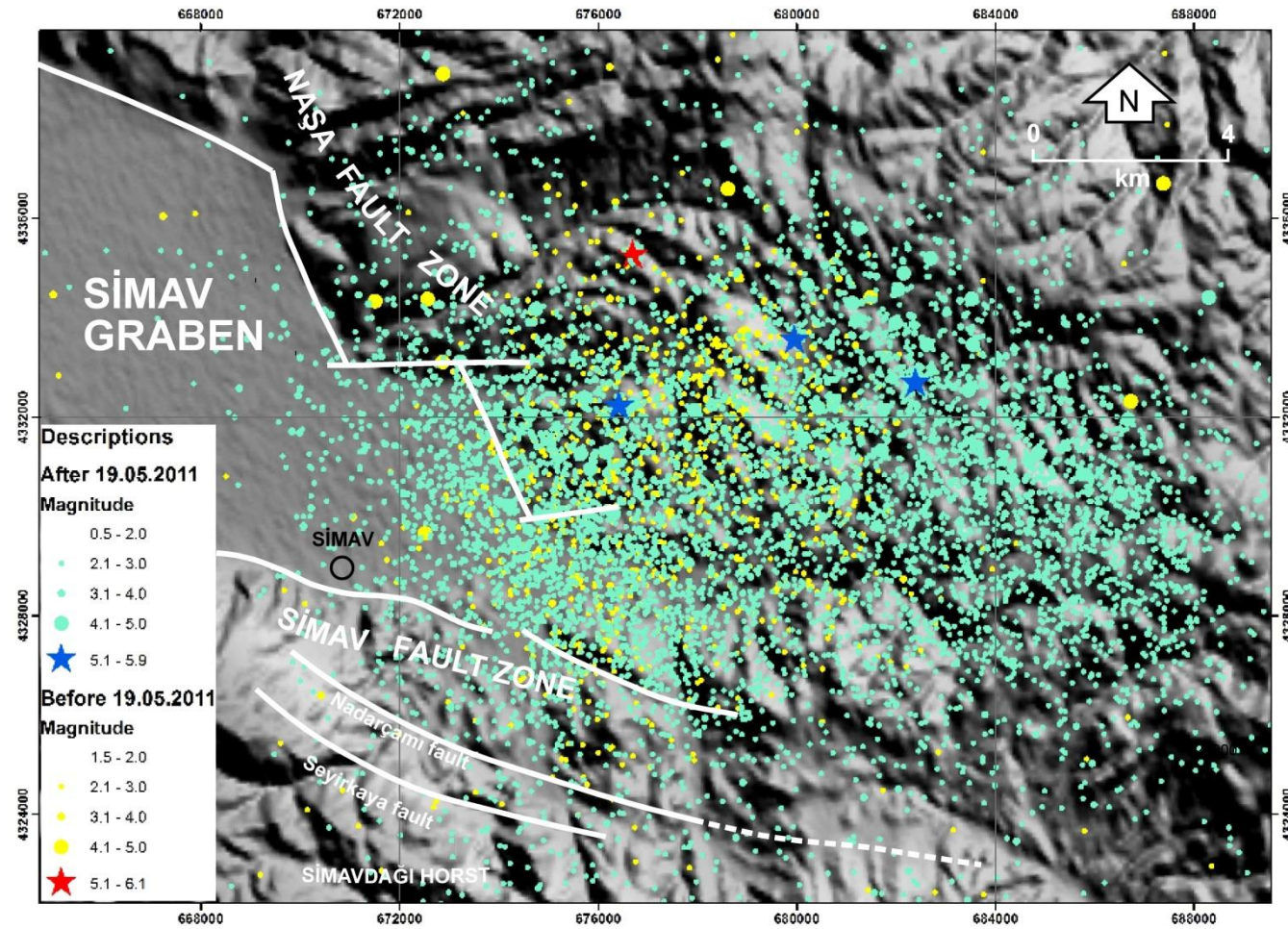


Figure 4-2: Seismotectonic map of the study area (Data is from ERD,2014b).

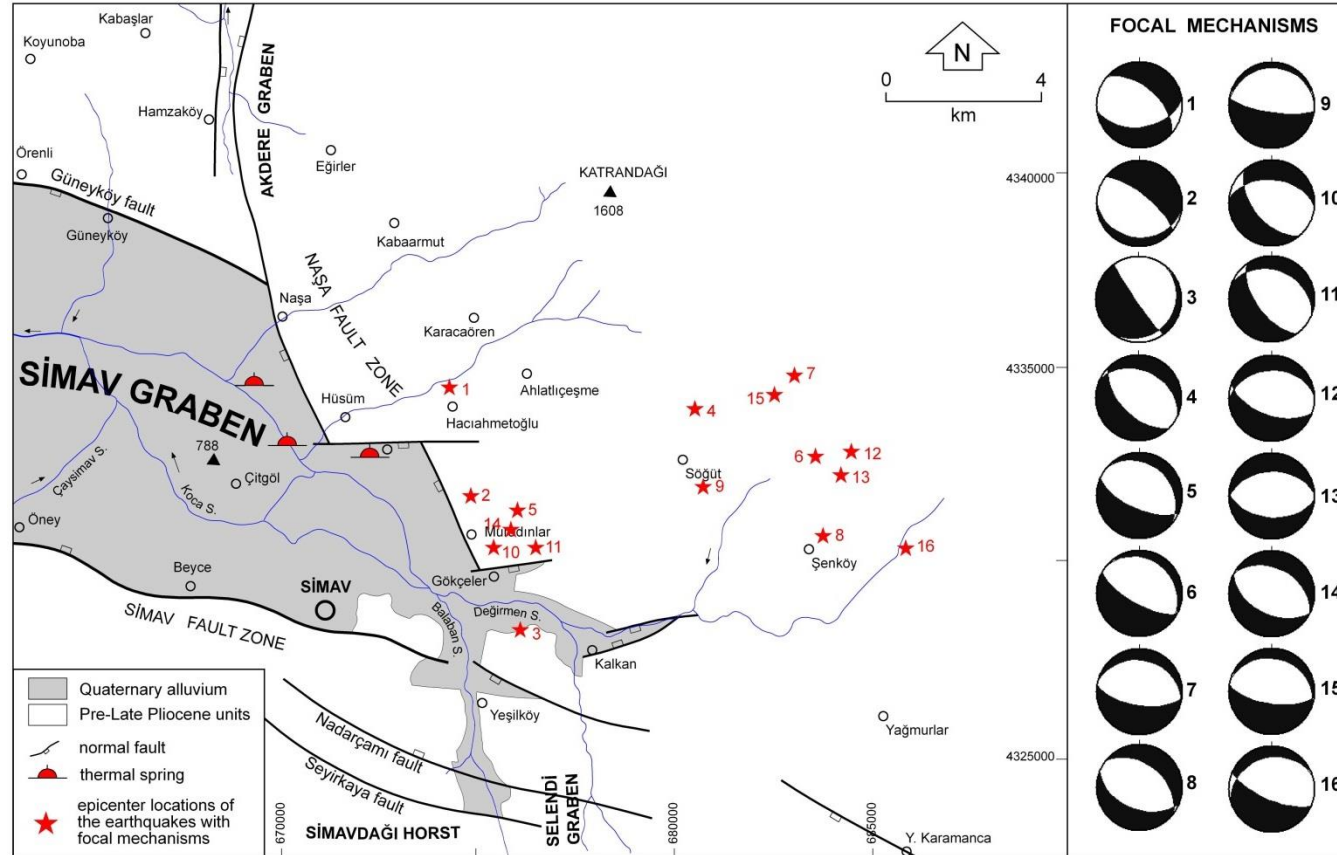


Figure 4-3: Focal mechanism solutions and their distribution in the study area. Seismic parameters are given in Table 4.1

Table 4-1: Seismic parameters of the focal mechanism solutions of earthquakes occurred in study area

No	Date	Time (UTC)	Latitude	Longitude	Depth	Magnitude	Strike	Dip	Rake	Institute
1	17.2.2009	07:28	39,15	28,98	16,8	5,2	262	46	-128	HARVARD
2	25.9.2009	09:23	39,12	29,02	20	3,7	276	20	-121	ERD
3	8.11.2009	09:05	39,08	29,04	5	3,6	218	16	162	ERD
4	19.5.2011	20:15	39,13	29,08	24,4	5,8	264	60	-90	ERD
5	19.5.2011	21:21	39,11	29,03	4	4	294	64	-98	ERD
6	19.5.2011	21:33	39,13	29,12	3,9	8	299	70	-99	ERD
7	27.5.2011	07:43	39,14	29,12	4,1	6	279	63	-91	ERD
8	28.5.2011	05:47	39,12	29,03	4,8	20	144	58	-72	KOERI
9	29.5.2011	01:31	39,12	29,09	4	4,3	279	76	-88	ERD
10	27.6.2011	21:13	39,11	29,02	4,8	6	321	55	-60	ERD
11	27.6.2011	21:28	39,11	29,05	4,2	6	324	61	-74	ERD
12	26.4.2012	22:05	39,13	29,11	5	4,5	290	57	-78	ERD
13	3.5.2012	15:20	39,12	29,11	10	5,3	274	48	-86	ERD
14	3.5.2012	16:16	39,10	29,04	6	4	297	50	-90	ERD
15	3.5.2012	21:45	39,14	29,11	6	4,2	279	66	-93	ERD
16	9.5.2012	17:49	39,10	29,15	5	4,1	293	69	-73	ERD

ERD: Earthquake Research Department (Turkey), KOERI: Kandilli Observatory Earthquake Research Institute

There are 16 focal mechanism solutions illustrated in Figure 4.3 and listed in Table 4.1. Each of these focal mechanisms has compressional and tensional axes calculated. Although focal mechanisms may give relatively varying nodal planes for each earthquake, their magnitude weighted statistical mean is coherent within acceptable error margins (Figure 4.4).

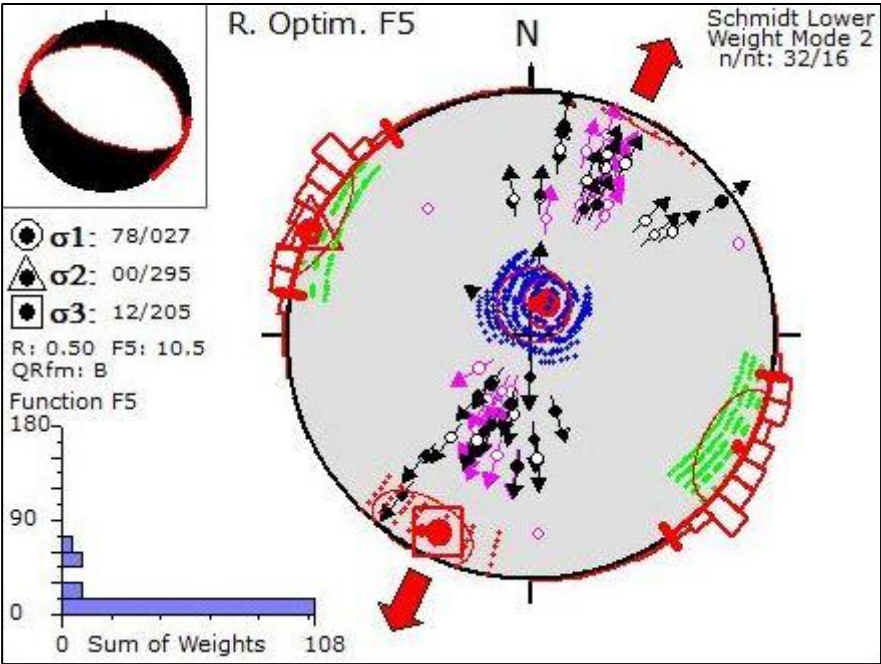


Figure 4-4: Schmidt lower hemisphere plot of Win Tensor rotational optimization solution of available focal mechanisms (Delvaux et al., 2003) (Red arrows indicate local extension direction of earthquake area).

Win Tensor is a free software that analyses fault slip and focal mechanism data (Delvaux et al., 2003). Rotational optimization method is used for analysis. This method makes a grid search to find an orthogonal principle stress configuration which has the minimum misfit to the overall dataset. This misfit is calculated using the weighing factor of each slip data and slip line deviation from the mean slip line that correspond to computed stress tensor. The measurements with angular deviation larger than 30° are omitted and iterative search is continued (Delvaux et al., 2003). Görgün (2014) calculated centroid moment tensors for 41 events with moment magnitudes (M_w) between 3.5 and 6.0 applying waveform inversion method. He suggested a stress field orientation from 41 focal mechanisms. This solution is also compatible with our calculation (Figure 4.5).

The source of earthquakes is normal faulting not strike-slip faulting and the local extension direction is NNE-SSW (Figure 4.4,4.5) .

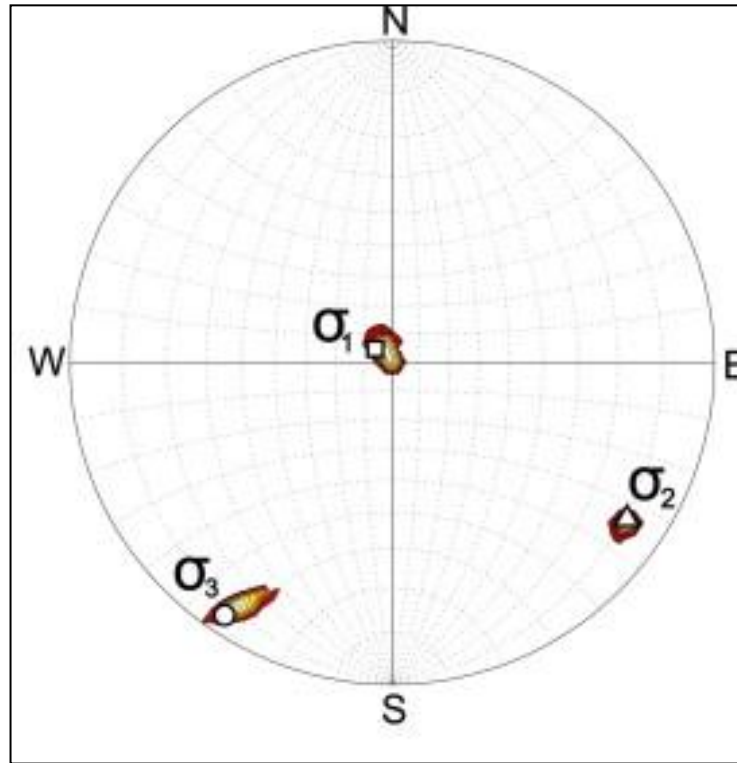


Figure 4-5: Stress field orientation derived from focal mechanisms (Görgün, 2014)

Based on these focal mechanisms solution diagrams, the source of the mainshock is the Seyirkaya fault and/or Nadarçamı fault which were observed and mapped in the field (Figure A-1 in Appendix) These are northerly steeply dipping (65° - 75°) normal faults located 10-12 km south of the epicenter. Besides focal mechanism solution also gives a dip amount of an approximately 40° for the fault plane at the focus of main shock. These seismological and geological data can be ascribed to that the source of the 19 May 2011 Simav earthquake is a listric fault in nature.

4.4 GPS Analysis of the region

Geoscientists, who mainly focus on tectonics, deal with the deformational processes and the resulting structures on the Earth through time. The ones that study active tectonics are more interested in recent deformation. Active tectonics movements

deform the crust by means of folding and faulting. Folding is a permanent plastic deformation process that occurs below and on the Earth surface where rocks behave ductile. Faulting is a process of brittle deformation of the crust that causes rapid ruptures and sudden release of energy termed to be earthquake. In either case, the total deformation is relatively slow in a given time period. Additionally, deformation is mostly compensated as sum of these two main processes in a region. Therefore, extremely precise measurement on a long time span is needed to observe current deformation of the Earth's crust. At this point, using the recently advanced Global Positioning System (GPS) comes into consideration.

4.4.1 Theoretical Background of GPS

Geodesy is a measurement and representation of the Earth in three dimensional time varying space. Satellite technology is advanced dramatically in the last decades and Global Positioning System is developed. GPS is a navigation system that provides location of the point of interest using GPS satellites. Since the satellites have relatively fixed orbits in a given reference frame, a GPS device can locate itself using several satellites in different directions. A GPS device locates itself in three main steps below: (a) GPS receiver reads the radio signals that are continuously broadcasted by the satellites, (b) Using the patterns inside the radio signal, GPS receiver calculates the distance to the satellite which is the source of the radio signal, and (c) GPS receiver locates its position using each distances from several different sources. Since the Earth is moving and rotating around the sun, the points on the Earth surface are not fixed in the universe. Hence, a global position which is relative to the Earth surface itself, i.e., has reference frame based on the Earth, cannot be useful. This situation causes another problem; the crust of the Earth is deforming due to plate tectonics movements and one cannot measure the deformation using already deformed reference point. Therefore a fixed coordinate system independent from Earth surface must be used. For this purpose, International Celestial Reference System is defined by using: (a) Vernal equinox which is the intersection of equatorial plane of the earth and its orbital plane, (b) The Earth's rotation axis and, (c) The axis 90° towards east from vernal equinox along equatorial plane of the Earth. This

reference frame is later adapted to the rotation of the Earth and International Terrestrial Reference Frame (ITRF) is introduced. This reference frame uses: (a) Greenwich meridian, (b) Mean pole between years 1900-1905 and, (c) Equatorial plane of the Earth. Current GPS receivers use this ITRF reference frame for ease of communication, this procedure involves conversion between ICRF and ITRF systems.

GPS measurement can be affected by various factors. These factors are: (a) the rotation of the earth can be affected by luni-solar tides, anisotropy of the earth, variation of rotation speed, earthquakes and electromagnetic coupling. These eventually change the rotation vector of the earth which is used to convert the universally fixed positions of ICRF to earth based ITRF coordinates, (b) The position of the satellite is changing from its predefined orbit because of gravitational forces due to topography, attraction forces of the sun and moon, solar radiation pressure and satellite maneuvers; these result in miscalculation of the position of the satellite which results in GPS error, (c) Atmospheric effects which are ionospheric effect resulted from ionospheric and tropospheric effects. These effects could change the path of the radio signal due to ion content or weather conditions, and (d) the device error; most of the handheld devices have more than 1-2 m positioning error due to antenna structure of the receiver, clock error, multipath error which is related to reflections from nearby surfaces, the stability of the GPS device setup and lastly the electronic noises of the area. The deformation rate is generally around 4 cm/yr in tectonically most active regions, therefore, the correction of these errors are obligatory to use GPS data in active tectonics. The most common methods to overcome errors are basically using better GPS devices, measuring positions for a long time and taking the best fitting line on position-time graph, measuring on different seasons, correcting the satellite orbit data from IGS, and using several GPS devices at one time to double check measurements.

4.4.2 Usage of GPS in Active Tectonics

As mentioned above, GPS technology is recently developed one that is used to measure the location of any point on the Earth at any time. If this measurement is

repeated through time, the change in the location of the point relative to reference frame gives the displacement of the point. This displacement is converted to GPS velocities later. Measuring a number of points in a region gives the GPS velocity field of the region. Calculating differential velocities of points relative to each other reflects the differential displacements and that consequently are used to determine deformation rate of the region relative to given coordinate system.

In general, GPS satellites which are above an in 160° line of sight are used for determining the position. This yields to higher precision in horizontal positioning which generally gives around three times more precise results than vertical positioning. Therefore it is a better application to use horizontal GPS velocities and calculate deformation in horizontal plane which will give the orientation and the type of horizontal strain axes and corresponding stress axes. For strike slip faulting systems, the magnitude of calculated strain axis could be correlated with the total magnitude of fault slip rate and shear strain rate. However, in the normal and reverse faulting cases, the dip of the fault will be important and should be considered while using horizontal strain magnitudes.

4.4.3 GPS Analysis in Western Anatolia and Simav Graben

GPS velocities used in this study are taken from McClusky et al. (2000), Reilinger et al. (2006) and Aktuğ et al. (2009). These velocities are illustrated in Figure 4.6.

Before the GPS analysis, some of the velocities are excluded from the process because: (a) the standart deviation is high, (b) duration of measurement is low, and (c) problems related to combination algorithm of different velocity fields. These velocities are processed on Velocity Interpolation to Strain Rates v2.0 (VISR2) software (Shen et al., 1996). This program assumes homogenous strain in the crust and uses the GPS velocities from points within a specified distance range and to calculate deformation at a point as rotation, translation and strain rates. The program uses a weighting algorithm that includes distance to the point, velocity uncertainties and velocity co-variances. The area is gridded as rectangular areas with 0.25 degree dimension. Maximum and minimum horizontal strain directions axes from the analysis are shown in Figure 4.7.

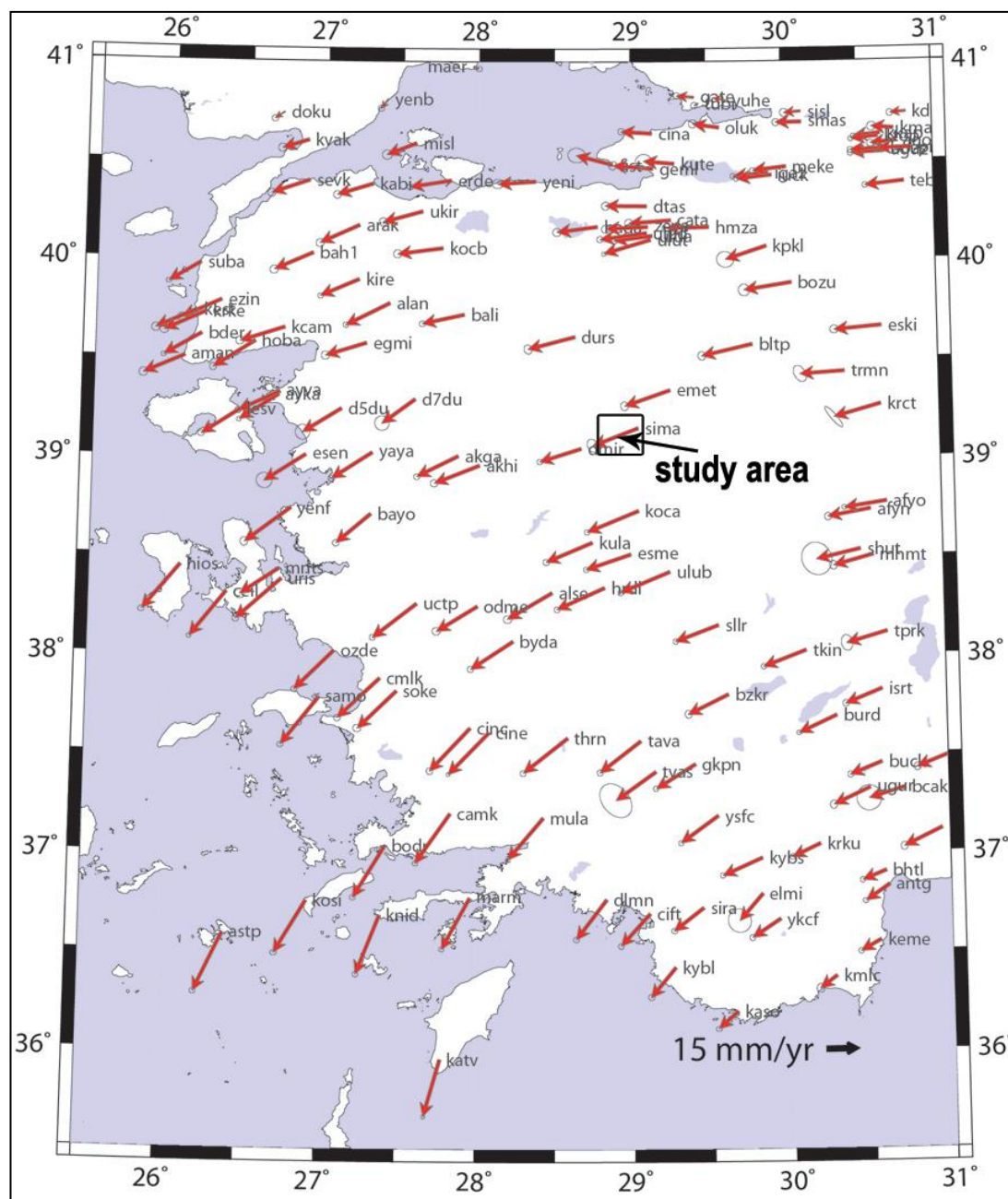


Figure 4-6: GPS velocity field of Western Anatolia which is relative to Eurasia fixed reference frame. Error ellipses are at 95% confidence interval. Simav graben is shown as black box inserted in the figure

These strain axes are compared to active faults map of Turkey (Emre et al., 2013) and World Stress Map project (Heidbach et al., 2008). According to horizontal strain axes, their type and relation to WSM project minimum horizontal stress orientations, a well fit is observed. Also the extension directions are generally perpendicular to the

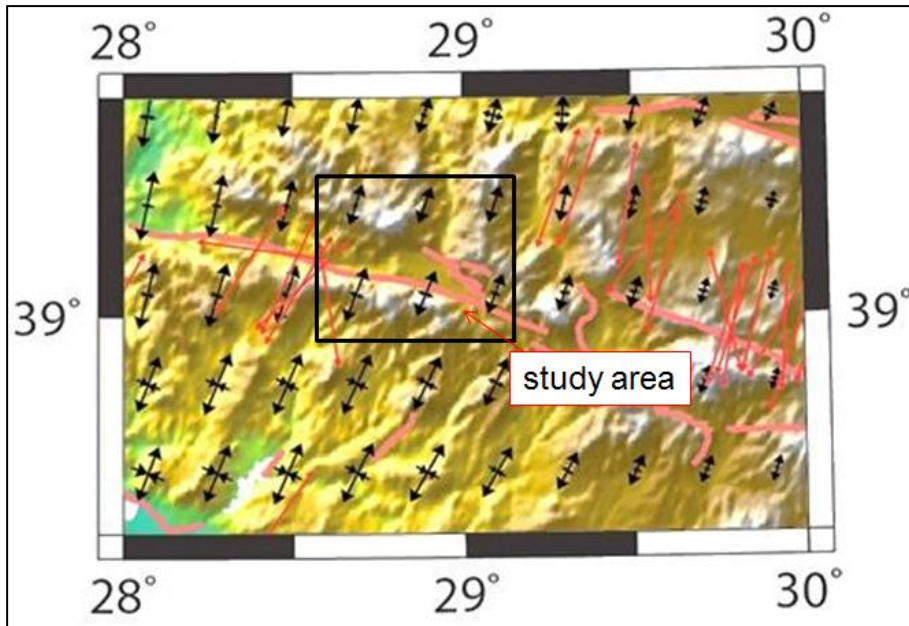


Figure 4-7: Maximum and minimum horizontal strain axes (black arrows), Minimum horizontal stress (extension) direction taken from World Stress Map project (red arrows) Heidbach et al., 2008

faults; therefore, these faults should be working as normal faults with small amount of strike slip components.

Rotation analysis of VISR2 assumes small rigid bodies bounded by the pre-defined grids and calculates the rotation of the grids relative to nearby regions. That shouldn't be confused with the Euler rotation of the crust. The rotation rates are calculated and illustrated in Figure 4.8.

Horizontal local rotations are observed generally near strike-slip and oblique-slip faults. For right lateral strike-slip faults, rotation will be clockwise and for left lateral strike-slip faults rotation will be counter-clockwise. For normal and reverse faults rotation will be small. GPS sites near Simav graben are sparse and have relatively higher uncertainty compared to GPS velocity differences. Therefore, a localized and more precise GPS analysis is needed for better resolution in GPS velocity analysis. Still, general trend of the deformation coming from GPS analysis can be compared and discussed with other methods within around 50 km resolution according to

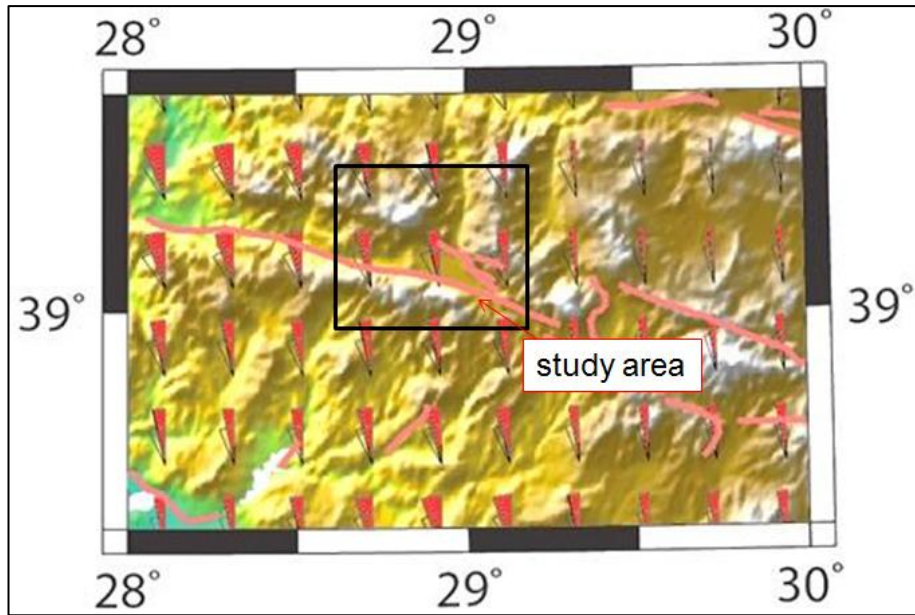


Figure 4-8: Rigid body rotations in the study area according to GPS velocities.

analysis results. According to GPS analysis, local extension direction in Simav Graben and around 100 km vicinity is about N20°E while orientation of the its margin-boundary fault is N80°W. This should result in small amount of right lateral strike-slip component if the faults have normal sense of motion. This result is also fitting well with the WSM results. Rotation amount is very small compared to its uncertainty, hence it is omitted.

CHAPTER 5

DISCUSSION ON EVOLUTIONARY HISTORY OF THE SIMAV AND AKDERE GRABENS

The discussion on the neotectonics of the western Anatolia covers a wide range of disciplines including tectonics, structural geology, stratigraphy, paleontology, geochemistry, petrology and geochronology. In the scope of this thesis, field based stratigraphic and structural evidences are obtained. Hence the discussion will be held in the light of these evidences as well as the available literature data reported by other authors.

The discussions on the neotectonics and evolution of the Southwest Anatolian graben-horst system (SWAGHS) are focused on two points: a) cause and onset age of extensional tectonic regime, b) corresponding evolutionary style of SWAGHS. Even there are numerous studies in the Western Anatolia in this scope there is not still a common agreement. Briefly, there are four views on the evolutionary model of SWAGHS: (1) Tectonic escape (extrusion) model (Şengör et al., 1985; Dewey and Şengör, 1979; Şengör, 1987) : the extension in SWAGHS is resulted from compression and westward extrusion of wedge-shaped Anatolian Platelet along the NAFS and EAFS after Tortonian due to Arabia-Eurasia collision took place in Langhian-Serravalian. Present kinematics of Western Anatolia supports the role of tectonic escape in the western Anatolian extension. However, the proposed age of the model contradicts to the formation age of NAFS, EAFS and the Anatolian Platelet which took place in Early Quaternary (Koçyiğit et al.,1999). Moreover, the Akdere and Selendi grabens with older fills of Early Miocene age which predates Arabia-Eurasia collision (Seyitoğlu et al., 1996); (2) Back-arc extension model

(McKenzie, 1978; Meulenkamp et al., 1988, Le Pichon and Angelier, 1979): the extension in SWAGHS is caused by southwestward migration of Hellenic arc due to the roll-back of northward subducting slab. Based on this model, the commencement age of extension is being proposed differently by different authors such as 13 Ma (Le Pichon and Angelier, 1979), 5 Ma (McKenzie, 1978) and at least 26 Ma (Meulenkamp et al., 1988); (3) Orogenic collapse model (Dewey, 1988; Seyitoğlu and Scott, 1991, 1992, 1996): the extension in SWAGHS was resulted from thinning and spreading of overthickened crust. Overthickening is due to collision and tectonic uplift (Dewey, 1988). Since collision built up vertical stress and created topographic high, after the lateral compressional force is removed, the isostatic and gravity forces took place and spread the overthickened crust as a rebound. The closure of İzmir-Ankara-Erzincan ocean took place in Latest Paleocene to Early Miocene. Immediately after the cessation of collision, the orogenic collapse took place (Seyitoğlu and Scott, 1991, 1992). Şengör et al. (1985) suggested that the crust in western Turkey was thickened up to 50-55 km which supports this model, and (4) Episodic two stage extension model with intervening contraction (Koçyiğit et al., 1999; Koçyiğit et al., 2000; Bozkurt, 2002; Koçyiğit and Özacar, 2003; Koçyiğit, 2005; Bozkurt and Sözbilir, 2004; Bozkurt and Rojay, 2005): first phase (Early-Middle Miocene) of the extension in SWAGHS is resulted from orogenic collapse occurred along the İzmir-Ankara-Erzincan suture zone. Second (Early Quaternary to recent) extension is characterized by combination of back-arc extension due to the roll-back process and tectonic escape models. Intervening compression is due to the change in the kinematics between Arabia and Eurasia or block rotations. This model is supported mainly by field evidences such as intensely deformed (folded and thrust to reverse faulted) Early Miocene-Lower Pliocene rock units deposited on supradetachment basins, and the presence of an angular unconformity between the deformed Early-Middle Miocene-Pliocene units and the undeformed modern graben fill of Quaternary age. Additionally there are different models such as the pulsed extension model (Purvis and Robertson, 2004, 2005) and two stage of extension separated by erosional period (Yılmaz et al., 2000). These models are slightly different from episodic extension model but they support it.

The field-based evidences allow commenting on evolutionary history of the Simav and Akdere grabens and lead to differentiate several deformation phases. These are from oldest to youngest: (a) N-S extensional phase and detachment faulting, (b) E-W extensional phase and Demirci and Selendi graben formation, (c) NW-SE compressional phase accommodated by NE-SW extension and deformation of older grabens and related fills, and (d) NNE-SSW extension (neotectonic regime) that forms the Simav graben (Figure 7.1).

During the first phase, a N-S extension was operating in the study area. The Simav detachment fault was formed after the cessation of Paleogene shortening during the closure of North Neotethys ocean (Seyitoğlu and Scott, 1992; Collins and Robertson, 1998; Koçyiğit et al., 1999). U-Th-Pb SIMS zircon dating of the Eğrigöz and Koyunoba syn-extensional granites gives 21 ± 0.2 to 20.7 ± 0.6 Ma (Ring and Collins, 2005). The Simav detachment fault was active until 18 Ma (Gessner et al., 2001; Ring et al., 2003; Işık et al., 2004; Bozkurt et al., 2011). Later on it must be locked due to doming resulted from intrusion of I-type syn-extensional granitoids (Ring and Collins, 2005). The Taşbaşı Formation was deposited on the top of exhumed footwall block of the Simav detachment fault (Ersoy et al., 2010). The Taşbaşı Formation is reddish colored, weakly cemented, poorly sorted and polygenetic boulder block conglomerate that was deposited as alluvial fans by high energy fluvial systems. Reddish color indicates terrestrial environment. Loose packaging and poorly sorting indicate short transportation distance and shallow-burial after the deposition. An angular unconformity between the Taşbaşı Formation and the Civanadağı Tuffs is observed in the field. This erosion could be resulted from doming of migmatites at the footwall block of the Simav detachment fault related to emplacement of granites (Bozkurt et al., 2011).

In the second phase, an E-W extension along the margins of the Selendi graben and syn-depositional faults were observed in the Akdere graben (Figures 3.18). The fill in the Akdere graben starts with the boulder-block conglomerates alternated with tuff and continues to tuff-sandstone dominated volcano-sedimentary sequence that passes to fluvio-lacustrine sedimentary package. Overall, graben fill is fining upward

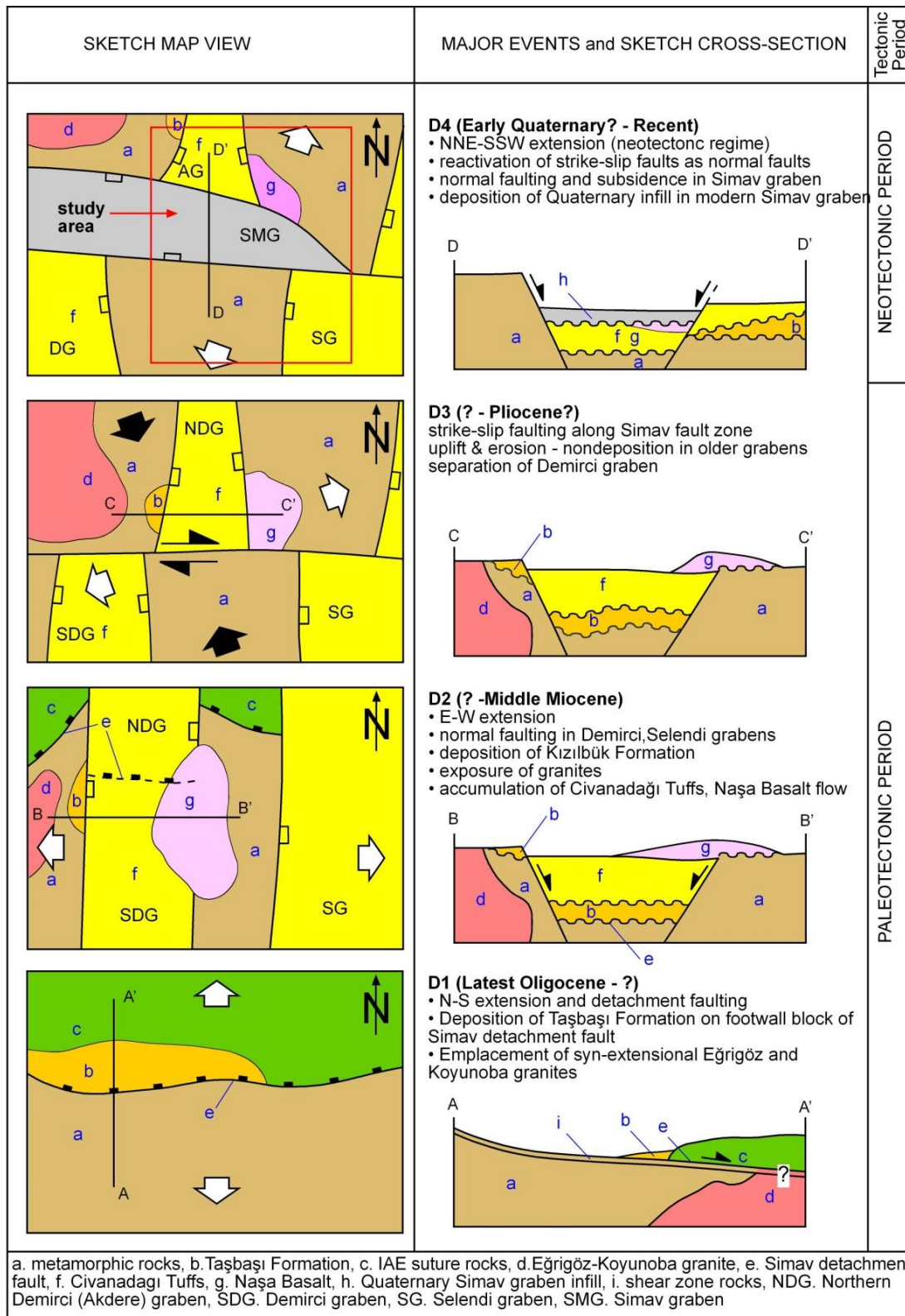


Figure 5-1: Sketch map view, cross-sections and major events depicting proposed evolutionary history of Simav and Akdere grabens

in nature which indicates receding of depocenter from the source (extension). It is also coherent with the stratigraphic relationships and the orientation of the units (Figure A-3 in Appendix). Granite blocks observed in the middle levels of the Civanadağı Tuffs indicate that the youngest exposure age of granites is Middle Miocene. This granite is possibly Koyunoba granite since the fill of the Akdere graben at that location is mainly derived from west according to the pinch-out geometry of pyroclastic basal flows. Moreover extensional faults controlling the Miocene sedimentation are proposed according to geothermal well logs (Section 3.4.4, C-D and G-H cross-sections in Figure A-2, A-3 in Appendix). The Naşa Basalt has flowed over both the Akdere graben (depocenter) and the eastern Katrandağı Horst. Since there is no deposition over the Middle Naşa Basalt, it is the time limit between second and third phases.

Third deformational phase is characterized by strike-slip faulting along the Simav fault zone, folding and uplift. The Demirci graben is cut, displaced up to 5.5-6 km in dextral direction (Konak, 1982) and separated into two parts by the intervening E-W-trending strike-slip fault zone (the ancestor of the present-day Simav fault zone of tensional origin). The northern part is named as the Akdere graben. This deformational phase was also recorded on the fault slickenside (Figures 3.21, 3.22, 3.23).

Fourth deformational phase (neotectonic regime) is governed by the NNE-SSW extension. Modern Simav graben was formed and some of the strike-slip faults have reactivated as normal faults (Figure 3.21). Also some of the faults inside the Akdere graben have reactivated and controlled the Quaternary deposition along the Simav modern graben (C-D and G-H cross-sections in Figure A-2, A-3 in Appendix). This neotectonic regime is also supported by stress inversion of fault planes (Figures 3.5, 3.11). Moreover focal mechanism solutions of the 19 May 2011 Söğüt earthquake and its aftershocks support the normal faulting character of active faults (Figures 4.2, 4.3). Furthermore, GPS analysis of the region gives NNE-SSW extension and normal faulting with minor strike-slip component (Figures 4.7, 4.8).

Consequently, considering the field evidences, the evolutionary history of the Simav and the Akdere grabens is episodic, not continuous.

CHAPTER 6

SEISMIC HAZARD ASSESSMENT OF SİMAV REGION

Earthquakes have always been a big problem for humanity throughout history. Since faults are suitable places for hot and/or cold water circulation and the areas near faults are good places for farming and reaching water, there are numerous old cities in western Anatolia built near active faults. Unfortunately, those cities were hit by earthquakes and the residents had to abandon the city after they realized that earthquakes damaged their cities because of location of the city. Now, developments in the Earth sciences guided people to have enough knowledge about faults and earthquakes. Still, in Turkey, earthquakes are the most important natural disasters that people have to come across. Large settlements and facilities are built in cities where there are a large number of people live and valuable economic activities are carried out. These buildings require enough and more precise earthquake hazard prediction studies in order to be more earthquake hazard safe. However, earthquake occurrence cannot be predicted precisely in terms of time, location and magnitude. Therefore, there is need for seismic hazard assessment studies that quantify the uncertainty of these variables and calculate the amount of ground shaking that a building should withstand in a given site.

6.1 Theoretical Background

Seismic hazard is the level of ground shaking and related effects of earthquake on a given site. The outcomes of seismic hazard assessment are design ground motion parameters which are peak ground acceleration, peak ground velocity, peak displacement and spectral acceleration amounts for given spectral periods (SSHAC, 1997). Seismic hazard and risk terms are often misused instead of each other but they

are different. Seismic risk describes the amount of damage to a building or a site in terms of structural, social, economic and environmental aspects. Basically seismic risk is equal to seismic hazard multiplied by building vulnerability (Wang, 2009).

There are two main approaches for seismic hazard analyses which are Deterministic Seismic Hazard Analysis (DSHA) and Probabilistic Seismic Hazard Analysis (PSHA). Probabilistic seismic hazard analysis (PSHA) includes all possible earthquake scenarios that are determined from geological and seismological data with all possible ground motion probabilities. Therefore, PSHA depends on good knowledge of geology to be successful on prediction. On the other hand, DSHA includes maximum credible earthquake (MCE) which is the largest earthquake that is capable of occurring on a nearby earthquake source (Abrahamson, 2006). The deterministic approach traditionally uses 0 or 1 standard deviation above the median for the ground motion, however, in probabilistic approach; larger numbers of standard deviations are used. The deterministic approach leads to a single ground motion for each scenario considered, whereas, the probabilistic approach guide to a hazard curve, giving the probability of exceeding various ground motion values (Abrahamson, 2000). Therefore, ground motion calculated from PSHA sometimes will be larger than DSHA but corresponding probability would be very small as low as zero. Therefore, DSHA seems to be safer than PSHA but it is highly dependent to expertise and may conclude expensive designs and must be applied for very important and long-living buildings such as dams, bridges and power plants (McGuire, 2001). The main idea of probabilistic approach is to provide a basis for selecting a “reasonable” design ground motion that is generally less than the worst case. In PSHA, maximum design earthquake (MDE) is defined that is expected to produce the strongest ground motion in a given site. MCE and MDE are often confused, MDE can be equal to MCE for critical structures but generally is less than MCE. Both PSHA and DSHA require an attenuation relationship which provides a means of predicting the level of ground shaking based on an earthquake magnitude, distance to earthquake source, site conditions, etc. As a result, PSHA and DSHA have pros and cons that should be considered according to the purpose and it is a

better practice to make both assessment studies for city-sized study areas. In the scope of this study, only DSHA will be carried out.

6.2 Deterministic Seismic Hazard Assessment of Simav Region

Deterministic approach includes individual earthquake scenarios as mentioned above. Simav graben is an active depression in which Simav County and numerous villages have been hit with large earthquakes recently. This provided up-to-date seismological information to assess the earthquake hazard.

6.2.1 Source Characterization

Major earthquake sources in the area are Simav Fault Zone (SFZ) and Naşa Fault Zone (NFZ). Due to short instrumental period, the seismic catalog shows maximum M_w 5.9 earthquake in the region. However, geological data show that these faults are capable of producing larger earthquakes. Therefore, MCE should be calculated using following formula proposed by Aydan et al. (2002).

$$L = 0.0014525M_s \times e^{1.31M_s} \quad (6.1)$$

The SFZ is a totally 80 km long zone of deformation characterized by normal faulting. It determines and controls the southern margin of the Simav graben. The Simav Fault Zone can produce a peak earthquake of M_s 6.74. The NFZ is another deformation zone of normal faulting bounding the northern margin of graben. It can produce a peak earthquake of M_s 5.34. Next step is selecting the correct attenuation relationship to be used throughout the analysis.

6.2.2 Selecting Reasonable Attenuation Relationship

While travelling in the ground, seismic waves lose their energy in terms of displacement, velocity and acceleration. This is called attenuation of a seismic wave. For this reason, earthquakes cannot be felt except from very sensitive recorders after a long distance. Attenuation relationship is an empirical definition that generally has log-normal distribution of different ground motion parameters that depend on

magnitude of the earthquake, distance to epicenter, faulting mechanism and site conditions. There are a number of attenuation relationships and the ones that will be discussed throughout this analysis are as follows: (a) Abrahamson and Silva (2008) Next Generation Attenuation (NGA) Model, (b) Boore and Atkinson (2008) NGA Model, (c) Campbell and Bozorgnia (2008) NGA Model, (d) Chiou and Youngs (2008) NGA Model, (e) Abrahamson and Silva (1997) Model, (f) Aydan et al. (2001) Model, (g) Ulusay et al. (2004) Model and (h) Kalkan and Gülkan (2004) Model.

It is essential to select correct attenuation relationship because they are developed from the earthquakes of different regions and different mechanisms. For this purpose, dataset of the attenuation relationship, comparison of PGA values calculated to accelerometer recordings are used. An example of accelerometer reading that is used for choosing attenuation relationships is seen on Table 6.1. In this example, resultant PGA is calculated by taking product of the PGA vectors in N-S, E-W and U-D directions.

Table 6-1: Earthquake and ground motion parameters of 24.05.2014 Gökçeada earthquake and properties of accelerometer installed in Simav County (ERD, 2014a)

STRONG GROUND MOTION RECORDS OF TURKIYE		
PLACE	:	KUTAHYA SIMAV HUKUMET KONAGI
EARTHQUAKE DATE	:	2014/05/24 09:25:00 (GMT)
EPICENTER COORDINATES	:	40.21080N-25.30730E
EARTHQUAKE DEPTH (km)	:	25.02
EARTHQUAKE MAGNITUDE	:	6.5 M_w
STATION ID	:	4309
STATION COORDINATES	:	39.09282N-28.97848E
STATION ALTITUDE (m)	:	828
RECORDER TYPE	:	GeoSig gmsplus
RECORDER SERIAL NO	:	101399
RECORD TIME	:	24/05/2014 09:25:28.0000 (GMT)
NUMBER OF DATA	:	27162
SAMPLING INTERVAL (sec)	:	0.01
RAW PGA VALUES (gal)	:	(N-S) 9.990711 (E-W) 8.592053 (U-D) 3.241706

The corresponding PGA vales on accelerometer readings are listed for different sized earthquakes from different sources and faulting mechanisms. Since the earthquake

parameters and site conditions of site of accelerometer should be known, they can be input to the attenuation relationship equations to select the correct attenuation relationship for the rest of the process. Some of the earthquakes are measured in local magnitude (M_L) and some attenuation relationships are designed for moment magnitude (M_w). Therefore a conversion is done by using the equations developed by Ulusay et al. (2004) based on Turkish earthquake data (Figure 6.1).

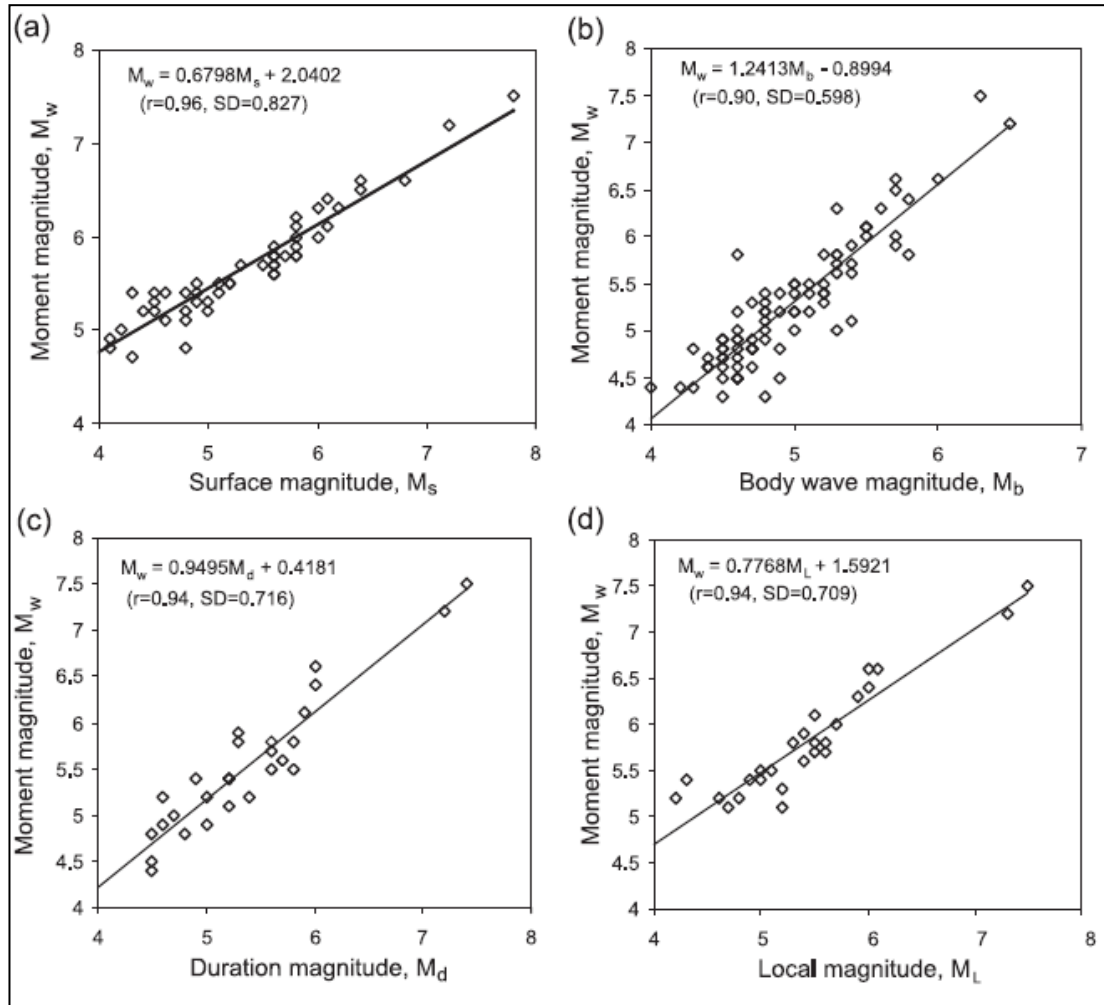


Figure 6-1: Correlations between earthquake magnitude values for Turkish earthquake catalogue (r : correlation coefficient; S.D.: standard deviation) (Ulusay et al., 2004).

The followings are the selected earthquakes of which accelerometer readings are available in the Simav and adjacent areas (Table 6.2).

Table 6-2: Accelerometer readings that are selected for attenuation relationship

Earthquake	Magnitude		Focal depth (km)	Location	PGA records (gal)			PGA (gal)	Epicenter Distance (km)	$V_{s,30}$ (m/s)
	Ml	Mw			N-S	E-W	U-D			
3.5.2012	5,4	5,8	10,9	Gediz	51	65	35	89,73	30	259
16.4.2012	4,7	5,2	6,9	Simav	31,5	19,79	14	39,75	13	259
19.5.2011	5,7	6,0	29	Gediz	91,83	104,6	67,1	154,5	11	343
15.9.2009	3,9	4,6	8,6	Simav	24,98	18,75	20,7	37,49	6,9	259

$V_{s,30}$: Shear wave velocity for 30 m depth, PGA: Peak ground acceleration

After selecting the accelerometer data, applicable and available attenuation models are employed to calculate peak ground acceleration (PGA) by using the parameters listed in Table 6.2. Abrahamson and Silva (2008) NGA Model, Boore and Atkinson (2008) NGA Model, Campbell and Bozorgnia (2008) NGA Model and Chiou and Youngs (2008) NGA Model PGA values are calculated by using the next generation attenuation (NGA) ground motion prediction equation program (Bozorgnia, 2014). Abrahamson & Silva (1997) Model PGA value is calculated by using attenuation relationship plotter (OpenSHA, 2014). Aydan et al, (2001) Model PGA value is calculated by using the formula below:

$$a_{max} = 2.8(e^{0.9M_s} - 1)e^{-0.025R} \quad (6.2)$$

Kalkan and Gülkan (2004) is calculated using equation 6.3.

$$\ln Y = b_1 + b_2(M - 6) + b_3(M - 6)^2 + b_5 \ln(r_{cl}^2 + h^2) + b_v \ln(V_s/V_A) \quad (6.3)$$

where b_1 , b_2 , b_3 , b_5 , h , b_v , V_A are the coefficients for attenuation relationship found by regression, M is earthquake magnitude, V_s is the shear wave velocity and r_{cl} is the distance to the horizontal projection of the rupture. Lastly Ulusay et al. (2004) Model PGA value is calculated by using the formula below:

$$PGA = 2,18 \times e^{(0,0218(33,3 \times M_w - R_e + 7,8427 \times S_A + 18,9282 \times S_B)} \quad (6.4)$$

In equation 6.4 M_w is earthquake magnitude, R_e is the epicentral distance and S_A to S_B are site condition parameters ($S_A = S_B = 0$ for rock sites, $S_A = 1$ and $S_B = 0$ for soil sites, and $S_A = 0$ and $S_B = 1$ for soft soil sites). Calculation results of PGA values for each earthquake and accelerometer readings are listed on Table 6.3.

Table 6.3: Recorded PGA values and calculated PGA values from attenuation relationships

Earthquake	3.5.2012	16.4.2012	19.5.2011	15.9.2009	Pearson's Correlation Coefficient (r)
Accelerometer PGA (g)	0.09	0.04	0.15	0.04	
Abrahamson & Silva 2008 PGA (g)	0.05	0.10	0.17	0.13	0.47
Campbell & Bozorgnia 2008 PGA (g)	0.06	0.08	0.15	0.07	0.79
Boore & Atkinson 2008 PGA (g)	0.07	0.11	0.19	0.11	0.67
Chiou & Youngs 2008 PGA (g)	0.04	0.09	0.16	0.09	0.61
Kalkan and Gülkan 1996 PGA (g)	0.08	0.12	0.21	0.12	0.71
Ulusay et al. (2004) PGA (g)	0.08	0.07	0.14	0.05	0.94
Abrahamson & Silva (1997) PGA (g)	0.06	0.09	0.22	0.09	0.80
Aydan et al. (2001) PGA (g)	0,07	0,05	0,15	0,03	0,97

In order to make a proper selection, Pearson's correlation coefficient is calculated. The coefficients indicated that Aydan et al. (2004) and Ulusay et al. (2004) attenuation relationships give the best fitting results. Since Ulusay et al. (2004) attenuation relationship considers site conditions, it is selected for DSHA.

6.2.3 Calculating Ground Motion

After selecting the most suitable attenuation relationship, study area is gridded down to 0.5x0.5 km grids. Each grid has been assigned with ground parameters described in Ulusay et al. (2004). Granites, metamorphic rocks and basalt are assigned as $S_A = S_B = 0$. Older graben fills are assigned as $S_A = 1$ and $S_B = 0$. Simav modern graben fill is assigned as $S_A = 0$ and $S_B = 1$. Maximum credible earthquakes were assigned to

SFZ and NFZ, using equation in Figure 6.1. Therefore, maximum $M_w=6.73$ for SFZ and $M_w=5.34$ for NFZ. Distances of each grid to the faults were calculated. PGA values calculated for each point were interpolated and then the deterministic seismic hazard map was prepared for the Simav graben and its near environ (Figure 6.2).

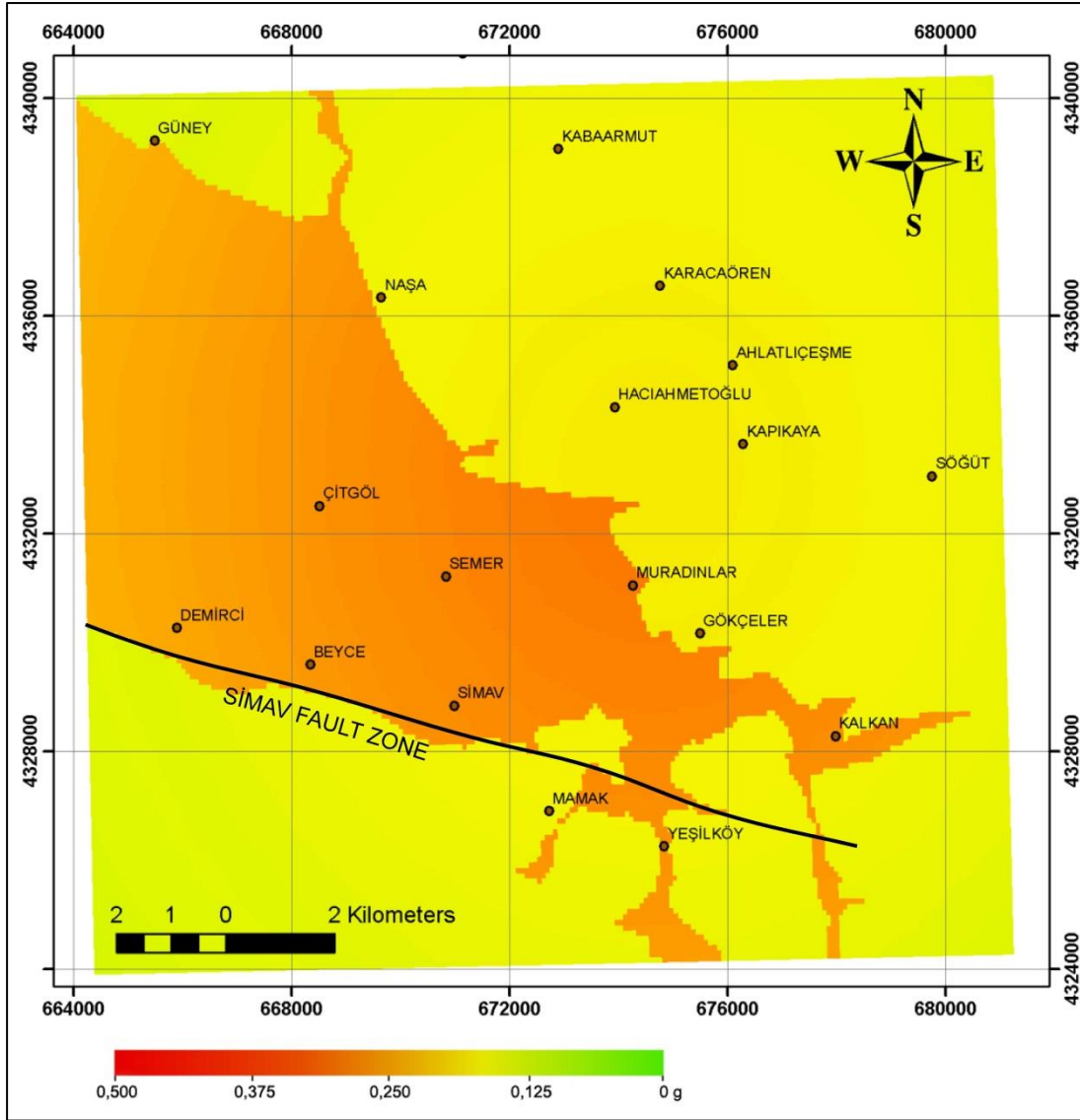


Figure 6-2: Deterministic seismic hazard map of Simav region prepared by using Ulusay et al. (2004) attenuation relationship formula and $M_w = 6.73$ scenario earthquake sourced from Simav fault zone.

Figure 6.2 shows that the peak ground acceleration (PGA) changes from 0.208 g to 0.398 g in the study area according to the site conditions and distance.

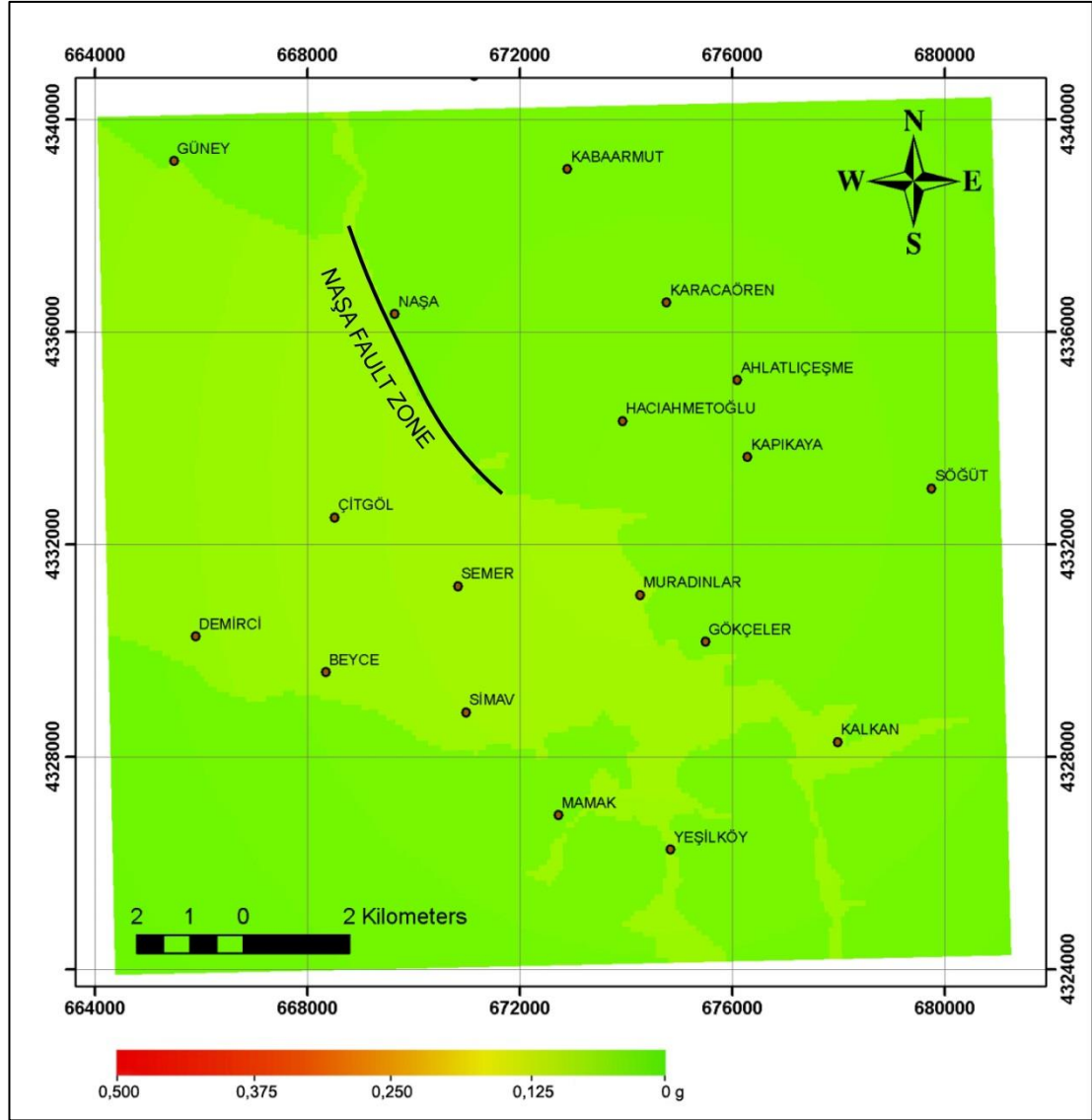


Figure 6-3: Deterministic seismic hazard map of Simav region prepared by using Ulusay et al. (2004) attenuation relationship formula and $M_w = 5.34$ scenario earthquake sourced from Naşa fault zone.

Figure 6.3 shows that the peak ground acceleration (PGA) changes from 0.076 g to 0.145 g in the study area. The calculated ground motions resulting from rupture of other fault segments are lower than the ones for Naşa fault zone. Therefore, apart from earthquake scenario sourced from Simav fault zone, only the scenario sourced from Naşa fault zone is included for comparison. For any calculation, major controlling factor for seismic hazard is ground conditions. Maximum PGA value for Simav County center is calculated 0.398g.

CHAPTER VII

CONCLUSIONS

In the light of the analysis of data collected in the field and the literature, the followings are concluded:

- 1) Three distinct paleostress orientations were found and ascribed to the different phases of deformation.
- 2) The units in the Akdere and Selendi grabens show that those grabens were active depocenters during the Latest Oligocene-Middle Miocene period. Later this deposition was interrupted and this interruption is recorded by angular unconformity between the deformed (folded) Miocene units and the Quaternary undeformed sedimentary package (modern or neotectonic graben fill).
- 3) Proposed tectonic evolution of the Akdere and Simav graben is episodic. According to field-based data and literature data of other disciplines of earth sciences, 1st phase is N-S extensional phase, 2nd phase is E-W extensional phase controlling the graben formation along the Demirci and Selendi paleobasins. 3rd phase is the NW-SE compressional phase, which deformed both the Demirci and Selendi paleotectonic grabens and their older fills. The 4th phase is the NNE-SSW extensional (neotectonic) phase which is still controlling the Simav graben formation and the reactivation of faults in the Akdere graben.
- 4) Simav Fault Zone is an active deformation zone let to the occurrence of both the historical and instrumental periods' earthquakes. Epicenter distribution and focus depths of the recent earthquakes indicate that their epicenters and foci should extend towards the further north and outside the of the Simav

graben, they are not located in the south of the Simav graben. This conclusion contradicts with the strike slip-faulting mechanism for the origins of recent earthquakes proposed by other authors.

- 5) Focal mechanism solutions of the 16 earthquakes occurred in the study area display either pure normal faulting or normal faulting with small amount of strike-slip component. Statistical mean of tension and pressure axes of the focal mechanism shows NNE-SSW extension in the study area.
- 6) Epicenter location and focal mechanism solution of the 19 May 2011 Simav earthquake indicate a normal faulting mechanism. Hence most reasonable candidates for the earthquake sources are the Nadarçamı and/or the Seyirkaya faults comprising the Simav Fault Zone. Since the dip of nodal plane of focal mechanism around 40° whereas dip amounts of the faults at the surface are around 75° , earthquakes might have been resulted from a normal fault with a listric geometry. According to analysis of the GPS velocities by using VISR2 software, extension around the the Simav graben is in the NNE-SSW direction. These results fit well with the World Stress Map project horizontal stress directions.
- 7) Seismic hazard assessment of the Simav graben shows that there is a high earthquake hazard potential. According to deterministic seismic hazard analysis by using Ulusay et al. (2004), the maximum PGA in the study area is 0.40g in the soil site conditions. It should be noted that detailed in-situ geotechnical tests are definitely required for site classification. The site classification method used in this study is based on geological map and gives a general idea about site specific ground motion.

REFERENCES

- Abrahamson, N.A., 2000. State of the practice of seismic hazard evaluation. GEOENG 2000 Conference Proceedings, Melbourne, Australia.
- Abrahamson, N.A., (2006). Notes on Probabilistic Seismic Hazard Analysis – An Overview. Rose School, Pavia, Italy.
- Abrahamson, N. A., and W. J. Silva (1997), Empirical Response Spectral Attenuation Relations for Shallow Crustal Earthquakes, Seismological Research Letters, 68(1), 94-127.
- Abrahamson, N., and W. Silva (2008). Summary of the Abrahamson & Silva NGA Ground-Motion Relations. Earthquake Spectra 24, 67--97. Atkinson, G. M., and D. M. Boore (2011). Modifications to Existing Ground-Motion Prediction Equations in Light of New Data. Bulletin of the Seismological Society of America 101, 1121--1135.
- Akay, E., (2009). Geology and petrology of the Simav Magmatic Complex (NW Anatolia) and its comparison with the Oligo-Miocene granitoids in NW Anatolia: implications on Tertiary tectonic evolution of the region. Int Geol Rev 98: 1655–1675.
- Akdeniz, N., 1980, Başlamış Formasyonu, Jeoloji Mühendisliği, v. 10 s.39-47
- Akdeniz, N., ve Konak, N. (1979). Simav-Emet-Tavşanlı-Dursunbey-Demirci yörelerinin jeolojisi. yayınlanmamış MTA Raporu. No:6547.
- Aktug, B., J. M. Nocquet, A. Cingoz, B. Parsons, Y. Ercan, P. C. England, O. Lenk, M. A. Gurdal, A. Kilicoglu, H. Akdeniz, and A. Tekgul (2009), Deformation of western Turkey from a combination of permanent and campaign GPS data: limits to block-like behaviour, Journal of Geophysical Research, 114, B10404.

- Ambraseys, N. (2009). *Earthquakes in the Mediterranean and Middle East: a multidisciplinary study of seismicity up to 1900*. Cambridge University Press.
- Angelier, J., (1989), Data base for tectonic orientations "Tector" Version 5.42, aug87-oct88-dec88-aou89 Copyright 1987, 1988, 1989.
- Angelier, J., (1994). Fault slip analysis and paleostress reconstruction. In: Hancock, P.L. (Ed.), *Continental Deformation*. Pergamon Press, Oxford, pp. 53–100.
- Aydan, Ö., Sedaki, M., & Yarar, R. 1996. The seismic characteristics of Turkish earthquakes. In: *Proceedings of Eleventh World Conference on Earthquake Engineering*. Paper no. 1270.
- Aydan, Ö, H. Kumsar, R. Ulusay (2002): How to infer the possible mechanism and characteristics of earthquakes from the strations and ground surface traces of existing faults. *JSCCE, Earthquake and Structural Engineering Division*, Vol. 19, No.2, 199-208.
- Bingöl, E., Delaloye, M., Ataman, G., 1982, Granitic intrusions in western Anatolia: a contribution to the geodynamic study of this area, *Eclogae Geologicae Helvetica*, 75,
- Boore, D. M., and G. M. Atkinson (2008). Ground-Motion Prediction Equations for the Average Horizontal Component of PGA, PGV, and 5%-Damped PSA at Spectral Periods between 0.01 s and 10.0 s. *Earthquake Spectra* 24, 99--138.
- Borsy, J., Ferrara, G., Innocenti, F. ve Mazzuoli, R., 1972. Geochronology and petrology of recent volcanics in the eastern Aegean Sea (West Anatolia and Lesvos Iceland). *Bullettin of Volcanology*, 36, 473-496.
- Bozkurt, E., (2002) Discussion on the Extensional Folding in the Alaşehir (Gediz) Graben, Western Turkey. "*Journal of Geological Society*", 179, p.105-109.
- Bozkurt, E. and Park, R. G., 1994. Southern Menderes Massif: an incipient metamorphic core complex in western Anatolia, Turkey. *Journal of the Geological Society*, London 151, 213-216.

- Bozkurt, E. and Mittwede, S. (2001) 'Introduction to the Geology of Turkey—A Synthesis', *International Geology Review*, 43: 7, 578 — 594
- Bozkurt, E. and Sözbilir, H., 2004. Tectonic Evolution of the Gediz Graben: Field Evidence for an Episodic, Two-Stage Extension in Western Turkey. *Geological Magazine* 141, 63–79.
- Bozkurt, E. and Rojay, B., 2005. Episodic, Two-Stage Neogene Extension and Short-Term Intervening Compression in Western Anatolia: Field Evidence from the Kiraz Basin and Bozdağ Horst. *Geodinamica Acta* 18, 299-312.
- Bozkurt, E., Satır, M. & Buğdaycıoğlu, Ç., (2011) Surprisingly young Rb/Sr ages from the Simav extensional detachment fault zone, northern Menderes Massif, Turkey. "Journal of Geodynamics", 52, p.406-431.
- Bozorgnia, Y. (2014, July 15), Next Generation Attenuation (NGA) Models. Retrieved from http://peer.berkeley.edu/ngawest/nga_models.html
- Campbell, K. W., and Y. Bozorgnia (2008). NGA Ground Motion Model for the Geometric Mean Horizontal Component of PGA, PGV, PGD, and 5% Damped Linear Elastic Response Spectra for Periods Ranging from 0.01 to 10 s. *Earthquake Spectra* 24, 139--171.
- Chiou, B. S.-J., and R. R. Youngs (2008). An NGA Model for the Average Horizontal Component of Peak Ground Motion and Response Spectra. *Earthquake Spectra* 24, 173--215.
- Collins, A., Robertson, A.H.F., 1998. Processes of Late Cretaceous to Late Miocene episodic thrust-sheet translation in the Lycian Taurides, southwest Turkey. *Journal of the Geological Society (London)* 155, 759 – 772
- Çağlayan, A., (2012), Kütahya-Simav-Demirciköy KSD-2011/7 Jeotermal Enerji Araştırma Sondajı Kuyu Bitirme Raporu, MTA Report. Compilation no:11527, Ankara. (Unpublished)
- Delvaux, D., Sperner, B., 2003, New aspects of tectonic stress inversion with reference to the Tensor program. In: NIEUWLAND, D. A. (ed.) *New Insights into*

Structural Interpretation and Modelling, Geological Society, London, Special Publications, 212, 75-100

Dewey, J.F., 1988, Extensional collapse of orogens: Tectonics, v. 7, p. 1123-1139.

Dewey, J.F. and Sengor, A.M.C., 1979. Aegean and surrounding regions: complex multiplate and continuum tectonics in a convergent zone: Geol. Soc. Amer. Bull., 90, 84-92.

Doğan, A. ve Emre, Ö., 2006, Ege Graben Sistemi'nin Kuzey Sınırı: Sındırgı-Sincanlı Fay Zonu. 59. Türkiye Jeoloji Kurultayı, 20-24 Mart 2006, Bildiri Özleri Kitabı, s. 83-84, Ankara.

Ercan, E., Dinçel, A., Metin, S., Türkecan, A. ve Günay, A. 1978. Uşak yöresindeki Neojen havzalarının jeolojisi. Bulletin of the Geological Society of Turkey, 21, 97-106.

Ercan, E., Satır, M., Sevin, D., Türkecan, A., 1996. Some new radiometric ages from Tertiary and Quaternary volcanic rocks from West Anatolia. Bulletin Mineral Research and Exploration Institute (Turkey), 119, 103-112.

Ercan, T., Günay, E. ve Savaşçın, M.Y. (1984). Simav ve çevresindeki Senozoyik yaşlı volkanizmanın bölgesel yorumlanması. MTA Dergisi, (97), 86-101.

ERD (Earthquake Research Department) (2014a, July 15), Strong-Motion Database. Retrieved from <http://kyh.deprem.gov.tr/ftpe.htm>

ERD (Earthquake Research Department) (2014b, July 15), Earthquake catalogue. Retrieved from <http://www.deprem.gov.tr>

Ergin, K., Güçlü, U., Uz, Z., 1967. Türkiye ve civarının Deprem Kataloğu (Milattan sonra 11 yılından 1964 sonuna kadar). İ.T.Ü., Maden Fak. Arz Fiziği Yayınları 24, 169 s.

Eriñç, T. Bilgin, M. Bener, K. Ata Sungur, S. Erer ve K. Göçmen, (1970) Gediz Depremi. Tatbikî Jeomorfolojik Etüd: İstanbul Üniversitesi Coğrafya Enstitüsü Yayınları, no. 60.

- Erişen, B., Dokuz, İ., Taşkın, İ., Yıldırım, N., (1985), Simav Eynal Kütahya Jeotermal Alanı Eynal-2 ve Eynal-3 Sondajları Kuyu Bitirme Raporu, MTA Report. Compilation no:7916, Ankara. (Unpublished)
- Erişen, B., Yıldırım, N., (1986), Simav Çitgöl Kütahya Jeotermal Alanı Çitgöl-1 Sondajı Kuyu Bitirme Raporu, MTA Report. Compilation no:8055, Ankara. (Unpublished)
- Erişen, B., Can, A., Yıldırım, N., (1989), Simav Eynal Jeotermal Alanı EJ1 ve EJ2 Jeotermal Sondajları Kuyu Bitirme Raporu, MTA Report. Compilation no:8916, Ankara. (Unpublished)
- Erkan, B., (1978), Simav Eynal J2 Kuyusu Sondaj Bitirme Raporu, MTA Report. Compilation no:8569, Ankara. (Unpublished)
- Erkan, B., Arslan, S., Başıkara, M., (1977), Simav Eynal J1 Kuyusu Sondaj Bitirme Raporu, MTA Report. Compilation no:8570, Ankara. (Unpublished)
- Ersoy, E.Y., Helvacı, C., Sözbilir, H., 2010. Tectono-stratigraphic evolution of the NE–SW-trending superimposed Selendi basin: implications for late Cenozoic crustal extension in Western Anatolia, Turkey. *Tectonophysics* 488, 210–232.
- Eyidoğan, H., and Jackson, J., A., 1985, A seismological study of normal faulting in the Demirci, Alaşehir and Gediz earthquake of 1969-1970 in western Turkey: implications for the nature and geometry of deformation in the continental crust, *Geophysical Journal of Royal Astronomical Society*, 81, 569-607.
- Ferrill, D. A. & Morris, A. P. 2001. Displacement gradient and deformation in normal fault systems. *Journal of Structural Geology* 23, 619–38.
- Gessner, K., Ring, U., Johnson, C., Hetzel, R., Passchier, C.W., Güngör, T., 2001. An active bivergent rolling-hinge detachment system: central Menderes metamorphic core complex in western Turkey. *Geology* 29, 611–614.
- Gürboğa, Ş., Koçyiğit A., and Ruffet, G., 2013. Episodic two-stage extensional evolutionary model for southwestern Anatolian graben–horst system: New field data

from the Erdođmuş-Yenigediz graben (Kütahya). *Journal of Geodynamics*, volume 65, p. 179-198.

Güven, M., Taşkın, İ., (1985), Simav Naşa Kütahya Sıcaksu Sondajı Kuyu Bitirme Raporu MTA Report. Compilation no:7903, Ankara. (Unpublished)

Hasözbek, A., Akay, E., Erdođan, B., Satır, M., Siebel, W., 2010a, Early Miocene granite formation by detachment tectonics or not? A case study from the northern Menderes Massif (Western Turkey). *Journal of Geodynamics* 50: 67-80

Hasözbek, Satır, M., Erdođan, B., A., Akay, E., Siebel, W., 2010b Early Miocene post-collisional magmatism in NW Turkey: geochemical and geochronological constraints. *International Geology Review* DOI: 10.1080/00206810903579302

Heidbach, O., Tingay, M., Barth, A., Reinecker, J., Kurfeß, D., and Müller, B., (2008) The World Stress Map database release 2008

Hempton, M.R., 1987. Constraints on Arabian plate motion and extensional history of the Red Sea. *Tectonics* 6, 687-705.

Işık, V., Seyitođlu, G. & Cemen, I. 2003. Ductile-brittle transition along the Alasehir shear zone and its structural relationship with the Simav detachment, Menderes massif, western Turkey. *Tectonophysics* 374, 1-18

Işık, V., Tekeli, O., Seyitođlu, G., 2004. The $^{40}\text{Ar}/^{39}\text{Ar}$ age of extensional ductile deformation and granitoid intrusion in the northern Menderes core complex: implications for the initiation of extensional tectonics in western Turkey. *Journal of Asian Earth Sciences* 23, 555–566.

Kahle H.-G., Straub C., Reilinger R., McClusky S., King R., Hurst K., Veis G., Kastens K., Cross P. 1998, The strain rate field in the eastern Mediterranean region, estimated by repeated GPS measurements. *Tectonophysics*; 294: 237-252.

Kalafat, D., Güneş, Y., Kekovalı, K., Kara, M., Deniz, P., Yılmaz, M. (2011) Bütünleştirilmiş Homojen Türkiye Deprem Katalođu (1900-2010; $M \geq 4.0$), Bođaziçi Üniversitesi, Kandilli Rasathanesi ve Deprem Araştırma Enstitüsü.

Kalafat, D., Polat, R., Poyraz , S., A. Kekovali K. and Akkoyunlu M.F., (2012). 19 May 2011 Simav Earthquake Sequence : Western Turkey, Geophysical Research Abstracts Vol. 14, EGU 2012-13091, 2012, 33rd General Assembly of the European Seismological Commission EGU General Assembly 2012, August 19-24, Moscow, Russia

Kalkan E. and Gülkan, P. 2004, Site-Dependent Spectra Derived from Ground motion Records in Turkey, Earthquake Spectra, Volume 20, No. 4, 1111-1138.

Kaya, O., 1972, Tavşanlı yöresi 'ofiyolit' sorununun ana-çizgileri: Türkiye Jeol. Kur. Bült., 15. 26-100

Koçyiğit, A., 1984. Güneybatı Türkiye Ve Yakın Dolayında Levha İçi Yeni Tektonik Gelişim, Geological Society of Turkey Bulletin 27, 1-16.

Koçyiğit, A., 2005. Denizli Graben-Horst System and the Eastern Limit of the West Anatolian Continental Extension: Basin Fill, Structure, Deformational Mode, Throw Amount and Episodic Evolutionary History, Sw Turkey. Geodinamica Acta 18, 167–208.

Koçyiğit, A., Yusufoglu, H. ve Bozkurt, E. 1999. Evidence from the Gediz graben for episodic two-stage extension in western Turkey. Journal of the Geological Society, London 156, 605-616.

Koçyiğit, A., Ünay, E. and Saraç, G., 2000. Episodic Graben Formation and Extensional Neotectonic Regime in West Central Anatolia and the Isparta Angle: A Key Study in the Akşehir-Afyon Graben, Turkey. In: Bozkurt, E., Winchester, J.A. and Piper, J.D.A. (Eds), Tectonics and Magmatism in Turkey and the Surrounding Area. Geological Society, London, Special Publications 173, 405–421.

Koçyiğit, A. and Özacar, A., 2003. Extensional Neotectonic Regime through the NE Edge of the Outer Isparta Angle, Sw Turkey: New Field and Seismic Data. Turkish Journal of Earth Sciences 12, 67–90.

Koçyiğit, A., and Deveci, Ş., 2005. Akşehir-Simav Fault System: commencement age of neotectonic regime and seismicity, SW Turkey. Deprem Sempozyumu, Kocaeli 2005, Özler Kitabı, s.26.

Konak, N., 1982, Simav dolayının jeolojisi ve metamorf kayaçların evrimi. İstanbul Yerbilimleri, 3, 313-337.

Le Pichon X. & Angelier, J., 1979, The Hellenic arc and Trench system: a key to the neotectonic Evolution of the Eastern Mediterranean Area: Tectonophysics, 60, 1-42.

McClusky S, Balassanian S, Barka A, Demir C, Ergintav S, Georgiev I, Gurkan O, Hamburger M, Hurst K, Kahle H, Kastens K, Kekelidze G, King R, Kotzev V, Lenk O, Mahmoud S, Mishin A, Nadariya M, Ouzounis A, Paradissis D, Peter Y, Prilepin M, Reilinger R, Sanli I, Seeger H, Tealeb A, Toksoz MN, Veis G., 2000, Global Positioning System constraints on plate kinematics and dynamics in the eastern Mediterranean and Caucasus. Journal of Geophysical Research-Solid Earth, 105 (B3): 5695-5719.

McGuire, K., 2001, Deterministic vs. probabilistic earthquake hazards and risks, Soil Dynamics and Earthquake Engineering, 21/5 377-384

McKenzie, D. P., 1978. Active tectonics of the Alpine-Himalayan belt: the Aegean and surrounding regions. Geophysical Journal of the Royal Astronomical Society 55, 217-254.

Meulenkamp, J.E., Wortel, M.J.R., Van Wamel, W.A., Spakman, W. & Strating, E.H. 1988. On the Hellenic subduction zone and the geodynamic evolution of Crete since the late Middle Miocene. Tectonophysics, 146, 203-215.

Morley, C. K., Nelson, R. A., Patton, T. L. & Munn, S. G. 1990. Transfer zones in the East African rift system and their relevance to hydrocarbon exploration in rifts. Bulletin of the American Association of Petroleum Geologists 74, 1234-53.

OpenSHA. (2014, July 18), Attenuation Relationship Plotter. Retrieved from <http://www.opensha.org/apps-AttenuationRelationship>

Oral, M.B., Reilinger, R., Toksoz, R., 1992. Deformation of the Anatolian block as deduced from GPS measurements. Transactions, American Geophysical Union, EOS 73, 120.

Oygür, V. ve Erler, A. 2000. Simav grabeninin metalojenisi (İç-Batı Anadolu, Türkiye). Türkiye Jeoloji Bülteni, 43(1), 7-19

Emre. Ö., Duman, T. Y., Özalp, S., Elmacı, H., Olgun, Ş. ve Şaroğlu, F. 2013, 1/1.125.000 Ölçekli Türkiye Diri Fay Haritası, Maden Tetkik ve Arama Genel Müdürlüğü Özel Yayınlar Serisi-, Ankara, Türkiye

Öcal, N., 1968, 1938-1955 yılları arasında Anadolu'da vukubulan bazı şiddetli zelzelelerde faylanma doğrultuları, M.E.H. Kandilli Rasathanesi , Sismoloji Yayınları No:2, İstanbul

Öztunalı, Ö., 1973, Uludağ (Kuzeybatı Anadolu) ve Eğrigöz (Batı Anadolu) Masiflerinin Petrolojileri ve Jeokronolojileri: İstanbul Üniv. Fen Fak. Monog., No 23, İstanbul, 115 s.

Pinar, N., Lahn, E., & Turkey. (1952). Türkiye depremleri izahli katalogu. Ankara: AKIN Matbaacılık Ltd. Ortaklığı.

Purvis, M. and Robertson, A.H.F., 2004. A pulsed extension model for the Neogene–Recent E–W trending Alaşehir Graben and the NE–SW trending Selendi and Gördes Basins, western Turkey. *Tectonophysics* 391, 171– 201.

Purvis, M. and Robertson, A.H.F., 2005. Miocene sedimentary evolution of the NE–SW-trending Selendi and Gördes Basins, Western Turkey: implications for extensional processes. *Sedimentary Geology* 174, 31-62.

Reilinger, R.E., McClusky, S.C., Oral, M.B., King, R.W., Toksoz, M.N., Barka, A.A., Kinik, I., Lenk, O. and Sanli, I. (1997). Global Positioning System measurements of present-day crustal movements in the Arabia-Africa-Eurasia plate collision zone. *Journal of Geophysical Research* 102: doi: 10.1029/96JB03736. issn: 0148-0227.

Reilinger, R., et al., 2006. GPS constraints on continental deformation in the Africa–Arabia–Eurasia continental collision zone and implications for the dynamics of plate interactions. *Journal of Geophysical Research* 111 (B05411), <http://dx.doi.org/10.1029/2005JB004051>.

- Reischmann, T., Kröner, A., Todt, W., Dürr, S., Şengör, A.M.C., 1991, Episodes of crustal growth in the Menderes Massif, W Turkey, inferred from zircon dating, *Terra Abstracts*, 3, 34.
- Ring, U., Johnson, C., Hetzel, R., Gessner, K., 2003. Tectonic denudation of a Late Cretaceous–Tertiary collisional belt: regionally symmetric cooling patterns and their relation to extensional faults in the Anatolide belt of western Turkey. *Geological Magazine* 140, 421–441.
- Ring, U. and Collins, A.S., 2005. U–Pb SIMS dating of syn-kinematic granites: timing of core-complex formation in the northern Anatolide belt of western Turkey. *Journal of the Geological Society, London* 162, 289–298.
- Rojay, B., Toprak, V., Demirci, C. and Süzen, L., Plio-Quaternary evolution of the Küçük Menderes Graben (Western Anatolia, Turkey). "*Geodinamica Acta*"18, (2005), p.317-331.
- Royden, L.H. (1993). Evolution of retreating subduction boundaries formed during continental collision. *Tectonics* 12: doi: 10.1029/92TC02641. issn: 0278-7407.
- Seyitoğlu, G., 1997, Late Cenozoic tectono-sedimentary development of the Selendi and Uşak–Güre basins: a contribution to the discussion on the development of east–west and north trending basins in western Turkey, *Geological Magazine*, 134, 163–75.
- Seyitoglu, G. & Scott, B. C., 1991. Late Cenozoic crustal extension and basin formation in west Turkey. *Geological Magazine*, 128, 155-166.
- Seyitoglu, G. & Scott, B. C., 1992. The age of Buyiik Menderes Graben (west Turkey) and its tectonic implications. *Geological Magazine*, 129,239-242.
- Seyitoğlu, G. & Scott, B. C., 1996. The cause of N-S extensional tectonics in western Turkey: Tectonic escape vs. Back-arc spreading vs. Orogenic collapse. *Journal of Geodynamics*, 22, 145 - 153.

Shen, Z.K., Jackson, D.D., and Ge, B.X., 1996, Crustal deformation across and beyond the Los Angeles basin from geodetic measurements: *Journal of Geophysical Research*, v. 101, p. 27 957–27 980.

SSHAC (Senior Seismic Hazard Analysis Committee). (1997) Recommendations for Probabilistic Seismic Hazard Analysis: Guidance on Uncertainty and Use of Experts, US Nuclear Regulatory Commission report CR-6372, Washington DC.

Şengör, A. M. C., 1979. The North Anatolian transform fault: its age, offset and tectonic significance, *Jour. Geol. Soc. Lond.*, 136, pp. 269-282.

Şengör, A. M. C., 1987, Cross-fault and differential stretching of hanging walls in regions of low-angle normal faulting: examples from western Turkey, *Continental extensional tectonics*, M. P Coward, J. F Deway, P. L Hancock, (Eds.), Geological Society Special Publication, 28, 575-589.

Şengör, A. M. C., Görür, N. and Şaroğlu, F., 1985, Strike-slip faulting and related basin formation in zones of tectonic escape: Turkey as a case study, *Strike-slip Deformation, Basin Formation, and Sedimentation*, Soc. Econ. Paleont. Min. Spec. Pub. 37 (in honor of J.C. Crowell), 227-264, 1985.

Tekeli, O., Işık, V., Seyitoğlu, G. & Çemen, İ. 2001. The Ar40/ Ar39 age of ductile extension and granitoid intrusions in the northern Menderes Massif, western Turkey. 4th Int. Turkish Geology Symposium. Abstract, p. 226.

Thurber, C.H. (1992), Hypocenter velocity structure coupling in local earthquake tomography, *Phys. Earth Planet. Int.*, 75, 55-62.

Ulusay, R., Tuncay, E., Sönmez, H. and Gökçeoğlu, C., 2004. An attenuation relationship based on Turkish strong motion data and isoacceleration map of Turkey. *Engineering Geology*, 74(3-4), 265-291.

Wang, Z., (2009) Seismic hazard vs. seismic risk, *Seismological Research Letters*, vol. 80, 5, 2009, p.673-674

Westaway, R. (1990). Block rotation in western Turkey . Observational evidence. *Journal of Geophysical Research* 95: doi: 10.1029/90JB00700. issn: 0148-0227.

Yılmaz, Y., Genç, Ş.C., Gürer, F., Bozcu, M., Yılmaz, K., Karacık, Z., Altunkaynak, Fi. and Elmas, A., 2000. When Did The Western Anatolian Grabens Begin To Develop? In: Bozkurt, E., Winchester, J.A. and Piper, J.D.A. (Eds), Tectonics and Magmatism In Turkey and The Surrounding Area. Geological Society, London, Special Publications 173, 353–384.

Yolsal-Çevikbilen, S. Taymaz, T., and Helvacı, C. (2013). Earthquake mechanisms in the Gulfs of Gökova, Sığacık, Kuşadası, and the Simav Region (western Turkey): Neotectonics, seismotectonics and geodynamic implications, Tectonophysics, doi:10.1016/j.tecto.2014.05.001

Zeschke, G. (1954): Simav grabeni ve taşlan. T.J.K. Bült., c. V, sayı 1-2, s. 179-198, Ankara.

APPENDIX A

TABLES AND PLATES

Table A-1: Seismic parameters of the earthquakes with magnitudes larger than 3.5 occurred in the period of 1944-2014. Epicenter distribution of the Simav graben between 38.5-39.5N 28.5-29.5E coordinates. Data source: Earthquake Research Institute (ERD, 2014b)

No	Date	Time	Latitude	Longitude	Depth (km)	Magnitude
1	10.10.1900	08:41	38.800	29.400	10	5.6
2	16.10.1900	17:30	38.800	29.400	10	4.8
3	11.3.1902	18:00	38.930	29.380	10	4.4
4	12.7.1902	00:00	38.800	29.300	10	4
5	30.4.1905	16:01	38.810	28.520	10	6.1
6	2.5.1905	00:00	38.800	28.500	10	5.4
7	4.6.1905	16:00	38.950	28.670	10	4.8
8	30.7.1905	23:16	38.950	28.670	10	4.8
9	31.10.1907	03:50	38.500	28.500	10	4.5
10	25.6.1944	04:16	38.790	29.310	40	6
11	25.3.1966	23:17	38.960	29.290	43	4.4
12	5.6.1966	09:14	39.070	29.340	36	4.4
13	3.11.1968	18:40	38.810	29.110	23	4.8
14	3.11.1968	18:44	38.600	28.700	56	4.5
15	22.3.1969	18:00	39.100	28.670	28	4.7
16	24.3.1969	01:59	39.110	28.510	30	5
17	24.3.1969	02:58	39.150	28.600	4	4.5
18	24.3.1969	11:23	38.900	28.600	53	4.5
19	24.3.1969	11:34	39.170	28.700	37	4.6
20	24.3.1969	12:13	39.080	28.650	20	4.7
21	25.3.1969	13:28	38.780	28.510	40	4.8
22	25.3.1969	14:40	39.020	28.900	25	4.6
23	17.4.1969	12:23	39.110	28.620	10	4.6
24	30.4.1969	20:20	39.120	28.520	8	5.2
25	3.5.1969	16:07	39.000	28.600	25	4.7
26	13.5.1969	17:48	39.030	28.570	35	4.6
27	19.5.1969	15:27	39.120	28.580	10	4
28	22.6.1969	17:27	39.120	28.600	10	4.5
29	27.6.1969	10:40	39.300	28.700	10	4.3
30	7.10.1969	18:49	39.160	28.540	49	4.9
31	28.3.1970	21:59	39.280	29.460	17	4.8
32	28.3.1970	22:40	39.020	29.430	43	4.2
33	28.3.1970	22:59	39.130	29.000	10	4.1
34	29.3.1970	01:47	39.000	29.400	13	4
35	29.3.1970	01:51	39.260	28.500	33	4.3

Table A-1 (continued)

36	29.3.1970	02:05	39.290	29.180	38	4.5
37	29.3.1970	03:34	39.000	29.100	10	4.2
38	29.3.1970	07:58	39.290	29.200	2	4.3
39	29.3.1970	09:52	39.160	29.410	47	4.3
40	29.3.1970	19:11	39.140	29.420	22	4.7
41	29.3.1970	22:12	39.200	29.200	10	4.4
42	30.3.1970	06:46	39.090	29.030	23	4.5
43	30.3.1970	06:49	39.430	29.400	33	4.6
44	30.3.1970	07:59	39.340	29.260	16	5
45	30.3.1970	08:35	39.290	29.240	36	4.7
46	30.3.1970	09:26	39.010	29.400	18	4.3
47	30.3.1970	13:48	39.340	29.130	21	4.3
48	30.3.1970	20:59	39.300	29.290	33	4.6
49	31.3.1970	00:51	39.330	29.410	18	4.6
50	31.3.1970	01:07	39.410	29.320	25	4
51	31.3.1970	04:10	39.010	29.200	9	4.2
52	31.3.1970	07:30	39.120	29.160	43	5
53	31.3.1970	08:30	38.930	29.300	55	4
54	31.3.1970	16:08	39.030	29.490	37	4.4
55	1.4.1970	03:46	39.300	28.700	25	4.4
56	1.4.1970	08:02	38.900	28.800	54	4.9
57	1.4.1970	15:56	39.320	29.270	35	4.8
58	2.4.1970	02:45	38.960	29.440	10	4.3
59	2.4.1970	13:05	39.040	29.200	15	4.2
60	5.4.1970	12:29	39.310	29.180	10	4.3
61	6.4.1970	08:12	39.190	28.540	33	5.1
62	7.4.1970	04:12	39.320	29.090	33	4.4
63	7.4.1970	17:05	39.340	29.320	33	5.1
64	9.4.1970	10:12	39.110	29.410	34	4.7
65	9.4.1970	20:43	39.210	29.350	30	4.2
66	10.4.1970	01:14	39.130	29.310	22	4.2
67	10.4.1970	23:13	39.130	29.310	10	4.3
68	11.4.1970	08:36	39.100	28.800	49	4.7
69	13.4.1970	05:16	39.320	29.030	15	4.4
70	15.4.1970	16:29	39.340	29.300	28	4.6
71	16.4.1970	01:07	39.210	29.130	17	4.2
72	18.4.1970	05:37	39.220	29.380	16	4.3
73	18.4.1970	05:52	39.370	29.300	10	4.4
74	19.4.1970	22:09	38.900	29.300	45	4.5
75	20.4.1970	03:47	38.860	29.400	67	4.5
76	20.4.1970	18:36	38.700	29.200	88	4.6
77	22.4.1970	18:38	39.080	29.430	48	4.6
78	23.4.1970	09:01	39.130	28.650	28	5.3
79	24.4.1970	02:40	39.060	28.600	21	4.2
80	24.4.1970	05:49	38.990	29.200	36	4.2
81	24.4.1970	16:54	39.120	28.740	37	4.2

Table A-1 (continued)

82	26.4.1970	18:24	39.370	28.790	46	4.1
83	27.4.1970	10:39	38.970	29.330	17	4
84	30.4.1970	14:58	39.310	29.310	25	4.6
85	30.4.1970	16:44	39.320	29.220	24	4.7
86	10.5.1970	16:07	39.000	29.100	33	4.7
87	11.5.1970	09:58	39.360	29.320	10	4.5
88	12.5.1970	07:41	38.600	29.300	33	5
89	12.5.1970	08:33	38.970	28.990	51	4.5
90	14.5.1970	07:56	39.020	29.100	38	5.1
91	24.5.1970	08:24	39.250	28.900	33	4.3
92	26.5.1970	05:51	38.920	29.440	59	4.4
93	30.5.1970	06:43	39.230	29.420	18	4.3
94	30.5.1970	19:49	39.400	28.800	10	4.3
95	10.6.1970	05:17	39.150	29.460	43	4.4
96	14.6.1970	00:58	39.250	29.170	23	4.4
97	10.7.1970	05:36	39.160	28.600	12	4.2
98	29.8.1970	18:03	39.010	29.360	34	4.3
99	1.9.1970	02:19	38.970	29.240	53	4.7
100	14.9.1970	07:10	39.240	29.320	37	4.2
101	9.11.1970	06:42	39.000	28.900	64	4.1
102	15.11.1970	03:14	39.320	29.280	10	4
103	17.12.1970	02:17	39.270	29.400	26	4.7
104	20.12.1970	11:01	39.360	29.240	26	4.8
105	21.12.1970	00:22	39.090	29.410	27	4.5
106	15.2.1971	08:19	39.195	29.361	32	4.9
107	10.4.1971	13:21	38.833	29.144	20	4.6
108	27.4.1971	17:19	38.906	29.057	13.5	4.4
109	30.4.1971	16:44	39.190	28.520	5	4.3
110	14.3.1972	14:05	39.320	29.470	38	5.5
111	23.6.1972	17:16	39.159	29.169	19.7	4.2
112	25.9.1972	22:34	39.110	29.210	51	4
113	4.10.1972	06:14	39.140	29.438	34.3	4.6
114	8.2.1973	14:33	39.247	28.728	38.3	4.2
115	25.2.1973	14:55	38.920	29.390	18	4
116	18.3.1973	18:08	39.249	29.145	18.4	4.1
117	12.5.1973	09:31	38.889	29.211	5.1	4.5
118	24.6.1973	00:15	38.784	29.250	10	4.1
119	5.7.1973	21:12	38.803	29.216	42.7	4.5
120	29.8.1974	08:02	38.845	29.284	18.8	4.2
121	29.9.1974	03:55	38.745	29.460	10	4.1
122	5.11.1974	07:00	39.163	29.300	15.8	4.1
123	12.2.1975	01:48	39.142	28.997	15.1	4.2
124	23.2.1976	10:13	39.096	28.667	17	4.3
125	8.5.1976	23:25	39.331	29.097	32.5	4.8
126	9.5.1976	02:55	39.256	28.761	10	4.2
127	9.5.1976	11:19	39.002	28.770	10	4.3

Table A-1 (continued)

128	9.5.1976	15:01	39.308	29.117	19.9	4.2
129	10.5.1976	12:01	39.277	29.166	26.5	4.4
130	10.5.1976	15:20	39.201	29.106	10	4.2
131	10.5.1976	23:54	39.258	29.171	33.2	4.4
132	11.5.1976	03:31	39.193	29.196	10	4.3
133	12.5.1976	05:11	39.333	29.162	21	4.3
134	14.5.1976	11:06	39.260	29.220	10	4
135	21.5.1976	09:37	39.277	29.165	23.9	4.5
136	22.5.1976	18:01	39.250	29.179	10	4.1
137	25.5.1976	18:43	39.308	29.089	14	4.6
138	28.5.1976	23:02	39.259	29.170	8	4.5
139	28.5.1976	23:09	39.350	29.364	5	4.2
140	29.5.1976	03:45	39.371	29.343	3	4.2
141	31.5.1976	05:10	39.477	29.136	39.5	4.9
142	9.6.1976	10:02	39.243	29.150	12	4.7
143	11.6.1976	00:52	39.182	29.002	11	4.1
144	11.6.1976	09:55	39.322	29.225	2	4.2
145	14.6.1976	06:52	39.339	29.275	22.7	4.7
146	15.7.1976	12:06	39.367	29.064	11	4.1
147	22.8.1976	13:28	39.347	29.029	23.2	4.8
148	24.8.1976	18:44	39.339	29.136	10	4.9
149	9.12.1977	20:36	39.362	29.131	10	4.3
150	4.10.1978	09:04	39.300	29.330	10	4.6
151	9.9.1979	16:10	39.320	28.830	8	4
152	14.2.1980	20:14	39.103	29.347	10	4.4
153	2.3.1980	05:32	39.255	29.387	6	4.6
154	27.4.1980	09:54	39.072	28.863	37.6	4.3
155	3.5.1980	04:26	39.141	28.985	34.8	4.1
156	4.5.1980	09:22	39.223	28.966	21.6	4.5
157	8.5.1980	22:06	39.198	28.904	10	4.5
158	11.7.1980	12:24	38.797	29.169	10	4.3
159	15.11.1980	16:11	39.202	28.896	10	4.3
160	28.12.1981	14:52	39.331	29.120	16.5	4.3
161	28.12.1981	14:53	39.389	29.056	10	4.5
162	8.2.1982	11:20	39.328	29.047	13	4
163	14.3.1982	14:14	39.271	29.060	10	4.2
164	15.2.1983	02:21	39.067	28.705	7.3	4.6
165	23.2.1983	16:53	39.168	29.295	2.8	4.1
166	6.3.1983	09:53	39.103	28.675	11.5	4.3
167	11.10.1983	12:08	38.850	29.215	10	4.2
168	6.11.1983	05:17	39.334	29.316	14	4.6
169	27.6.1984	18:16	39.246	28.790	7.7	4.1
170	12.6.1986	06:42	39.086	28.698	10	4.1
171	19.8.1986	06:03	39.038	28.786	10	4.7
172	14.11.1986	03:38	39.361	29.062	10	4.5
173	15.11.1986	21:52	39.372	28.905	10	4.5

Table A-1 (continued)

174	3.9.1990	14:16	39.050	28.510	11	3.9
175	27.2.1991	17:37	38.740	29.330	1	3.7
176	27.2.1991	18:02	39.090	29.380	1	3.8
177	22.4.1991	20:38	38.920	28.800	10	3.6
178	18.6.1991	14:38	39.210	29.410	11	3.7
179	11.7.1991	18:41	39.410	29.460	18	3.6
180	3.8.1991	18:11	39.120	28.600	20	3.5
181	1.4.1992	12:23	39.400	28.680	12	4
182	1.4.1992	12:36	39.430	28.710	10	3.7
183	6.4.1992	19:15	38.971	29.210	4.6	4.3
184	15.6.1992	04:21	39.110	29.420	11	3.9
185	22.12.1992	22:15	39.290	28.802	10	4
186	23.12.1992	23:02	39.330	28.800	9	3.7
187	24.12.1992	13:03	39.310	28.810	11	3.6
188	25.12.1992	22:36	39.220	28.820	10	3.9
189	9.3.1993	09:41	39.162	28.797	10	4.1
190	30.5.1993	15:42	39.293	29.115	4	4.1
191	18.2.1994	23:23	38.930	29.040	1	3.5
192	19.5.1994	11:46	38.610	28.510	1	3.8
193	21.5.1994	09:31	38.630	28.860	1	3.8
194	25.6.1994	18:45	39.295	29.178	6	4
195	8.7.1994	23:08	39.319	29.140	10	4
196	15.7.1994	23:54	39.333	29.198	1	4
197	8.8.1994	05:28	38.975	29.145	44	4
198	10.9.1994	06:50	39.250	28.860	1	3.5
199	29.10.1995	13:35	38.510	29.000	11	3.6
200	5.6.1998	22:31	38.960	28.780	10.8	3.5
201	29.9.1999	16:46	39.099	28.995	3.3	4.1
202	18.1.2002	21:15	39.250	29.470	1	3.5
203	5.9.2002	00:26	38.650	29.020	9.8	3.7
204	18.9.2002	21:40	39.340	29.160	5.2	3.5
205	14.1.2005	02:19	39.121	28.563	18.9	3.7
206	8.8.2005	02:05	39.122	28.854	20	3.5
207	23.4.2006	22:58	38.823	29.345	10	3.5
208	8.7.2007	12:39	39.373	28.783	6.95	3.6
209	18.7.2007	02:51	39.329	29.293	5.35	3.6
210	20.9.2007	06:18	39.220	29.420	5	4
211	5.10.2007	17:12	39.135	29.050	14.77	3.7
212	19.10.2008	10:54	39.130	29.434	10	4
213	20.1.2009	05:15	39.186	29.448	14.31	3.8
214	17.2.2009	05:28	39.149	29.045	7	5.2
215	17.2.2009	05:52	39.123	29.041	21.2	3.5
216	17.2.2009	09:37	39.131	29.062	17.9	3.7
217	17.2.2009	10:45	39.122	29.066	7.02	3.6
218	19.2.2009	22:25	39.124	29.030	10.28	4
219	20.2.2009	00:31	39.129	29.067	10.59	3.6

Table A-1 (continued)

220	24.2.2009	07:41	39.130	29.023	7	3.6
221	25.2.2009	13:27	39.120	29.070	10.3	3.6
222	28.2.2009	16:30	39.351	29.154	15.22	3.6
223	19.4.2009	20:48	39.088	29.043	7.69	3.5
224	20.4.2009	12:22	39.103	29.038	4.76	3.8
225	23.4.2009	02:56	39.135	29.060	7.69	3.6
226	27.4.2009	09:50	39.102	29.052	9.29	3.5
227	31.7.2009	13:24	39.118	29.033	17.57	3.9
228	12.8.2009	03:35	39.108	29.040	14.3	3.6
229	19.8.2009	22:36	39.116	29.021	10.13	3.9
230	11.9.2009	14:01	38.717	28.860	6.97	3.6
231	15.9.2009	09:23	39.090	29.050	11	4
232	23.10.2009	01:07	39.114	29.023	22.43	3.5
233	8.11.2009	09:05	39.081	29.036	6.99	3.8
234	2.3.2010	00:43	39.134	29.071	2.8	4.2
235	2.3.2010	00:59	39.140	29.100	7	4.3
236	2.3.2010	00:59	39.157	29.076	3.66	3.7
237	18.3.2010	08:03	39.285	29.069	9.94	3.7
238	14.9.2010	14:05	39.130	29.083	10.06	3.6
239	10.2.2011	03:56	39.141	29.039	5.31	3.5
240	29.3.2011	00:53	39.160	29.067	6.97	4.3
241	4.4.2011	03:44	39.128	29.089	7	3.5
242	5.4.2011	19:53	39.127	29.065	14.53	3.5
243	13.5.2011	12:52	39.108	29.059	6.98	3.7
244	19.5.2011	19:59	39.121	29.091	3.03	3.8
245	19.5.2011	20:15	39.133	29.082	24.46	5.9
246	19.5.2011	20:17	39.136	29.110	6.99	3.9
247	19.5.2011	20:25	39.144	29.108	7	4.6
248	19.5.2011	20:41	39.100	29.130	5	4
249	19.5.2011	20:43	39.120	29.090	2	4
250	19.5.2011	20:59	39.116	29.054	7.02	3.9
251	19.5.2011	21:01	39.096	29.090	7.06	3.5
252	19.5.2011	21:01	39.078	29.073	6.98	3.7
253	19.5.2011	21:05	39.109	29.001	7	3.9
254	19.5.2011	21:06	39.080	29.069	7.03	3.6
255	19.5.2011	21:06	39.132	29.112	7	3.8
256	19.5.2011	21:08	39.110	29.034	7.06	4.2
257	19.5.2011	21:09	39.127	29.013	7.14	3.6
258	19.5.2011	21:12	39.113	29.038	7.74	4.8
259	19.5.2011	21:20	39.202	29.068	7	3.7
260	19.5.2011	21:21	39.113	29.032	6.99	4.3
261	19.5.2011	21:24	39.106	29.025	33.85	3.9
262	19.5.2011	21:25	39.064	29.045	7	3.7
263	19.5.2011	21:33	39.131	29.124	20.83	4.3
264	19.5.2011	22:05	39.126	29.102	24.9	3.8
265	19.5.2011	22:19	39.115	28.989	6.95	4

Table A-1 (continued)

266	19.5.2011	23:27	39.146	29.138	7.01	3.7
267	20.5.2011	00:03	39.099	29.019	6.98	3.7
268	20.5.2011	00:13	39.141	29.107	16.92	4.1
269	20.5.2011	00:15	39.108	29.052	8.33	3.5
270	20.5.2011	00:23	39.120	29.110	15.76	3.8
271	20.5.2011	00:58	39.115	29.084	17.38	4.3
272	20.5.2011	02:10	39.116	29.025	14.66	3.9
273	20.5.2011	02:31	39.104	28.969	7.01	3.8
274	20.5.2011	03:32	39.104	29.068	6.99	3.5
275	20.5.2011	04:00	39.144	29.002	6.97	4
276	20.5.2011	04:16	39.164	29.112	2.33	3.5
277	20.5.2011	05:00	39.120	29.087	7.09	4.2
278	20.5.2011	05:20	39.122	29.019	6.85	3.9
279	20.5.2011	05:37	39.097	29.026	6.97	3.7
280	20.5.2011	06:07	39.127	29.111	6.75	3.5
281	20.5.2011	07:22	39.116	29.093	18.27	3.9
282	20.5.2011	07:35	39.134	29.108	11.44	3.7
283	20.5.2011	07:43	39.133	29.099	6.53	3.6
284	20.5.2011	08:03	39.093	29.030	4.83	3.9
285	20.5.2011	08:16	39.095	29.034	6.91	3.5
286	20.5.2011	10:14	39.108	29.075	5.5	3.5
287	20.5.2011	11:30	39.123	29.003	7	4
288	20.5.2011	11:50	39.104	29.004	12.42	3.8
289	20.5.2011	15:35	39.127	29.041	5.83	3.7
290	20.5.2011	20:13	39.109	29.012	4.8	3.5
291	20.5.2011	20:56	39.126	29.046	8.5	3.5
292	20.5.2011	22:01	39.183	29.111	5.95	3.5
293	21.5.2011	00:09	39.139	29.098	4.03	3.5
294	21.5.2011	03:38	39.108	28.997	7.42	3.5
295	21.5.2011	04:02	39.255	28.931	8.79	3.5
296	21.5.2011	04:43	39.112	29.008	9.89	3.5
297	21.5.2011	21:43	39.104	29.051	7	4
298	22.5.2011	07:04	39.089	29.056	7	3.5
299	22.5.2011	07:10	39.097	29.058	6.99	3.6
300	22.5.2011	09:14	39.099	29.045	7	3.6
301	22.5.2011	10:32	39.111	28.994	7	3.5
302	22.5.2011	16:49	39.116	29.021	1.89	3.9
303	23.5.2011	18:26	39.144	29.005	5.25	3.5
304	24.5.2011	02:55	39.101	29.022	16.8	4.2
305	24.5.2011	04:55	39.235	29.146	19.02	3.5
306	24.5.2011	08:57	39.100	29.015	3.1	3.6
307	24.5.2011	16:40	39.115	29.085	6.87	3.6
308	24.5.2011	16:54	39.135	29.145	11.5	3.6
309	24.5.2011	17:47	39.126	29.061	19.32	3.8
310	24.5.2011	19:47	39.137	29.109	2.33	3.5
311	24.5.2011	20:57	39.111	29.035	7.07	3.6

Table A-1 (continued)

312	24.5.2011	23:08	39.108	29.049	6.99	3.6
313	25.5.2011	10:48	39.140	29.003	6.45	3.6
314	25.5.2011	12:15	39.126	29.114	6.99	3.8
315	25.5.2011	17:55	39.135	28.998	3.05	3.5
316	26.5.2011	09:42	39.123	29.104	4.29	3.7
317	26.5.2011	10:10	39.109	29.113	6.61	3.6
318	26.5.2011	10:15	39.111	29.103	7.82	3.5
319	26.5.2011	17:34	39.108	29.067	11.08	3.5
320	26.5.2011	20:04	39.112	29.077	6.98	3.5
321	27.5.2011	07:43	39.139	29.124	19.42	4.4
322	28.5.2011	05:47	39.122	29.041	23.02	5.1
323	28.5.2011	07:06	39.095	29.048	7	3.5
324	28.5.2011	07:35	39.110	29.130	8	4
325	28.5.2011	09:28	39.112	29.026	13.8	3.6
326	28.5.2011	09:55	39.135	29.111	4.68	3.7
327	28.5.2011	10:23	39.115	29.015	10.3	3.6
328	28.5.2011	11:21	39.099	29.057	14.46	3.6
329	28.5.2011	13:26	39.113	29.016	8.09	3.5
330	28.5.2011	18:06	39.112	29.028	16.62	4
331	29.5.2011	01:31	39.143	29.085	5.04	4.5
332	29.5.2011	19:46	39.113	29.035	6.99	3.7
333	30.5.2011	08:52	39.099	29.062	11.49	3.8
334	30.5.2011	14:52	39.127	29.014	18.1	3.5
335	30.5.2011	17:57	39.137	29.011	7.62	3.8
336	30.5.2011	22:03	39.157	29.011	15.29	4
337	31.5.2011	04:27	39.114	28.981	17.79	3.9
338	31.5.2011	21:26	39.139	28.997	14.02	3.5
339	1.6.2011	13:55	39.136	29.030	2.13	3.7
340	2.6.2011	04:35	39.137	29.020	6.9	3.6
341	3.6.2011	16:38	39.124	29.131	6.78	3.9
342	4.6.2011	13:51	39.112	29.102	15.63	4.1
343	5.6.2011	19:06	39.132	29.013	5.45	3.7
344	5.6.2011	21:29	39.143	29.095	6.98	4
345	6.6.2011	22:24	39.126	29.039	8.14	3.5
346	7.6.2011	22:52	39.110	29.058	18.68	3.7
347	9.6.2011	13:26	39.122	29.028	6.82	3.5
348	11.6.2011	05:28	39.122	29.087	17.15	3.8
349	11.6.2011	10:17	39.073	29.058	6.98	3.9
350	21.6.2011	00:55	39.161	29.088	10.42	3.5
351	25.6.2011	18:23	39.169	29.068	5.93	3.6
352	25.6.2011	21:07	39.100	29.112	16.69	3.5
353	27.6.2011	21:13	39.120	29.020	9	5
354	27.6.2011	21:28	39.122	29.044	12.15	4.4
355	27.6.2011	21:45	39.122	29.010	8.33	3.5
356	27.6.2011	22:24	39.121	29.018	5	3.9
357	27.6.2011	22:25	39.117	29.002	11.19	3.7

Table A-1 (continued)

358	27.6.2011	22:41	39.113	29.021	3.09	3.5
359	27.6.2011	23:41	39.070	29.000	8	4
360	28.6.2011	00:13	39.053	29.068	7.08	3.5
361	28.6.2011	06:48	39.150	29.116	7	3.5
362	28.6.2011	08:21	39.150	29.008	7.3	3.6
363	29.6.2011	11:40	39.123	29.003	9.28	4
364	29.6.2011	12:10	39.108	29.006	6.99	3.5
365	30.6.2011	01:03	39.127	29.003	9.8	3.6
366	30.6.2011	19:06	39.117	29.072	9.64	3.8
367	3.7.2011	14:16	39.104	29.015	10.78	4.1
368	5.7.2011	15:43	39.133	29.095	6.63	3.6
369	5.7.2011	18:55	39.117	29.023	7.29	3.8
370	6.7.2011	06:22	39.097	29.008	8.75	3.8
371	6.7.2011	18:56	39.104	29.088	6.84	3.8
372	6.7.2011	20:00	39.080	29.011	10.2	3.8
373	13.7.2011	01:31	39.123	29.033	14.7	4.3
374	17.7.2011	19:51	39.064	29.124	13.84	4
375	18.7.2011	06:19	39.155	29.054	15.15	3.9
376	18.7.2011	10:57	39.127	29.082	5.03	3.5
377	19.7.2011	17:58	39.111	29.111	7.01	3.5
378	19.7.2011	21:16	39.105	29.093	17.66	4.1
379	19.7.2011	21:32	39.100	29.083	21.35	3.8
380	20.7.2011	01:53	39.100	29.081	15.95	3.7
381	20.7.2011	03:30	39.115	29.008	18.49	3.7
382	20.7.2011	17:51	39.114	29.025	16.71	3.8
383	18.8.2011	04:35	39.100	29.033	7	3.5
384	19.8.2011	02:05	39.111	29.059	7.16	3.9
385	22.8.2011	15:00	39.130	29.037	7.03	3.8
386	22.8.2011	20:21	39.131	28.984	6.96	3.8
387	23.8.2011	17:47	39.126	28.953	7.03	3.5
388	23.8.2011	19:20	39.122	28.988	7	3.8
389	25.8.2011	04:19	39.139	29.096	22.54	4.3
390	2.9.2011	03:30	39.130	29.057	7.02	3.6
391	6.9.2011	05:07	39.114	29.093	8.5	3.6
392	12.9.2011	06:16	39.086	29.100	5	3.6
393	20.9.2011	07:01	39.112	29.125	7.01	3.5
394	28.9.2011	05:07	39.100	29.032	2.51	3.5
395	8.11.2011	21:39	39.133	29.096	20.98	3.5
396	10.11.2011	13:11	39.154	29.110	21.19	3.7
397	11.11.2011	14:06	39.147	29.108	4.63	3.6
398	5.12.2011	21:15	39.074	29.099	7.01	3.8
399	8.12.2011	01:07	39.125	29.090	14.11	3.8
400	11.1.2012	03:44	39.123	29.141	20.85	3.7
401	29.2.2012	01:29	39.112	29.035	2.11	3.9
402	3.3.2012	21:05	39.129	29.130	6.26	3.7
403	14.3.2012	04:12	39.127	28.996	5.62	3.8

Table A-1 (continued)

404	16.4.2012	10:10	39.123	29.122	6.9	4.7
405	16.4.2012	10:11	39.110	29.136	7	4.6
406	16.4.2012	10:22	39.102	29.112	10.56	3.5
407	16.4.2012	12:19	39.114	29.123	6.99	3.9
408	17.4.2012	20:45	39.147	29.114	6.99	4.5
409	17.4.2012	21:02	39.079	29.126	4.4	3.5
410	17.4.2012	21:26	39.118	29.116	7	3.6
411	18.4.2012	12:46	39.119	29.129	7	3.5
412	19.4.2012	19:52	39.111	29.138	7.49	4.5
413	20.4.2012	02:43	39.108	29.096	8.11	3.6
414	20.4.2012	02:48	39.098	29.147	7	3.5
415	20.4.2012	02:54	39.092	29.109	7.26	3.5
416	20.4.2012	16:39	39.153	29.098	20.59	4.4
417	22.4.2012	07:01	39.113	29.120	6.96	3.5
418	23.4.2012	16:14	39.124	29.144	6.31	4.3
419	23.4.2012	16:14	39.055	29.149	6.96	4
420	23.4.2012	17:47	39.102	29.155	5	3.9
421	23.4.2012	18:52	39.126	29.113	5	3.9
422	23.4.2012	23:47	39.102	29.162	7	3.8
423	26.4.2012	22:02	39.103	29.160	7	3.5
424	26.4.2012	22:05	39.131	29.113	25.54	4.8
425	26.4.2012	23:46	39.106	29.121	10.35	3.5
426	3.5.2012	15:20	39.125	29.110	10.59	5.2
427	3.5.2012	15:24	39.100	29.149	6.99	3.7
428	3.5.2012	15:25	39.121	29.126	6.99	4
429	3.5.2012	15:28	39.066	29.104	7	3.6
430	3.5.2012	15:40	39.166	29.023	6.45	3.8
431	3.5.2012	16:07	39.125	29.123	7	3.5
432	3.5.2012	16:16	39.102	29.039	25.41	4.6
433	3.5.2012	17:10	39.136	29.097	23.7	4.4
434	3.5.2012	18:10	39.097	29.112	16.79	3.5
435	3.5.2012	18:32	39.123	29.135	7	3.7
436	3.5.2012	20:44	39.111	29.091	7.03	3.7
437	3.5.2012	21:45	39.135	29.106	14.22	4.7
438	4.5.2012	02:00	39.120	29.102	23.94	4.5
439	4.5.2012	05:30	39.105	29.124	6.59	3.5
440	5.5.2012	02:56	39.088	29.079	6.96	3.9
441	5.5.2012	10:23	39.109	29.167	2.07	3.5
442	8.5.2012	02:31	39.097	29.090	8.39	3.6
443	9.5.2012	17:49	39.097	29.146	10.33	3.6
444	9.5.2012	17:49	39.103	29.157	8.98	4.3
445	25.5.2012	20:44	39.095	29.111	7.09	3.6
446	11.6.2012	03:49	39.117	29.166	6.99	3.9
447	11.6.2012	03:51	39.105	29.164	6.99	3.6
448	13.6.2012	06:40	39.107	29.148	21.58	4.3
449	19.6.2012	01:46	39.117	29.159	25.91	4.9

Table A-1 (continued)

450	30.6.2012	03:11	39.116	29.135	7.11	3.7
451	5.8.2012	13:51	39.104	29.125	9.3	3.9
452	25.8.2012	23:33	39.113	29.074	8.4	3.5
453	16.9.2012	10:35	39.108	29.132	17.52	3.6
454	4.10.2012	01:07	39.125	29.090	7.13	3.6
455	5.10.2012	12:58	39.120	29.146	6.91	3.8
456	10.10.2012	16:48	39.099	29.161	6.99	3.6
457	10.10.2012	16:53	39.100	29.153	6.99	3.5
458	30.10.2012	00:12	39.139	29.179	21.35	4.1
459	4.3.2013	02:59	39.141	29.106	7	3.6
460	12.3.2013	20:47	39.120	29.058	12.81	4.1
461	29.5.2013	14:43	39.136	29.098	7	4
462	9.6.2013	14:18	39.139	29.022	15.61	4.1
463	9.7.2013	23:28	39.126	29.092	6.99	3.5
464	24.7.2013	11:49	39.340	29.022	12.08	3.6
465	28.7.2013	14:14	39.365	29.020	4.45	3.6
466	7.8.2013	05:20	39.209	29.416	20.86	4.4
467	23.9.2013	16:54	39.095	29.175	7.06	3.6
468	15.7.2014	12:25	39.130	29.004	9.92	4.1

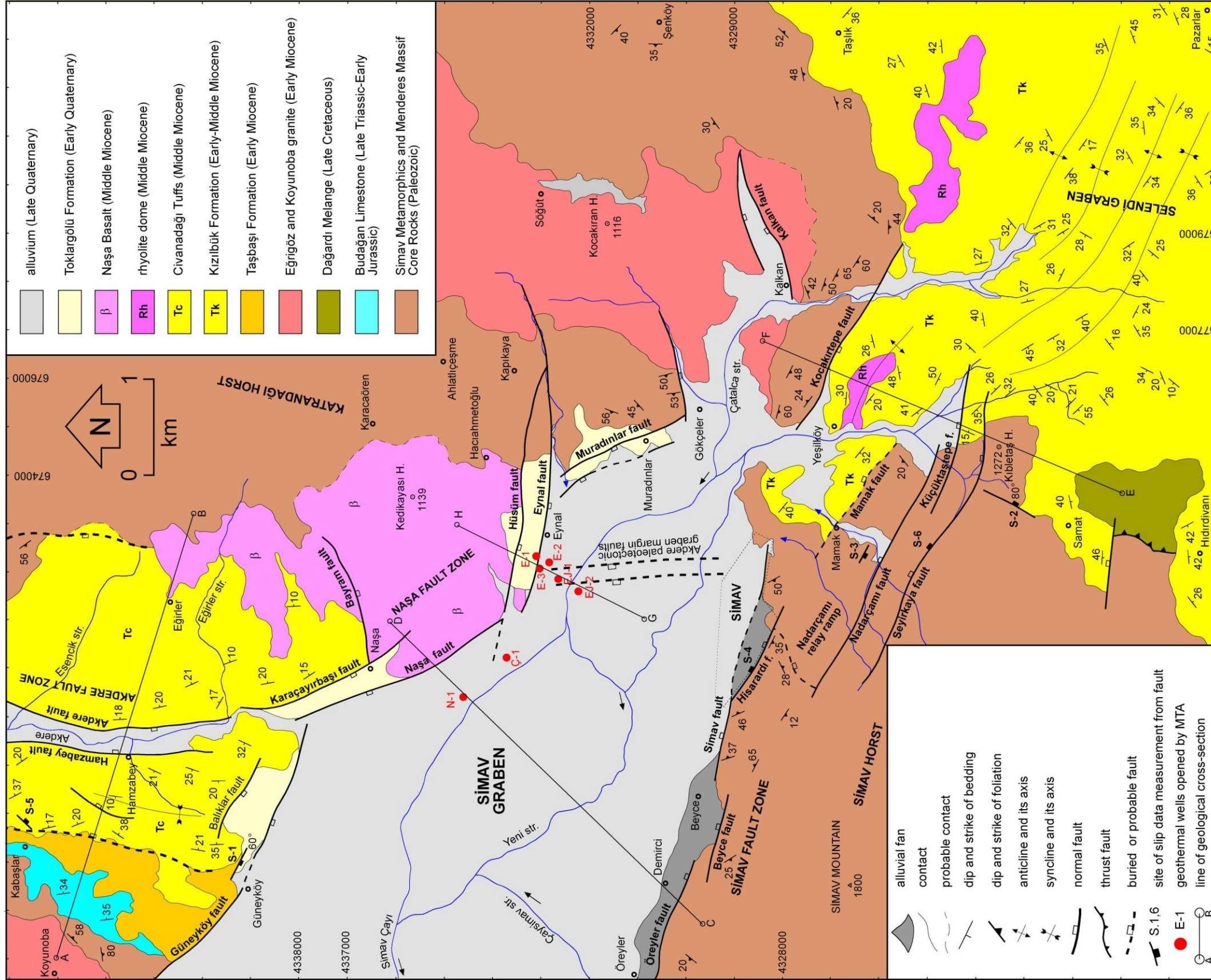


Figure A-1: Geological map of the study area

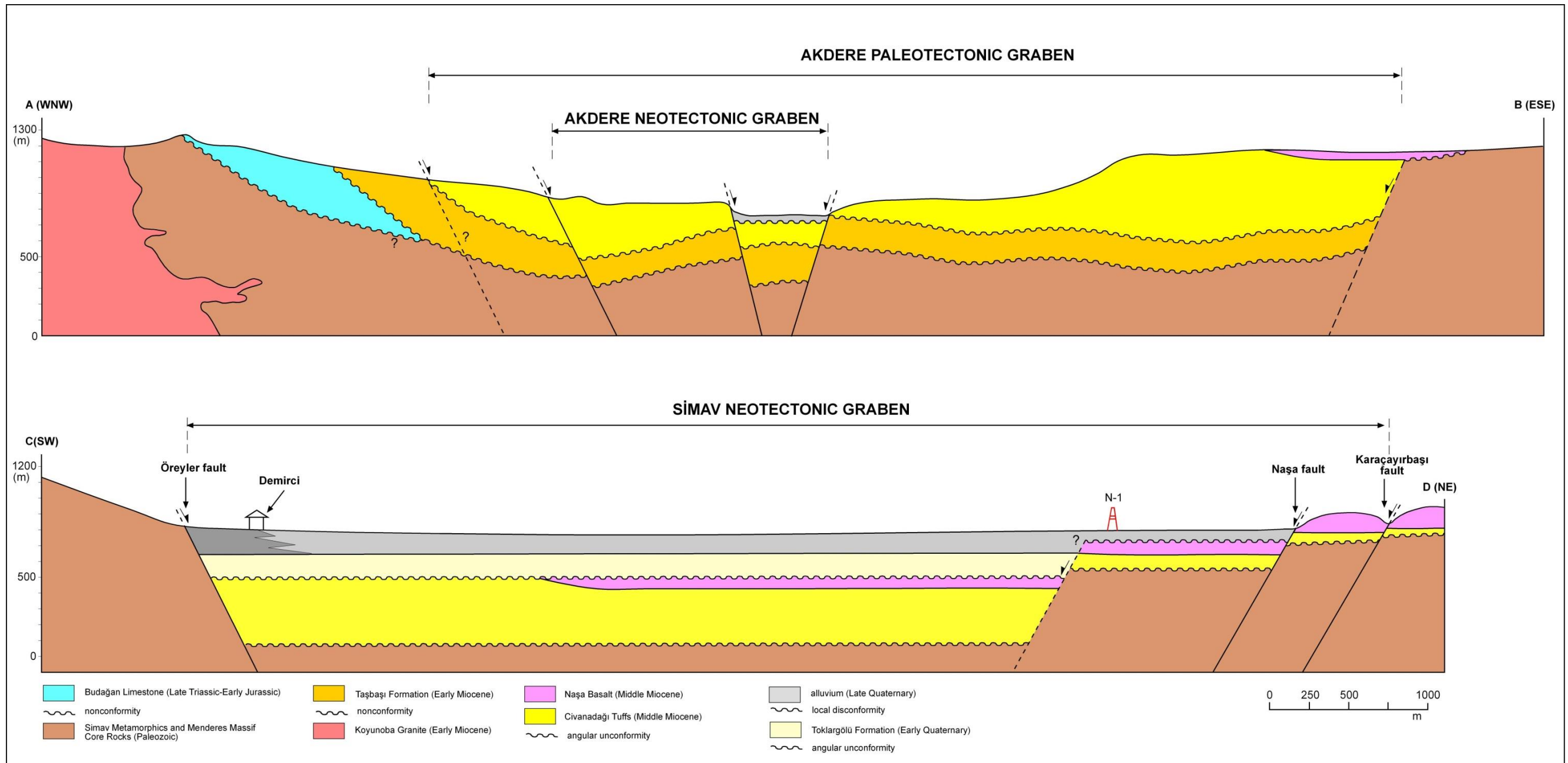


Figure A-2: Geological cross sections along A-B and C-D lines (position of the lines are shown in figure A-1). For details of the well logs readers are referred to see (Güven et al., 1985)

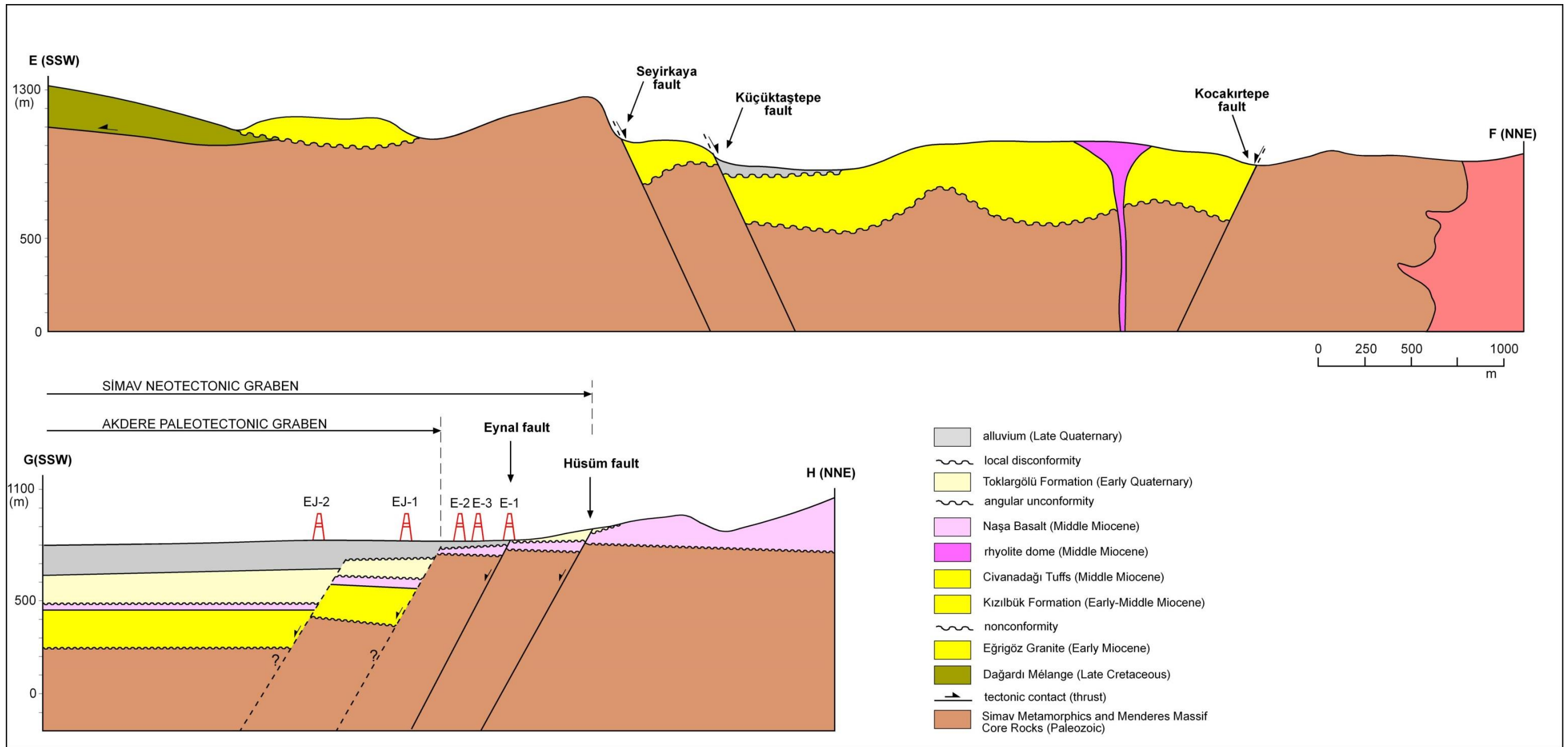


Figure A-3: Geological cross sections along A-B and C-D lines (sites of the lines are shown in figure A-1). For details of the well logs readers are referred to see (Erkan et al.,1977; Erkan, 1978; Erişen et al.,1985; Erişen et al.,1986; Erişen et al.,1989)